

STATUS OF THESIS

Title of thesis

Design, Simulation and Modeling of a Micromachined U-shaped Cantilever Device for Application in Magnetic Field Detection

I, WADDAH ABDELBAGI TALHA MOHAMMED hereby allow my thesis to be placed at the Information Resources Center (IRC) of Universiti Teknologi PETRONAS (UTP) with the following conditions:

1. The thesis becomes the property of UTP.
2. The IRC of UTP may make copies of the thesis for academic purposes only.
3. This thesis is classified as

Confidential

Non – confidential

If this thesis is confidential, please state the reason:

The contents of this thesis will remain confidential for _____ years.

Remarks on disclosure:

Endorsed by

Signature of Author

WADDAH ABDEBAGI TALHA
Permanent Address:
Faculty of Engineering & Technology
University of GEZIRA
Wad Medan, Sudan

Date: _____

Signature of Supervisor

Dr. JOHN OJUR DENNIS
Universiti Teknologi PETRONAS
Malaysia

Date: _____

UNIVERSITI TEKNOLOGI PETRONAS

Approval by Supervisor (s)

The undersigned certify that they have read, and recommend to The Postgraduate Studies Programme for acceptance, a thesis entitled **“Design, Simulation and Modeling of a Micromachined U-shaped Cantilever Device for Application in Magnetic Field Detection”** submitted by (**Waddah Abdelbagi Talha Mohammed**) for the fulfillment of the requirements for the degree of (Master of Science in Electrical and Electronics Engineering).

Date

Signature : _____

Main Supervisor : Dr. John Ojur Dennis

Date : _____

Signature : _____

Co-Supervisor : Dr. Nor Hisham B Hamid

Date : _____

TITLE PAGE

UNIVERSITI TEKNOLOGI PETRONAS

**Design, Simulation and Modeling of a Micromachined U-shaped Cantilever
Device for Application in Magnetic Field Detection**

By

Waddah Abdelbagi Talha Mohammed

A THESIS

SUBMITTED TO THE POSTGRADUATE STUDIES PROGRAMME

AS A REQUIREMENT FOR THE

DEGREE OF MASTER OF SCIENCE IN ELECTRICAL AND ELECTRONICS
ENGINEERING

ELECTRICAL AND ELECTRONICS ENGINEERING

BANDAR SERI ISKANDAR,

PERAK

August, 2009

DECLARATION

I hereby declare that the thesis is based on my original work except for quotations and citations which have been duly acknowledged. I also declare that it has not been previously or concurrently submitted for any other degree at UTP or other institutions.

Signature: _____

Name : WADDAH ABDELBAGI TALHA MOHAMMED

Date : _____

DEDICATION

**To my parents
for their Patience.**

waddah

ACKNOWLEDGEMENT

Firstly, I would like to thank Almighty ALLAH for the innumerable gifts that He has granted me, for guiding me along in completing this work and for giving me an opportunity to undertake higher education.

I would like to express my total appreciation to the people for their support and for guiding me to complete this thesis. Very special and great thanks to my supervisor, Dr. John Ojur Dennis who offered numerous helpful, information, ideas, suggestions and guidance on this work. Also for my co-supervisor Dr. Nor Hisham B Hamid and Mr. James Osurow.

I would like to express my utmost appreciation to my dearest parents Ust. Abdelbagi Talha and Ust. Aishah Elobaid, my three sisters and my aunt Aishah Talha for their bearding up a lot with me, without their love and support my achievement would mean nothing. I would like also to thank all other family members.

I would like to thank all my friends particularly Dr. Mohammed Tom, Ust. Abd elrahman Burir, Abdelazeim, Ustazes: Sumiah, Aleiah, Yousif, Naji, Abubakr, Jalal eldeen, Gassan, Abdelaziz, Hani, Mahmud, Sohaila and Hajeir. Also Dr. Almalih, Dr. Ahmad Ali and Dr. Aseem for their supporting and friendship through good and bad times.

Finally, Thanks and gratitude must be given to the PETRONAS company and University for their grant me this opportunity and facilities to completion this research.

ABSTRACT

The research explores the potential applicability of the Lorentz force actuation of a MEMS based U-shaped cantilever which is made entirely of aluminum. The main objective of the study is to design, simulate and derive mathematical models for the behavior of the cantilever. The design is based on CMOS fabrication technology and bulk micromachining implemented in CoventorWare simulation environment using a Si substrate and SiO₂ insulating layer supporting the Al U-shaped cantilever. Analytical models describing 3-D vibration modes (mode 1, 2 and 3) of the cantilever and their verification by simulation are discussed based on the direction of the current through the cantilever and the direction of the orthogonal external magnetic field. The response of the cantilever is discussed in two situations: static and dynamic. The static motion is obtained when a constant force, representing the Lorentz force due to a direct current through the cantilever placed in a static magnetic field, is applied. On the other hand, the dynamic vibration is realized when a periodic force is applied representing the Lorentz force due to a static external magnetic field acting on an alternating current through the cantilever. Results show that the displacement of the cantilever is significantly large indicating that high sensitivity can be achieved when it is driven at its resonant frequency. Three resonant frequencies were obtained for the three modes of vibration of 3, 8 and 86.6 kHz for mode 1, 2 and 3 respectively when the thickness is 5 μm , width is 20 μm , length of the base is 760 μm and length of the arm is 1000 μm . Results show the resonant frequency and sensitivity of mode 1 depend on the thickness and length of the arms only, mode 2 depends on the length of the base, length of the arms and thickness. While the resonant frequency and sensitivity of mode 3 are depend on the length of the base, length of the arms and width. The displacement as a function of the applied force is shown to be perfectly linear. The quality factors (Q -factor) of the system for the three modes were determined to be the same at the same damping coefficient. The systems response is found to decrease exponentially with increasing damping. Finally polysilicon piezoresistors in Wheatstone's bridge configuration is used to convert the response of the cantilever to electrical measurements at various voltages for different dimensions of the cantilever. The highest sensitivity of about 64 V/T without amplification is obtained for a thin beam of 0.6 μm polysilicon embedded in 2 μm thick silicon cantilever beam.

ABSTRAK

Tesis ini mengkaji potensi aplikasi 'Lorentz force actuation' pada tiang penyangga berbentuk U yang berdasarkan kepada 'MEMS' dan diperbuat sepenuhnya daripada aluminium. Objektif utama kajian ini adalah untuk merekabentuk, menjalankan simulasi dan seterusnya menghasilkan model-model matematik bagi kelakuan tiang penyangga. Rekabentuk adalah berdasarkan kepada teknologi fabrikasi CMOS dan 'bulk micromachining' yang dijalankan di persekitaran simulasi 'ConventorWare' menggunakan produk Silikon ('Si') dan lapisan penebat Silikon oksida ('SiO₂') yang menyokong tiang penyangga berbentuk U tersebut. Model-model analitikal yang menggambarkan tiga keadaan getaran 3 dimensi (3-D) (mod 1, mod 2 dan mod 3) bagi tiang penyangga tersebut dan pengesahannya melalui simulasi dibincangkan didalam kajian ini berdasarkan kepada arah arus elektrik yang melalui tiang penyangga dan arah medan magnet luaran yang bersudut tepat. Tindak balas tiang penyangga bagi tiga keadaan tersebut di bincangkan dalam dua situasi, iaitu statik dan dinamik. Situasi statik adalah apabila daya yang tetap di kenakan. Daya yang tetap ini mewakili daya 'Lorentz' yang disebabkan oleh medan magnet luaran yang statik. Situasi getaran dinamik pula adalah apabila daya dikenakan secara berkala. Daya ini mewakili daya 'Lorentz' yang disebabkan oleh medan magnet luaran yang statik yang bertindak ke atas arus ulang-alik di dalam tiang penyangga. Hasil kajian menunjukkan pergerakan tiang penyangga dari tempat asal adalah sangat ketara apabila ia digerakkan pada frekuensi resonan dan ini menunjukkan bahawa tahap sensitiviti yang tinggi boleh dicapai pada frekuensi ini. Bagi tiga mod getaran yang dijalankan, tiga frekuensi resonan yang berbeza diperolehi, iaitu 3 kHz bagi mod 1, 8 kHz bagi mod 2 dan 86.6 kHz bagi mod 3. Spesifikasi tiang penyangga yang digunakan dalam ujian ini ialah ketebalan 5 μm , lebar ialah 20 μm , panjang dasar ialah 760 μm dan panjang lengan ialah 1000 μm . Keputusan menunjukkan bahawa bagi mod 1, frekuensi resonan dan sensitiviti hanya bergantung kepada ketebalan dan panjang lengan sahaja dan bagi mod 2, ia bergantung kepada panjang dasar, panjang lengan dan ketebalan. Manakala bagi mod 3, frekuensi resonan dan sensitiviti bergantung kepada panjang dasar, panjang lengan dan lebar tiang penyangga. Pergerakan tiang penyangga adalah berkadar terus dengan daya yang dikenakan ke atasnya. Faktor kualiti ('Q-factor') sistem bagi ketiga-tiga mod pula adalah sama pada 'damping coefficient'

yang sama. Tindakbalas sistem didapati berkurangan secara eksponen apabila 'damping' bertambah. Seterusnya, 'Polysilicon piezoresistors' di dalam konfigurasi jambatan 'Wheatstone' digunakan untuk menukar tindakbalas tiang penyangga kepada sukatan elektrik bagi nilai voltan yang berlainan pada dimensi tiang penyangga yang berlainan. Tiang penyangga yang berukuran $2\ \mu\text{m}$ dengan $0.6\ \mu\text{m}$ 'polysilicon' terpancang di dalamnya memberikan kadar sensitiviti paling tinggi iaitu $64\ \text{V/T}$ tanpa sebarang amplifikasi.

TABLE OF CONTENTS

STATUS OF THESIS.....	i
APPROVAL PAGE.....	ii
TITLE PAGE	iii
DECLARATION.....	iv
DEDICATION.....	v
ACKNOWLEDGEMENT.....	vi
ABSTRACT.....	vii
ABSTRAK.....	viii
TABLE OF CONTENTS.....	ix
LIST OF TABLES.....	xii
LIST OF FIGURE.....	xiii
ABBREVIATIONS AND SYMBOLS	xvi
Chapter 1 INTRODUCTION.....	1
1.1 BACKGROUND.....	1
1.2 PROBLEM STATEMENT.....	3
1.3 OBJECTIVES OF THE STUDY.....	5
1.4 SCOPE OF THE PROJECT.....	5
1.5 THESIS OUTLINE.....	5
Chapter 2 LITRATURE REVIEW.....	7
2.1 FORCE AND PRESSURE TRANSDUCTION.....	7
2.1.1 Principle of Lorentz Force Actuation.....	8
2.1.2 Static and Dynamic Response Characteristics in Lorentz Force Actuation.....	9
2.1.3 Linearity property of a vibrating system.....	11
2.1.4 Q-factor.....	12
2.1.5 Damping coefficient.....	14
2.1.6 Peizoresistive transducers.....	15
2.2 MEMS AND CMOS-COMPATIBLE MICROMACHINING OF CANTILEVER STRUCTURES.....	17

2.2.1 Surface Micromachining.....	18
2.2.2 Bulk Micromachining.....	18
2.3 FINITE ELEMENT MODELS (FEM) SIMULATORS.....	19
2.4 REVIEW OF RELATED STUDIES.....	21
2.4.1 Fabricated and Characterized a MEMS based Cantilevers.....	21
2.4.2 Simulation Studies on a MEMS Devices base Cantilever.....	26
Chapter 3 METHODOLOGY.....	28
3.1 U-SHAPE CANTILEVER DEVICE STRUCTURE.....	28
3.2 LORENTZ FORCE FOR ACTUATION OF THE U-SHAPED CANTILEVER.....	30
3.3 SIMULATION AND MODELING OF THE DEVICE.....	32
3.3.1 Device Simulation software.....	32
3.3.2 Materials selection.....	35
3.3.3 Device design.....	36
3.3.4 Mesh Creation.....	39
3.3.5 Simulation and characterization of the U-shaped cantilever.....	41
3.3.6 Piezoresistor for output signal measurement.....	47
3.4 MATHEMATICAL MODELING.....	52
Chapter 4 RESULTS AND DISCUSSION.....	58
4.1 STATIC AND DYNAMIC CHARACTERIZATION AND MODELING.....	58
4.1.1 Static Characterization.....	58
4.1.2 Dynamic Characterizatio.....	61
4.1.3 Comparison between the static and dynamic mode.....	63
4.2 THE EFFECT OF THE CANTILEVER DIMENSIONS ON ITS DYNAMIC CHARACTERISTICS.....	64
4.2.1 Variation of the cantilever thickness.....	64
4.2.2 Variation of the cantilever width.....	69
4.2.3 Variation in length of arms.....	72
4.2.4 Variation in length of the base.....	75
4.3 RELATIONSHIP BETWEEN APPLIED FORCE AND DISPLACEMENT.....	80
4.3.1 Static mode.....	80
4.3.2 Dynamic mode.....	81

4.4 MECHANICAL QUALITY FACTOR.....	83
4.5 EFFECT OF DAMPING-COEFFICIENT.....	85
4.6 PIEZORESISTOR TRANSDUCTION.....	88
4.6.1 Effect of arms deflection on Resistivity.....	88
4.6.2 Sensitivity estimation.....	92
Chapter 5 CONCLUSION AND RECOMMENDATIONS.....	95
5.1 CONCLUSION.....	95
5.2 RECOMMENDATIONS AND LIMITATIONS OF RESEARCH.....	96
REFERENCES.....	Er
ror! Bookmark not defined.	
APPENDIX-A.....	104
APPENDIX-B.....	109
APPENDIX-C.....	111
LIST OF PUBLICATIONS.....	116

LIST OF TABLES

Table 3-1 Properties of materials used in the software	36
Table 3-2 Calculated values of forces applied to the base and both arms of the cantilever	44
Table 3-3 Dimensions of the Aluminium cantilever determined in the software.....	46
Table 3-4 The thickness of the silicon beam and piezoresistor grown inside	48
Table 4-1 Maximum displacement and sensitivity of the cantilever in the three modes of vibration for static and dynamic cases	63
Table 4-2 Theoretical and simulation results of resonant frequency for various thicknesses of the U-shaped cantilever for the three modes of vibrations.....	68
Table 4-3 Theoretical and simulation results of Resonant frequency for various widths for the three modes of vibration	71
Table 4-4 Simulation results of the length of the arms effect on the value of the resonant frequency for mode 1, mode 2, mode 3a ($b/l > 0.82$) and mode 3b ($b/l < 0.82$)	73
Table 4-5 Simulation results of the effect of length of base on the resonant frequency for mode 1, mode 2, mode 3a ($b/l > 0.82$) and mode 3b ($b/l < 0.82$)	75
Table 4-7 Simulation and theoretical resonant frequency various length of the arms for mode 3a and 3c	79
Table 4-8 Calculated Q-factor for mode 1, mode 2 and mode 3	84
Table 4-9 Maximum displacement at the resonant frequency for various values of the damping coefficient for the three modes of vibration.....	86
Table 4-10 Calculated Δf and Q-factor for the three modes for various damping coefficients.....	87
Table 4-11 Simulation results of ΔR_p % for different values of the cantilever deflections	89
Table 4-12 Calculated values of ΔR_p (Ω) and simulation results of the voltage output for different values of the cantilever deflections.....	91
Table 4-13 Sensitivity for mode 1, mode 2 and mode 3	92
Table 4-14 Simulation results showing changes in various parameters for different thicknesses of the piezoresistor.....	93
Table 4-15 Calculated values of the voltage output and the sensitivity for difference thickness of piezoresistor.....	94

LIST OF FIGURES

Figure 2-1 Transduction of a force via spring and sensor element into electrical output [27].....	7
Figure 2-2 A straight wire in a magnetic field that is constant along its length [19].....	8
Figure 2-3 Frequency response of a vibrating system [19, 28].....	10
Figure 2-4 Mass-Spring System [21, 22].....	10
Figure 2-5 Frequency response of the mass and band wide at -3dB of the amplitude [35].....	13
Figure 2-6 Micromachining techniques: (a) Surface micromachining steps and (b) Bulk micromachining.....	19
Figure 2-7 SEM photograph of two U-shape cantilevers [22].....	22
Figure 2-8 Principle of Lorentz force actuation of the U-shaped cantilever [15, 46].....	23
Figure 2-9 Visualization of the (a) symmetric S and (b) antisymmetric A flexural vibration modes [14].....	24
Figure 2-10 The piezoresistive magnetic field sensor [31].....	25
Figure 2-11 SEM photograph of the polysilicon specimens [32].....	25
Figure 2-12 Simulation result of the cantilever under load by the Lorentz force [24].....	26
Figure 3-1 Schematic diagram of the metal U-shaped cantilever.....	28
Figure 3-2 Schematic drawing of the layers of micro machined U-shaped cantilever device.....	29
Figure 3-3 Cross sectional view of a U-shaped cantilever device.....	29
Figure 3-4 The three modes of vibration of a U-shaped cantilever.....	31
Figure 3-5 The main window of the Coventor soft ware.....	33
Figure 3-6 Flow chart of the methodology in CoventorWare.....	34
Figure 3-7 Material Properties Database (MPD) window in CoventorWare.....	35
Figure 3-8 Process Editor for layer deposition and patterning.....	36
Figure 3-9 2-D Layout Editor showing layout of the U-shaped cantilever.....	37
Figure 3-10 3-D solid model of the (a) front side and (b) back side etched U-shaped cantilever.....	38
Figure 3-11 Compared accuracy of the diffrent values of mesh.....	40
Figure 3-12 The mesh results of the 3D solid model of the device.....	41
Figure 3-13 MemMech Settings dialog box of the CoventorWare.....	43

Figure 3-14 Preprocessor view of (a) meshed cantilevered beam, (b) meshed piezoresistor (c) combined model showing geometry placement.....	47
Figure 3-15 Applied voltage to the Piezoresistor Model.....	48
Figure 3-16 Settings Window of MemPZR.....	49
Figure 3-17 U-shaped cantilever with incorporation of piezoresistors.....	50
Figure 3-18 Cross sectional view of the (a) arm width (b) arm Length of the U-shaped cantilever device with polysilicon piezoresistor.....	50
Figure 3-19 Wheatstone's bridge circuit diagram for strain gauges.....	51
Figure 3-20 Cantilever beam motion.....	53
Figure 3-21 Model for mechanical vibration of a U-shaped cantilever in (a) mode 1, (b) mode 2 and (c) mode 3.....	54
Figure 3-22 Mode 3 of the cantilever-two forces acting on the base.....	56
Figure 3-23 Three different submodes for mode 3.....	57
Figure 4-1 3D simulation of constant applied force (a) 0.9 μN downward on the base (mode 1), (b) 1.2 μN applied to the arms in opposite direction (mode 2) and (c) 1.2 μN and 0.9 μN inwards on the arms and base respectively (mode 3)	60
Figure 4-2 Maximum displacement versus frequency for a periodic force of 0.9 μN amplitude applied to the base of the cantilever (mode 1).....	61
Figure 4-3 Maximum displacement versus frequency for a periodic force of 1.2 μN amplitude applied to the arms of the cantilever (mode2).....	62
Figure 4-4 Displacement versus frequency for a periodic force of 0.9 μN amplitude applied to the base and 1.2 μN to both arms of the cantilever (mode3).....	62
Figure 4-5 Vector representation of displacement for a 5 μm thick U-shaped cantilever for the three modes of vibration.....	65
Figure 4-6 Maximum displacement of U-shaped cantilever vs. frequency at various thicknesses for (a) mode 1(b) mode 2 and (c) mode 3.....	67
Figure 4-7 Theoretical and simulation results of resonant frequency various thickness for the three modes of vibration.....	68
Figure 4-8 Maximum displacement of U-shaped cantilever various frequency at various widths for (a) mode 1, (b) mode 2 and (c) mode 3.....	70
Figure 4-9 Theoretical and simulation results of resonant frequency various cantilever width for (a) mode 1 and mode 2 (b) modes 3.....	71

Figure 4-10 Simulation results of the three submodes for mode 3 of the cantilever's mechanical vibration for (a) $l = 1000 \mu\text{m}$, $b = 1000\mu\text{m}$, $b/l > 0.82$, (b) $l = 1000 \mu\text{m}$, $b = 820 \mu\text{m}$, $b/l = 0.82$ and (c) $l=1000 \mu\text{m}$, $b=760\mu\text{m}$, $b/l < 0.82$	72
Figure 4-11 Simulation results of the resonant frequency various length of arms for (a) mode 1 and 2 (c) mode 3a and mode 3c.....	74
Figure 4-12 Simulation results of the resonant frequency various length of the base for (a) mode 1 and 2 (b) mode 3a and mode 3c.....	76
Figure 4-13 Simulation and theoretical resonant frequency vs. length of arm for (a) mode 1 and (b) mode 2.....	78
Figure 4-14 Simulation and theoretical resonant frequency various length of arm for mode 3a and 3b.....	79
Figure 4-15 Simulation and theoretical values of the displacement as function of a constant applied force for the three modes.....	80
Figure 4-16 Displacement amplitude versus frequency at various applied periodic force for (a) mode 1 (b) mode 2 and (c) mode 3.....	82
Figure 4-17 Simulation and theoretical values of the displacement amplitude at the resonance frequency as function of a periodic applied force for the three modes....	83
Figure 4-18 Frequency response of the cantilever and band wide at -3dB of the amplitude for mode 1.....	84
Figure 4-19 Frequency response for mode 1at different values of the damping coefficient.....	85
Figure 4-20 Maximum displacement at the resonant frequency versus damping coefficient for the three modes of vibration.....	87
Figure 4-21 Cross sectional view of the arm of the U-shaped cantilever device with embedded polysilicon piezoresistor.....	88
Figure 4-22 ΔR_p % various cantilever deflections for mode 1.....	89
Figure 4-23 Conditioning circuit for strain gauges at $5 \mu\text{m}$ deflection of the cantilever in $-z$ direction.....	90
Figure 4-24 Calculated values of ΔR_p and estimated output voltage (mV) versus cantilever deflection.....	91
Figure 4-25 Simulated values of ΔR_p % various cantilever deflections for various beam thickness.....	93

ABBREVIATIONS AND SYMBOLS

MEMS	Microelectromechanical System
CMOS	Complementary- Metal- Oxide Semiconductor
IC	Integrated Circuits
DNA	Deoxyribonucleic Acid
SQUID	Superconducting Quantum Interference Device
CAD	Computer Aided design
FEM	Finite Element Model
3-D	Three Dimensions
2-D	Two dimensions
Si	Silicon
SiO ₂	Silicon Oxide
SiC	Silicon Carbide
Al	Aluminum
AlN	Aluminum Nitride
Au	Gold
FSBM	Front-Side Bulk Micromachining
BSBM	Back-Side bulk Micromachining
KOH	Potassium Hydroxide
TMAH	Tetramethylammonium hydroxide
F	Force
q	Charges
V	Velocity
B_{ext}	External magnetic flux density
L	Length of wire

i	Current
t	Time
T	Time of the period
k	Stiffness
m	Mass
c	Damping
u	Static displacement
ψ	Amplitude of the dynamic displacement
ω_0	Resonance angular frequency
f_0, f_{res}	Resonance frequency
U_{diss}	Energy dissipated
U_{stored}	Energy stored
Q -factor	Quality-factor
Δf_{-3dB}	3dB band width of frequency
d	Damping factor
R	Resistance
ρ	Specific resistance
A	Cross-section Area
ΔR_p	The change of the resistance of Piezoresistor
S	Sensitivity
S_{stat}	Static sensitivity
S_{res}	Resonant sensitivity
V_{out}	Output Voltage
BEM	Boundary Element Method
MemMech	Mechanical Simulation tap

MPD	Material Properties Database
MemPZR	Piezoresistor simulation tap
$V_{out-wheat}$	Output Voltage of Wheatson bridge
$V_{r.m.s}$	Root mean square Voltage
I	Moment of inertia
E	Young's modulus
h	Thickness
w	Width
l	Length of the arm
b	Length of the base
p	Distributed load
ζ	Spatial coordinates (x, y, or z) direction

Chapter 1

INTRODUCTION

1.1 Background

In the last few years, microfabricated cantilevers have been proposed as mechanical transducers for different sensing applications and many researchers have explored this area. Use of cantilevers for these applications has the advantages of reasonably good sensitivity, smaller sizes and lower costs. These cantilevers consist of microscopic bars free to move at one end and fixed at the opposite end. They are produced using standard silicon microfabrication techniques. The shape of the cantilever beam differs based on the type of the application: Single rectangular-shape for chemical application [1, 2] and biomolecular analysis [3], U-shape, V-shaped and cantilever-inside-cantilever structure for magnetic field sensing [4, 5, 6] and measurement of liquid viscosity [7]. Cantilever systems have also been designed and used to measure a variety of other quantities such as surface stress, temperature, heat generation and electric field [8, 9].

The design and fabrication techniques for these micro electromechanical system (MEMS) devices are based on Complementary Metal Oxide Semiconductor (CMOS) and bulk micromachining technology using a CMOS wafer with electronic parts on it. Important reasons for the successful application of cantilever sensors to measure these quantities are the reduced dimensions of the transducer. Therefore, improved sensitivity and resolution can be achieved for the measurement of extensive quantities, whereas for intensive quantities the advantage of cantilever sensors is mainly due to reduced sensor dimensions and potential compatibility with IC fabrication [10].

Two modes of operation for cantilever sensors can be distinguished: static and dynamic. First, in static operation the deflection of the cantilever by bending induced in one direction is employed to measure physical quantities. As an example, using static cantilever deflections, the surface stress due to DNA hybridization and receptor-ligand binding on cantilever have been measured [10, 11]. Second, for the dynamic mode the cantilever is excited harmonically [12] and a basic understanding of the mechanical behavior of cantilever beam is critical in order to successfully develop cantilever-based microsensors. The knowledge of spring constant, resonance frequency, damping coefficient and corresponding quality factor of a cantilever sensor have to be taken into account to determine sensitivity and resolution. This way the resonator cantilever combines the advantage of high sensitivity of the sensor. Resonance beam gas sensor is an example of the resonator sensors [13]. Microcantilevers can be operated either as microbalances or as surface stress sensors. By monitoring the shifts in its resonant frequency it is possible to follow the absorption processes which change its mass.

One of such devices, a micromachined U-shaped cantilever, offers measurement possibilities for a variety of physical parameters. They can be used for magnetic field measurement [4, 10, 14], chemical gas sensing [13], measuring the viscosity of liquids [7], and for moving and buckling at micrometer distance in the micro scaling industry [15]. In terms of stress sensing applications, the smaller dimensions of the cantilever causes a reduction in the magnitude of forces detected. The surface stress can be determined with the deflection of the cantilever either optically or electrically. The optical method commonly used is the optical lever technique, which involves alignment of the system consisting of lasers, photodetectors and focusing optics [16, 17]. On the other hand, the piezoresistive method is simple and directly measures the change in deflection of the cantilever [4, 10].

Numerous types of the micro magnetometers are designed and used for multiple applications such as magnetic flux detection and new applications like hydrocarbon exploration and metal detection. The sensitivity and the range of the measurement of

these devices are however limited and non directional like hall magnetometer, while others are expensive, bulky and have complicated design. These include the highly sensitivity vector magnetometers such as fluxgate or superconducting quantum interference device (SQUID) [18]. U-shaped cantilever device is a simple vector magnetic flux detector. The elastic properties of thin-films of some metals such as aluminium or gold are important in applications involving the deflection of these films under various applied forces that can simultaneously measure three orthogonal components of an external magnetic field. In actual application, the movements of the cantilever, made up of aluminium thin film, are accomplished by the Lorentz force acting on direct current (static mode) or alternating electric current (dynamic mode) through the aluminium thin film when the cantilever is placed in an external magnetic field. The orthogonal magnetic field components are able to excite different modes of vibrations of the cantilever. Consequently, the response of the cantilever can be used to detect the magnitude and direction of the external magnetic field.

1.2 Problem statement

The actuation of U-shaped cantilever device based on Lorentz force [14, 16, 19] is still not widely and systematically explored and few studies have been carried out in this field. There is need for more characterization and optimization of the device to extend the range of measurement of magnetic fields. The effect of the different parameters of the U-shaped cantilever such as the effect of its dimensions on the value of the natural frequency (resonant frequency) requires systematic investigation.

The use of industrial CMOS processes for the fabrication of MEMs devices leads to systems that rely on standard IC processes combined with a few additional post processing steps [4, 14, 20, 21]. In the application of CMOS and IC technology for the fabrication of CMOS-integrated sensor systems, three approaches can be distinguished: pre-processing, intermediate processing, and post-processing. These processes lead to high development and overall production costs for a sensor system. The number of

samples of these devices that can be produced by trial and error and simulate is therefore limited. For example F. Keplinger, et al [14] designed and characterized one sample of a U-shaped cantilever with a given dimensions while V. Beroulle, et al [22] investigated two sample devices. This method does not therefore allow systematic characterization of more parameters such as the effect of varying dimensions of the device and effect of damping factor on the performance of the device in terms of its response and sensitivity. However versatile Computer-Aided Design (CAD) programs of MEMS fabrication and FEM simulation software such as ANSYS software [17, 23, 24] and more recently CoventorWare [25] allow for designing and simulating MEMS devices with full control and manipulation of the device dimensions and layers and comprehensively investigate the electrical and physical properties of these layers. Furthermore, different models of the device could be designed, characterized and optimized by trial and error before the actual factory fabrication. This results in considerable reduction in the cost and time for the designer and researchers.

FEM simulation study is therefore very useful for optimizing a device by varying its materials and dimensions before the actual industrial fabrication of the device and selected samples that are suitable for certain application and range of the measurement. In this research, CoventorWare finite element models (FEM) simulation software developed by Coventor Inc 2006 is used to perform finite element simulation (fabrication, design, analysis) of the micromachined U-shaped cantilever. There are very few researches on MEMS using this software, however the results obtained from its application in the last few years has revealed its efficiency [26].

1.3 Objectives of the study

The main aim of this study is to design and simulate a U-shaped cantilever for possible application in 3-D magnetic field detection. The specific objectives of the study are:

- To design and simulate the U-shaped cantilever device.
- To validate the simulation results with mathematical modeling.
- To investigate the effect of cantilever deflection on piezoresistive transducer for application in magnetic field measurement.

1.4 Scope of the project

This study undertakes FEM simulation of a U-shaped cantilever based on CMOS-compatible and bulk micromachining technology. Different samples of the U-shaped cantilever device are simulated and optimized. The effect of the cantilever dimensions such as thickness, width, length of arms, and length of the base on the resonant frequency and sensitivity of the device is investigated. Other important parameters such as the effect of the damping coefficient on the system response are also studied. Furthermore this research identifies the parameters required to achieve a high response and sensitivity of the piezoresistor transducer element implanted in the U-shaped cantilever.

1.5 Thesis outline

- **Chapter-1** presents an introductory part of this thesis and discusses the background of the microcantilever sensors in general. It also outlines U-shaped microcantilever device and its application to magnetic field sensing. The problem statement of this research project is described in this chapter as well. The objectives for the characterization and optimization of this system are dealt with in this chapter.
- **Chapter-2** presents literature review and is divided into two sections, the first section deals with the theoretical background of the system and its basic principle of operation. Other quantities related to the system modeling are also mentioned. And the second part explains the previous work done related to this work.

- **Chapter-3** explained in detail our methodology for investigating the design and characterization the system using CoventorWare (software) to fabricate and simulate different samples of two types (front side block micromachining) and (back side block micromachining) of U-shaped cantilever device. And how to mechanical characterization of the cantilever by applying force (static and dynamic) is also presented in this chapter. Similarly the conversion of the response of the cantilever into an electrical signal for measurement is treated as well. Derivation of the theoretical beam equations to U-shaped cantilever structure is also dealt with in this chapter.
- **Chapter-4** presents and explains the results of the research. First, the comparison between the static mode and dynamic mode for the three different modes of cantilever motion in addressed. Second, the effect of the cantilever dimensions on the resonant frequency and the sensitivity of the cantilever for certain motion of vibration is discussed in detail. These simulation results are validated by the theoretical results obtained by solving the equation of the modes of vibration analytically. The third part of the results concerns with the effect of damping coefficient on cantilever response and the quality factor of vibration. The linear relationship between the force produced by the Lorentz force and the deflection of the cantilever also realized in this section. The last part of the results explains the response of the piezoresistor transducer to convert the deflection of the cantilever to an electrical signal (voltage output). It also compares the sensitivity of the system for the different thicknesses of polysilicon piezoresistor embedded inside the silicon lead.
- **Chapter-5** concludes and summarizes the results of our research work. It also includes the conclusion drawn from our research work as well as comments and recommendations for future work.

Chapter 2

LITERATURE REVIEW

2.1 Force and Pressure Transduction

There are several techniques to measure force and pressures. Very often, the force to be measured is converted into change in length or height of a piece of material, the spring element. The change in dimensions is subsequently measured by a sensor element. Figure 2.1 shows the overall transduction process [27]. Three categories of transduction process are distinguished based on the read out mechanism: piezoresistive (strain gauge or a changing resistivity), capacitive (strain gauge or a changing capacitance) and resonant sensors. Sometimes it is not easy to distinguish the sensor element and the spring element; the sensor itself may also be the spring element and dimensions of the element. For example in piezoelectric and piezoresistive force transducers, the deformed crystal both supports the load and supplies the output signal.

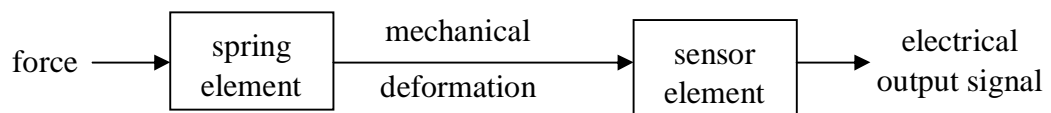


Fig 2-1 Transduction of a force via spring and sensor element into electrical output [27]

The applied force to the sensor either directly produced by some object or due to a physical phenomenon such as Lorentz force.

2.1.1 Principle of Lorentz Force Actuation

Lorentz force is a well known physical phenomenon [19]. This force is generated when a conductor carrying an electrical current is placed in a magnetic field as shown in Figure 2.2.

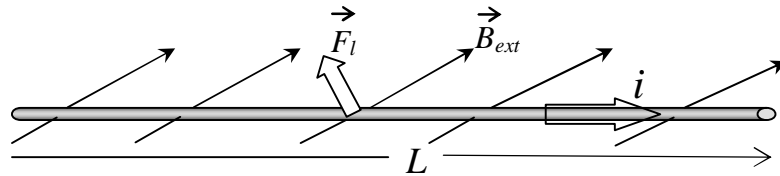


Fig 2-2 A straight wire in a magnetic field that is constant along its length [19]

Each of the moving charges in the wire, which comprise the current, experiences the Lorentz force, and together they can create a macroscopic force on the wire given by the Equation 2.1 for a straight and stationary wire.

$$F_L = iB_{ext}L \sin\theta \quad (2.1)$$

Where F_L is the magnitude of the Lorentz force, i the current in the conductor measured in amperes (A), B_{ext} is the static external magnetic flux density, L is length of the conductor, and $\sin\theta$ is sine of the angle between the magnetic field and the current through the conductor. And when the magnetic field perpendiculars to the current equation 2.1 are becomes:

$$F_L = iB_{ext}L \quad (2.2)$$

Measurement of magnetic flux densities is an important task in many research areas and is commonly associated with physical phenomena such as Lorentz force. The mechanical excitation of a micro machined structure by the Lorentz force can be used as an alternative transducer mechanism. Besides that, such actuators have a fundamental linear dependence between force and electrical current, as well as between force and magnetic

flux density [15]. By adapting the electrical current, the sensor offers a high sensitivity and a large dynamic range enabling measurement of both strong and weak magnetic fields.

2.1.2 Static and Dynamic Response Characteristics in Lorentz Force Actuation

There are two situations that may be considered in the response of a current carrying wire exposed to a static external magnetic field: static and dynamic response characteristics. In the static behavior, a constant Lorentz force acts on a wire carrying a direct current placed in an orthogonal static external magnetic field that results in a fixed displacement in a given direction. For small deflections, the behavior of the wire is governed by the well-known Hook's law that relates the applied force F to the resultant bending by the following relation

$$F = -k .u \quad (2.3)$$

Where u is static displacement in the x -, y - or z -directions and k is the wire stiffness constant that depends on the wire material and dimensions.

On the other hand, the dynamic behavior results from an application of an alternating current in the wire that induces it to vibrate periodically as a result of the Lorentz force induced by a static orthogonal external magnetic field. The response of a vibrating system will depend on the relationship between the frequency of the externally applied periodic force and the natural frequency of the vibration system. For instance if a mass on a spring is moved and then released, it will oscillate at its natural frequency. When a periodic force is applied at this frequency, the amplitude of the response (maximum displacement) will increase dramatically and the highest response (displacement) can be achieved when the cantilever driven at this frequency. This phenomenon is known as resonance and is the fundamental principle applied in all resonating sensors. Figure 2.3 shows frequency response of the cantilever to a periodic force [19, 28].

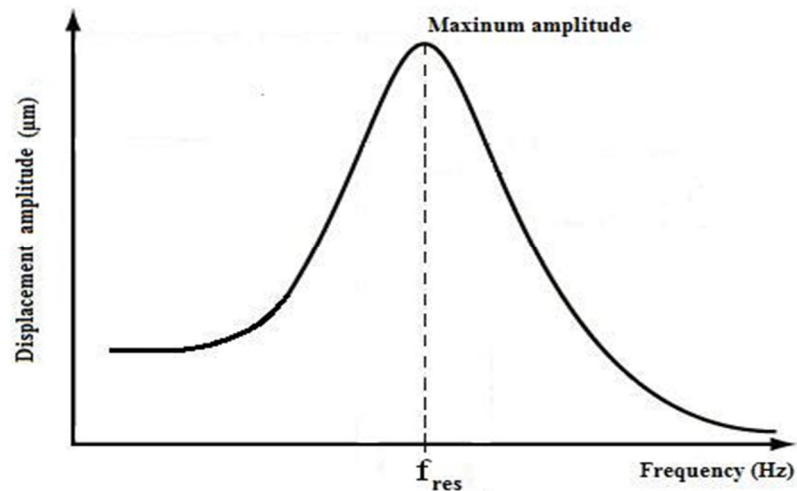


Fig 2-3 Frequency response of a vibrating system [19, 28]

In order to determine the resonant frequency, the resonator has to be brought into vibration and the vibration has to be detected. Usually an oscillator circuit is realized where the resonator is the frequency determining element. The value of this frequency is dependent on physical properties of the material such as density, stiffness and dimensions (thickness, width, and length) of the beam for a certain mode of vibration [19, 28, 29, 30]. A description of the behaviour of a general simple dynamic problem can be done by modeling it as a mass oscillating on a spring of stiffness k and damping factor D [21, 22] as shown in Figure 2.4.

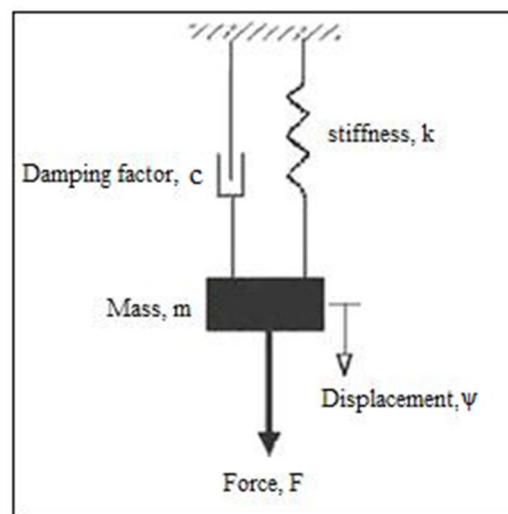


Fig 2-4 Mass-Spring System [21, 22]

The internal force in the spring is given by $k\psi$ and so its dynamic equation of motion is given by [31, 32]:

$$m\psi'' = -k\psi - c\psi' - F \quad (2.4)$$

where ψ is the displacement, m the mass, k the spring constant measured in (N/m) and c the damping factor. If the periodic force is considered sinusoidal, that is $F = F_0 \sin(\omega t)$, the solution of equation 2.5 gives the maximum displacement amplitude ψ_{\max} at the resonant frequency as

$$\psi_{\max} = \frac{F_0}{c \left(\frac{k}{m} - \left(\frac{c}{2m} \right)^2 \right)^{\frac{1}{2}}} \quad (2.5)$$

where F_0 is the amplitude of the applied force. For low-damped systems with forced oscillation, the resonance angular frequency is given by

$$\omega_0 = \sqrt{\frac{k}{m}} \quad (2.6)$$

and the actual frequency calculated from

$$f_0 = \frac{1}{2\pi} \sqrt{\frac{k}{m}} \quad (2.7)$$

2.1.3 Linearity property of a vibrating system

Generally, linearity is a desirable characteristic of all systems where an output responds to an input. The system is said to be a linear system when the response of system to inputs is given simply by the sum of the responses due to individual input. In addition, if input is multiplied by a common constant factor, the resulting response is multiplied by the same factor. The motion produced by the Lorentz force as the input of a vibrating system and the deflection in the system as the output response is called Linear Electromagnetic Actuation [33]. This is because for measurement over a given range for

small deflections, the displacement of the wire is a linear function of the Lorentz force [6, 34]. The sensitivity for this given combination of magnetic field strength B and spring constant k is measured in $\mu\text{m/mN}$. The direct proportionality is an advantage for designing a simple signal conditioning circuit.

2.1.4 Q -factor

Mechanical quality factor (Q) is an important parameter in the study of vibrating systems. It is a measure of the energy losses of the resonator or, in other words, a measure of mechanical damping. Q -factor is defined as the ratio between the total energy stored on the vibration, U_{stored} , and the energy loss (dissipated) per cycle, U_{diss}

$$Q = \frac{U_{\text{stored}}}{U_{\text{diss}}} \quad (2.8)$$

Low energy losses imply a high Q -factor. The Q -factor cannot be determined directly, but instead can be deduced from the response characteristics of the resonator. One common method of determining Q is from the steady-state frequency plot of a resonator excited by a periodic force with constant amplitude [4] and Q is given by the equation:

$$Q = f_{\text{res}} / \Delta f_{\text{3dB}} \quad (2.9)$$

where f_{res} is the resonant frequency of a given mode, Δf_{3dB} is 3dB band width of the frequency that is at $\frac{1}{\sqrt{2}}$ of maximum amplitude [35]. Figure 2.5 shows the frequency response of a U-shaped cantilever and how to determination the band wide at 3dB of the amplitude.

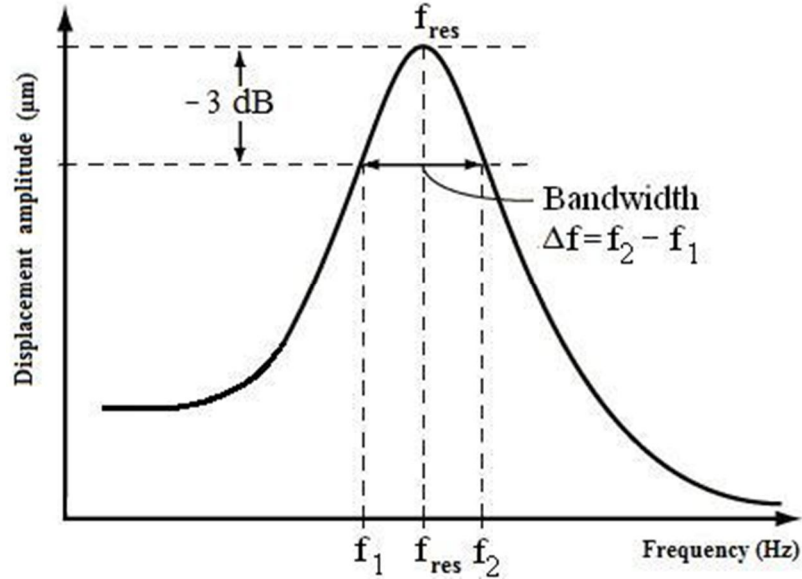


Fig 2-5 Frequency response of the mass and band wide at -3dB of the amplitude [35]

In the two methods of actuation of a mechanical structure discussed in section 2.1.2, the static method uses a calibrated dc current. The displacement value can be converted in a measurement circuit to indicate the voltage level at the output that is directly proportional to the magnetic induction. The ratio between this output voltage and the magnetic induction is defined as the static sensitivity $S_{(stat)}$ [36]. The other actuation method is realized when an alternating current is used. The amplitude of the output signal is then modulated by the value of the static (or low frequency) magnetic induction. The ratio between the output amplitude and the magnetic induction then represents the sensitivity. The best sensitivity is obtained with an actuation current frequency equal to the resonance frequency (f_{res}) of the mechanical structure. The ratio between the resonant sensitivity, $S_{(res)}$, and $S_{(stat)}$ is a measure of the Q value that is:

$$Q = f_{res} / \Delta f_{-3dB} = S_{(res)} / S_{(stat)} \quad (2.10)$$

A high Q -factor means a sharp resonance peak and has the advantages of low energy required to maintain the vibration, minimal effect of the electrical circuitry on oscillation and low sensitivity to mechanical disturbances.

2.1.5 Damping coefficient

If an undamped structure is allowed to vibrate freely, the magnitude of the oscillation is constant. In reality, however, energy is dissipated by the structure's motion, and the magnitude of the oscillation decreases under the effect of the damping and the motion environment. This energy dissipation is known as damping. Damping is usually assumed to be viscous or proportional to velocity. And the Q -factor of the vibration is strongly inversely proportional to the damping. Therefore the damping factor is an important parameter to consider when performing a harmonic analysis. The dynamic equilibrium equation of the natural oscillation of a vibrating damped mechanical structure is [37]

$$m\psi'' + c\psi' + k\psi = 0 \quad (2.11)$$

where m is the mass, c the damping, k the stiffness, and ψ the modal amplitude. The solution is of the form:

$$\psi = A \exp \beta t \quad (2.12)$$

where A is constant and β is function of c .

Damping coefficient also can be expressed mathematically as a fraction of the critical damping for each eigenmode and the dimensional damping c correlated with the non-dimensional damping ratio d as [34]

$$d = \frac{c}{c_{\text{crit}}} \quad (2.13)$$

where the critical damping is given by

$$c_{\text{crit}} = 2\sqrt{mk} \quad (2.14)$$

2.1.6 Piezoresistive transducers

This section discusses the principles of the transformation of a deformation in a micro cantilever into an electrical output and the electronic interface circuits needed for such purposes. The transfer of a deformation in a mechanical construction by an external load to an electrical signal is called transduction. The most important mechanisms for transduction of mechanical microsensors use the following effects: piezoresistivity, the dependency of the capacitance on the geometric arrangement of conductor, optical resonance and optical interferometry [17].

Since Smith documented the piezoresistive effect in silicon in 1945. Piezoresistive MEMS devices have been implemented in a variety of sensing application, including pressure, acceleration, force and displacement sensing [38]. Piezoresistivity is a material property where the bulk resistivity of a material is influenced by the mechanical stress applied to it. Silicon, especially in the monocrystalline form, exhibits a high piezoresistivity [39, 40, 41]. Combined with excellent mechanical properties, this makes it a preferable material for mechanical sensors. Whereas metals show a change in resistance due to mechanical stress or strain mainly because of geometric effects, the piezoresistive effect in silicon results from a change in resistivity and exhibits significantly higher sensitivities. Because of this and the easy fabrication of resistors in standard IC fabrication, piezoresistive detection is a widely applied sensing principle for mechanical microstructures for measurements using an electrical signal. The piezoresistive effect in silicon depends strongly on the crystal orientation, doping type, and concentration. Piezoresistive property of polysilicon is used as piezoresistor transducer in this research. The general relation between the relative changes of a resistance R , which for polysilicon is equal to the change in resistivity ρ , is given by [17]:

$$\frac{dR}{R} = \frac{d\rho}{\rho} \quad (2.15)$$

The electrical resistance of a piece of any material depends on its dimensions, shape and the specific resistance ρ . For a rod with cross-section A and length l the resistance R (Ω) is given by

$$R = \frac{\rho l}{A} \quad (2.16)$$

Therefore the change of the resistance of a material (ΔR) is directly proportional to the change in its resistivity ($\Delta\rho$). The simulation software will realize the results in percentage values of the unstressed resistance value of the piezoresistor

$$\Delta R\% = \frac{(\textit{stressed} - \textit{unstressed})}{\textit{unstressed}} \% \quad (2.17)$$

where $\Delta R\%$ is percent change in resistance.

Using equation 2.17, the value of the change of the resistance (in Ω) can be obtained by

$$\Delta R_p = \frac{\Delta R\%}{100} \times R \quad (2.18)$$

where R is the original (unstressed) value of the resistance of the piezoresistive material.

Many solid state sensors for mechanical signals are based on the piezoresistive effect. The change in resistivity of a piezoresistive material subject to a mechanical deformation is used to measure many physical quantities such as pressure, force, and acceleration. The advantages of piezoresistor technology implementation in circuits include low cost fabrication opportunity, mature processing technology, readout circuitry can either be on-chip or discrete, various sensitivities can be obtained, and different pressure levels can be achieved according to the application [26]. Piezoresistive pressure sensors are one of the very-first products of MEMS technology. Those products are widely used in automotive applications such as air pressure detection, in biomedical applications such as blood pressure measurement and in household appliance such as washing machines, dishwashers and vacuum cleaners.

The sensitivity, S , of all magnetic field sensors is a ratio between the voltage output V_{out} of the measurement circuit and the magnetic flux density B_{ext} detected and is given by

$$S = \frac{V_{out}}{B_{ext}} \quad (2.19)$$

There are two sensitivities of the system: static sensitivity S_{stat} for the static mode of the cantilever and resonant sensitivity S_{res} for the dynamic mode at the resonant frequency of vibration. The maximum deflection in the static mode is too small if the output voltage and sensitivity compared to that in dynamic resonance response.

2.2 MEMS and CMOS-compatible micromachining of cantilever structures

Microelectromechanical Systems (MEMS) is a logical expansion of the silicon processes used to fabricate integrated circuits. These processes were originally developed to build microelectronic and micromechanical devices having structures capable of motion in a microscopic scale. MEMS devices are built in much the same way as a silicon integrated circuit. Various films including polysilicon, silicon nitride, silicon dioxide, aluminum and gold are deposited and patterned to produce complicated, multilayer three-dimensional structures. However, the major difference is the release step at the end. In a MEMS device, some of the layers materials are removed using a selective etch, leaving a device with moveable elements. Complementary metal–oxide–semiconductor (CMOS) based MEMS manufacturing technology employs standard CMOS processes to fabricate microstructures within the metal–dielectric layers that are deposited during the standard CMOS processing flow, resulting in mechanical structures that are just microns away from the analog and digital electronics.

CMOS is a well-known and the dominant semiconductor technology. CMOS-chips generally consist of a substrate, the transistor components, the metal layers and a passivation layer [20]. The substrate is a silicon wafer, the thickness of which depends on the wafer size. Some metal such as aluminum or copper are used to wire the electric

component. Intermetal oxide (Si-oxide) layers are used as electrical insulator between the different metal layers. Finally, silicon nitride, silicon oxinitride, or silicon oxide layers passivate the device and protect the electronics. The overall CMOS device is fabricated in a defined sequence of material deposition, doping, lithography and etching steps.

Micromachining structures such as membranes and cantilevers are widely used in microsensors fabrication. The micromachining techniques are categorized into surface micromachining and bulk micromachining processes.

2.2.1 Surface Micromachining

Surface micromachining encompasses a number of techniques to create microstructures from thin films previously deposited onto a substrate and is based on a sacrificial-layer method [20]. In surface micromachining the features are built up layer by layer on the surface of substrate and in contrast to bulk micromachining, surface micromachining leaves the substrate intact [42]. A sacrificial layer is deposited and patterned on a substrate. After that, a structural thin film, in most cases polysilicon, is deposited and patterned, which will perform the mechanical or electrical functions in the device. A selective etchant then removes exclusively the sacrificial-layer material. The thickness of the sacrificial layer determines the distance of the structural parts from substrate surface as shown in Figure 2.6 (a). Clamped beams and microbridges can be fabricated this way.

2.2.2 Bulk Micromachining

Unlike surface micromachining, bulk micromachining defines structures by selectively etching inside a substrate. It is one approach to develop the functionality of IC-based devices by micromachining the bulk substrate, which consists of silicon. Bulk micromachining techniques can be classified into two structure geometries isotropic and anisotropic etching techniques as shown Figure 2.6 (b). The two etching techniques that can be used are wet etching which typically uses liquid solvents such as potassium hydroxide (KOH) or tetramethylammonium hydroxide (TMAH) and dry (gaseous)

etching that is used to dissolve silicon which has been left exposed by the photolithography masking step. The etching can be implemented by two methods: Back-side or Front-side etching. More details on CMOS and micromachining techniques can be found in dedicated references on micro systems technology [42, 43, 44].

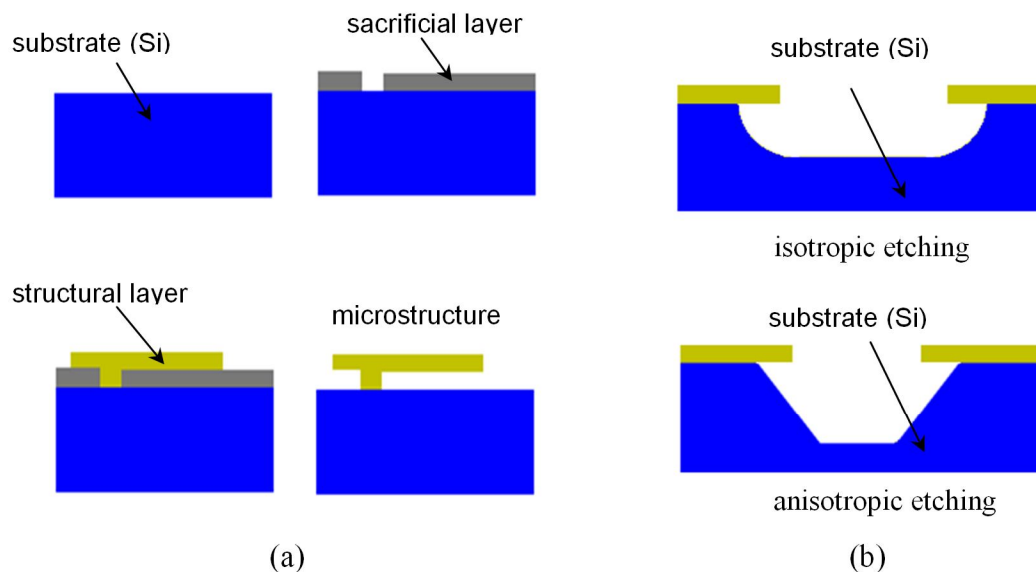


Fig 2-6 Micromachining techniques: (a) Surface micromachining steps and (b) Bulk micromachining.

2.3 Finite Element Method (FEM) simulators

Finite element method (FEM) is a powerful technique originally developed for numerical solution of complex problems in structural mechanics, on the other word FEM is numerical technique for finding approximate solutions of partial differential equations as well as of integral equations. And it remains the method of choice for complex systems. In the FEM, the structural system is modeled by a set of appropriate finite elements interconnected at points called nodes. Elements may have physical properties such as thickness, coefficient of thermal expansion, density, Young's modulus, shear modulus and Poisson's ratio.

Most commonly used modeling approach for MEMS devices is based on the use of finite elements method (FEM). Numerous finite element programmes have been developed which are able to solve linear, non linear, static, dynamic, elastic, plastic, steady state, transient, and other problems, during the last years. A given technical problem must be expressed in physical terms so that it can be formulated mathematically by means modelling. The model should reflect the reality as exactly as possible. However, it should also be as simple as possible. Furthermore, the model must be described in such a way that it can be implemented in computers. These are used whenever analytical solutions are difficult to achieve such as for MEMS with complex geometry or multiple actuation modes. Such modes, coupled with an FEM simulator, provide accurate simulation results for various physical domains such as mechanical, thermal, or magnetic [5].

FEM simulators are still not able to easily prepare the system parts and couple it with mixed signal electrical simulators. Moreover, a long simulation time is consumed for the high accuracy that is unwanted particularly during the optimization process. FEM simulators are efficient and accurate at the device level, whereas other solutions are necessary at the circuit or system level. It then becomes necessary to deal with analytical models that may be integrated in a microelectronic design flow in order to simulate electromechanical behaviors. Such asset of equations may result from finite-element parametric analysis and interpolation [13, 23]. This is often the only solution to handle complex systems. For simple structures, the modeling can be conducted analytically by using well-established results from the concerned scientific fields. In this case physical parameters such as technological constants or device dimensions are directly part of equations, leading to a faster, intuitive optimization method [45]. An example being successfully applied with significant contribution of widely used simulation software such as ANSYS 6.0 and CoventorWare are already contributing to the comprehensive understanding of device behavior and performance.

2.4 Review of Related Studies

In this section studies that are directly related to U-shaped cantilever structure is reviewed. The review is subdivided into studies in which actual devices were fabricated and simulation based research.

2.4.1 Review of fabrication and Characterization MEMS based Cantilevers

The principle of the Lorentz force is used for actuation a MEMS based U-shaped cantilever of flexible thin-film aluminum reported by Raphael H, et al [15] and [34]. Conventional semiconductor fabrication technology (surface micromachining) is used to produce the actuators. To fabricate one sample on 2-inch-diameter silicon wafer, 3 thin-film layers are deposited by sputtering. The 1 μm SiO_2 layer provides insulation and the 2 μm polysilicon layer serves as a sacrificial layer for releasing the Aluminum structure from the Si wafer. The displacement amplitude as a function of frequency was investigated. Maximum displacement of about 50 μm at the resonant frequency is obtained as compared 20 μm for the static mode. The relation between the current and the displacement has been measured with a laser displacement meter. A natural frequency of 2.65 kHz and a quality factor Q of 2.5 are reported. Equations (2.5), (2.6), and (2.7) are used for the dynamic modeling and a theoretical resonant frequency of 2.6 kHz is obtained that is close to the experimental results. The paper also demonstrated the linearity relationship between the displacement of the cantilever and the applied force. However, the paper considers only testing and characterization of the structure for vibrations due to Lorentz force in one direction.

N. Dumas et al have also published three papers on the application of the U-shaped cantilever [10, 22, 46]. Figure 2.7 shows SEM micrograph of a fabricated U-shaped cantilever device in the first paper [22]. Front-Side Bulk Micromachining (FSBM) was used to fabrication the device. FSBM is preferable over the Back-Side Bulk Micromachining (BSBM) due to its self alignment capability and thus lowering the cost of the post process [47, 48]. Figure 2.7 shows two samples of the device that have been

designed and tested. Piezoresistive technique using Wheatstone bridge circuit was used for the measurement of the output voltage. The graph of the frequency response indicates a value of the resonant frequency of about 22.5 kHz and a maximum output voltage of 0.9 Volt.

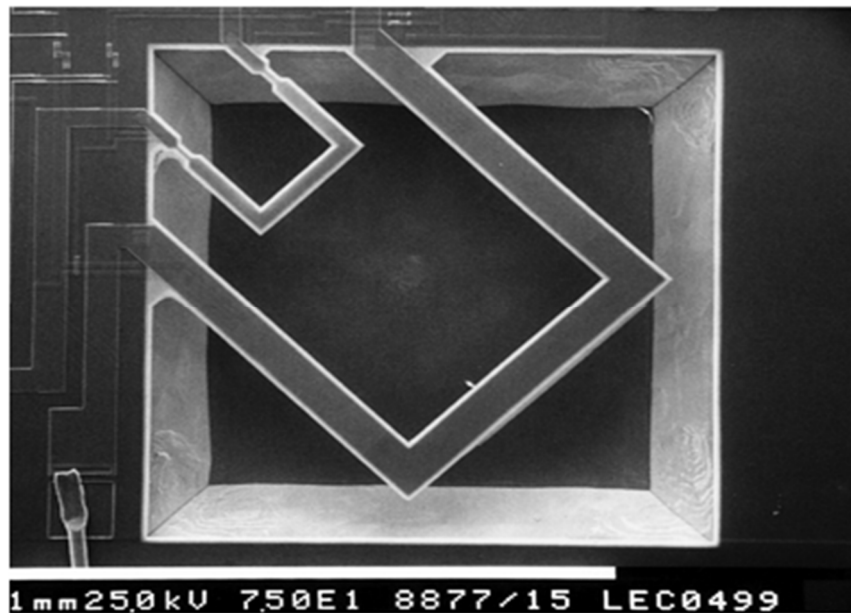


Fig 2-7 SEM photograph of two U-shape cantilevers [22]

A second paper published by the same author [46], compared between the static and resonant sensitivity of the cantilever sensor. The output voltage of the static measurement is found to be about 14 mV/T while it is 350 mV_{rms}/T at the resonant frequency. Another paper written by these authors [10] focuses on the modeling equations of the motion and Q-factor of the system and optimized the circuit for measurement. The testing and characterization in these three papers considered only Lorentz force actuation of the cantilever for one mode of vibration.

Figure 2.8 shows typically schematic representation of the behavior of the U-shaped cantilever beam in these papers when the Lorentz force is acting on the base of the cantilever.

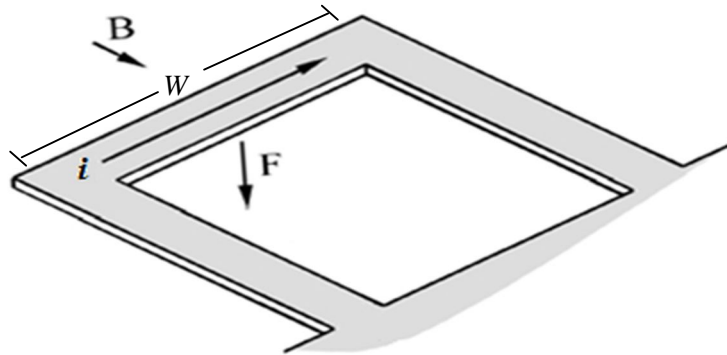


Fig 2-8 Principle of Lorentz force actuation of the U-shaped cantilever [15, 46]

An electrical current (i) pass through the beam by means of aluminum planar coils. Lorentz force (F) results from the interaction between an external magnetic field (B) and current (i). This force depends on the width (W_c) of the cantilever: $F = iW_cB$. The author showed how the Lorentz force law can be used to calculate the applied force that generates the vibration. A resonant frequency of 22.5 kHz and a quality factor of 114 were measured, while the resonant sensitivity obtained is about $0.85 \text{ V}_{\text{rms}}/\text{T}$ at damping factor of $7.83 \times 10^{-7} \text{ N s m}^{-1}$. The paper also focuses on the optimization of the electrical measurement circuit.

F. Keplinger, et al [14] carried out simultaneous measurement of two magnetic field components using a U-Shaped cantilever device. The U-shaped cantilever was used to detect the external magnetic field from two directions. Vibration in one direction was called the symmetric mode and in the other antisymmetric mode as shown in Figure 2.9 (a) and (b). The paper described the shape of the two modes of vibration and presents the value of the resonant frequency for each mode.

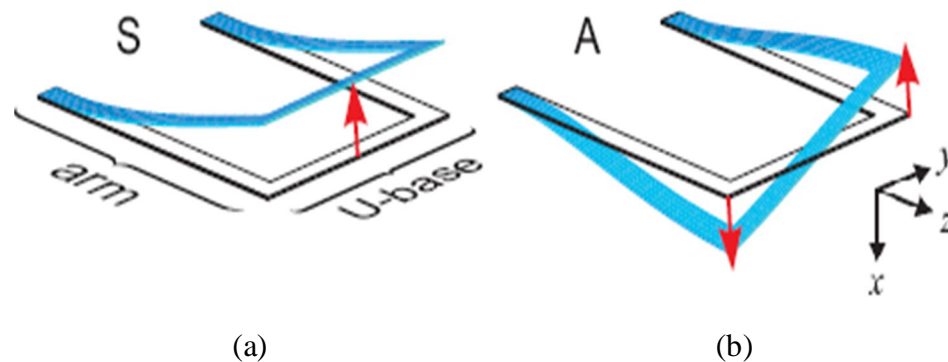


Fig 2-9 Visualization of (a) symmetric and (b) antisymmetric vibration modes [14]

The U-shaped cantilever device was fabricated using Back Side Bulk Micromachining (BSBM) with a length of $1500\ \mu\text{m}$, base of $1100\ \mu\text{m}$, a beam width of $100\ \mu\text{m}$, and a thickness of $15\ \mu\text{m}$. It carries a $0.5\ \mu\text{m}$ thick and $60\ \mu\text{m}$ wide gold (Au) lead. Optical readout is used for measurements. The resonant frequency value is about $5.8\ \text{kHz}$ for symmetric (mode-1), while it is $16\ \text{kHz}$ for the antisymmetric. In another paper [45] the authors focused on the mathematical equations of the different modes of vibration of the U-shaped cantilever. Making some assumptions, the classical Euler-Bernoulli beam dynamics theory is adopted to analyze the problem of the flexural deflections of the cantilever.

Z. Djuri, et al [6] designed and fabricated cantilevers with “U” and “V” shapes. A homogenous composition of the microcantilever made of a conductive material (gold) is chosen in order to avoid the adverse bimaterial effect. Preliminary experimental results obtained by measuring interaction between a permanent magnet and current carrying cantilever are given (Lorentz force actuator). This work realized the linearity relationship between the Lorentz forces generated (in nN) and the current through the cantilever (in mA), and also linearity relationship between the cantilever displacement (in nm) and the force obtained by using permanent magnet and changing the current through the cantilever.

In another experimental work [31], a piezoresistor transducer and the conditioning circuit (typically a Wheatstone bridge) was designed and optimized to reject power supply noise. Figure 2.10 shows the bulk device with piezoresistor embedded inside the cantilever. FSBM wet anisotropic etching of silicon is used to release the U-shaped structure. This paper discussed the electrical measurement circuit in detail, rather than the characterization of the cantilever and vibration modes.

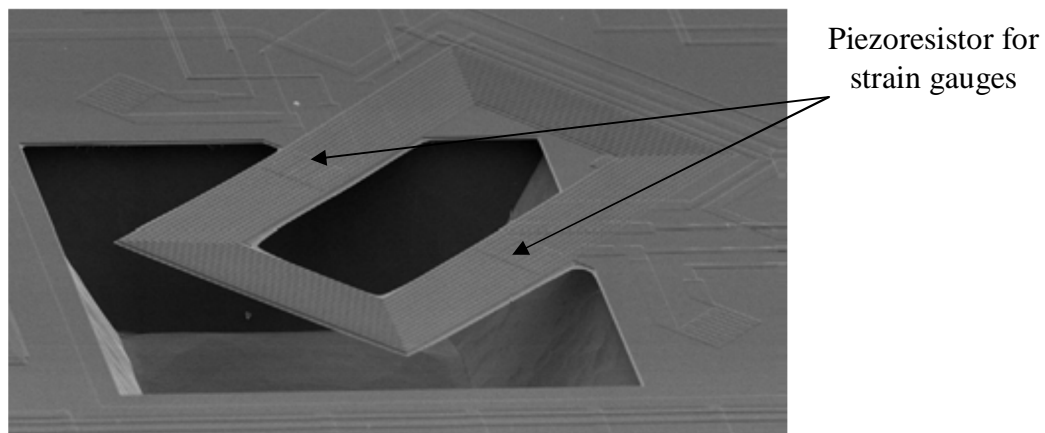


Fig 2-10 The piezoresistive magnetic field sensor [31]

Jeng-Nan Hung et al [32] investigated the effect of cantilever dimensions by varying one and keep the others constant for single rectangular polysilicon cantilever beam. Just the effect of the Length and width of the cantilever is characterized in this work. Figure 2.11 shows the samples of the cantilever of different lengths fabricated.

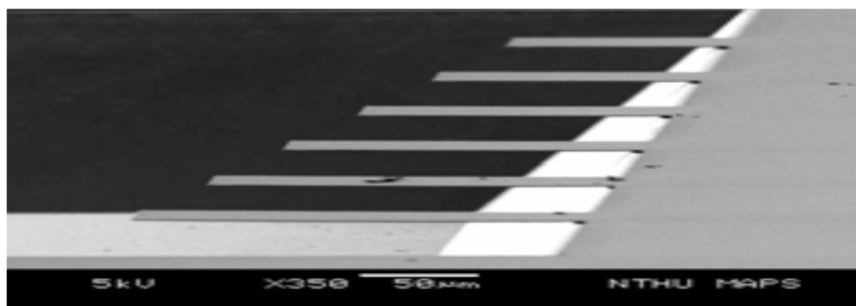


Fig 2-11 SEM photograph of the polysilicon specimens [32]

2.4.2 Simulation Studies on a MEMS Devices base Cantilever

A few simulation studies in this area have been carried out. In one instance, ANSYS 6.0 software was used by Franz K, et al [24] to simulate a U-shaped cantilever with the geometrical dimensions of the cantilever of length of arms of $1100\ \mu\text{m}$, overall base of $1000\ \mu\text{m}$, beam width of $100\ \mu\text{m}$ and beam thickness of $10\ \mu\text{m}$. Estimation of the sensor behaviour and the model optimization was performed on the device. Static analysis was used to determine the displacement due to the loads. Deflections of $13\ \mu\text{m}$ in z -direction was obtained under load by the Lorentz force of $80\ \mu\text{N}$ calculated by taking the external magnetic field in the x -direction to be $40\ \text{T}$ and the current through the cantilever to be $2\ \text{mA}$. Figure 2.12 shows the mode for the estimation and optimization was conducted. The conclusion it is suggested that utilizing the Lorentz force on a micro machined Si cantilever with thin film conductors provides a promising sensor principle for measuring high quasistationary magnetic fields.

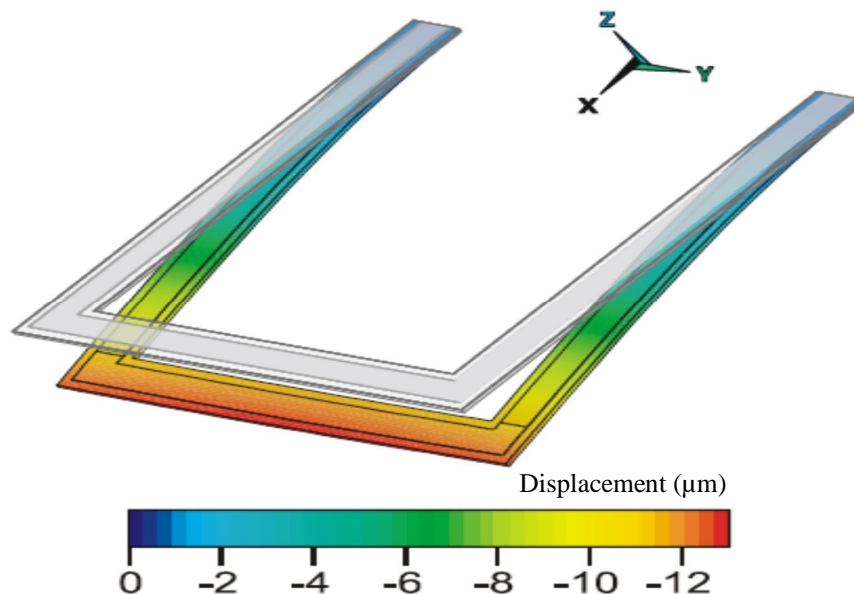


Fig 2-12 Simulation result of the cantilever under load by the Lorentz force [24]

In another recent research [26], the researchers used CoventorWare to design and characterize a MEMS piezoresistive pressure sensor for ocean depth measurements. The designer used BSBM of Si of dimensions $1500\mu\text{m}\times 1500\mu\text{m}$, and applied pressure (in psi) to realize the output response of the Wheatstone bridge (in mV). They also compared experimental work with the simulation results. Very small error ratio between them was observed, indicating the effectiveness of the software in modeling the behavior accurately.

Chapter 3

METHODOLOGY

3.1 U-shape cantilever device structure

Figure 3.1 shows the metal line of a U-shape cantilever consisting of two parallel cantilever beams (arms) that are connected at their free extremity by a linking arm that will be called the base in this thesis. The cantilever is anchored at the contact pads. Figure 3.2 shows schematic 3-D structure of the device layers, that consist of the Al metal line, the silicon oxide (SiO_2) insulating layer to which it is anchored and silicon (Si) substrate, while Figure 3.3 shows the cross sectional view of the structure.

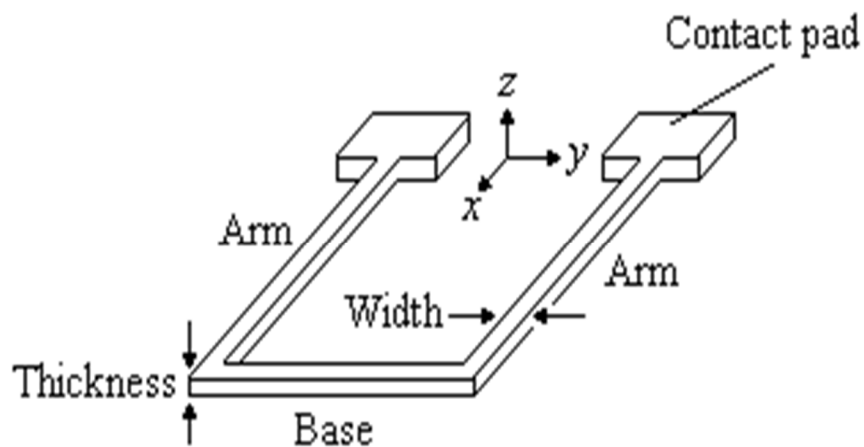


Fig 3-1 Schematic diagram of the metal U-shaped cantilever

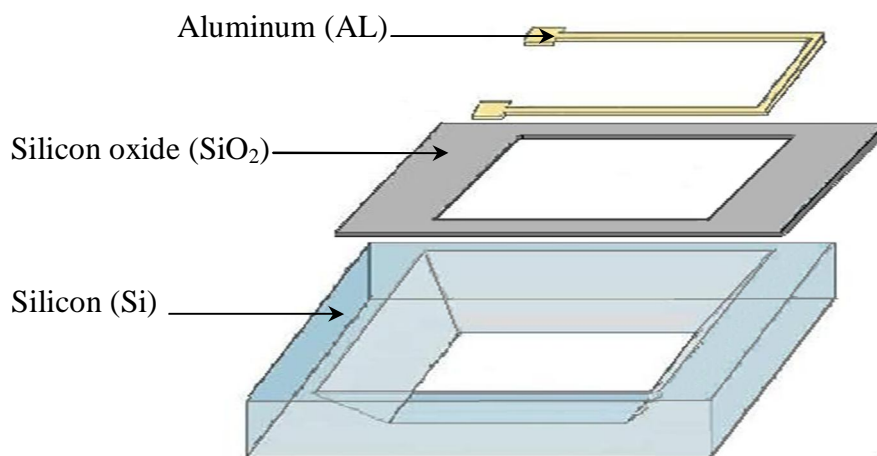


Fig 3-2 Schematic drawing of the layers of micro machined U-shaped cantilever device

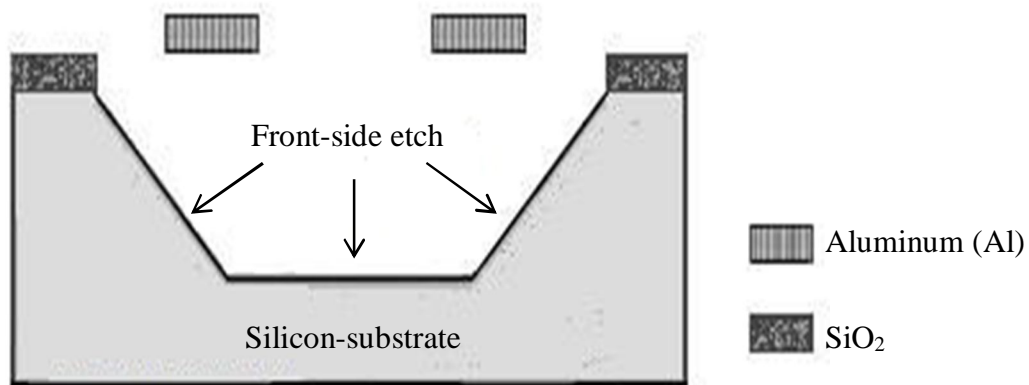
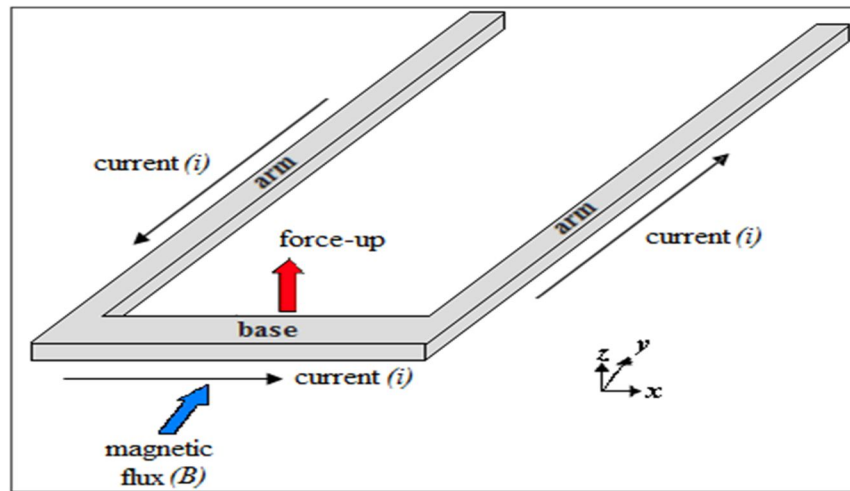


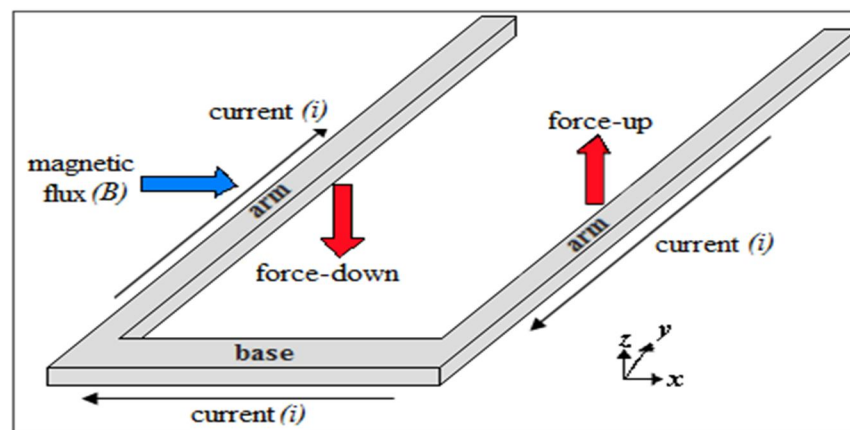
Fig 3-3 Cross sectional view of a U-shaped cantilever device

3.2 Lorentz force for actuation of the U-shaped cantilever

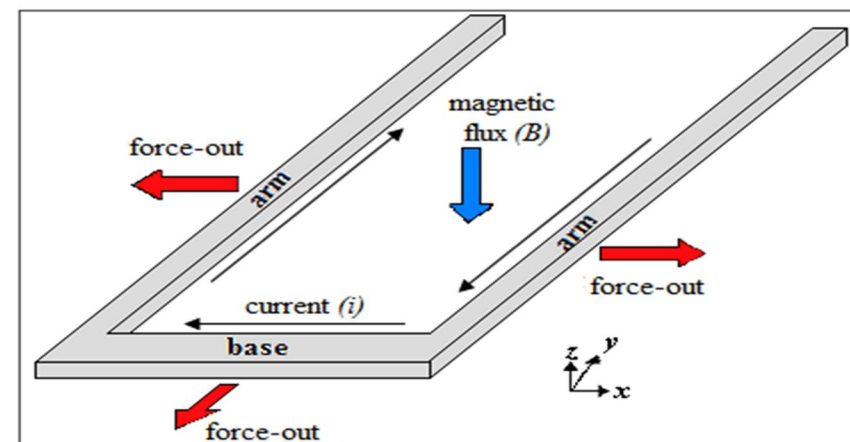
Three modes of motion generated by the Lorentz force will be considered in our work based on the direction (x , y , or z) of the external magnetic field and direction of the current through the parts of the cantilever. Figure 3.4 shows the cantilever motion when the external magnetic field and the current are perpendicular to each other. Mode 1 is characterized by the up and down vibrations of the cantilever base in the z -direction. The external magnetic field is perpendicular to the base of the cantilever and parallel or antiparallel with the current in the arms and therefore no force acts on the arms. On the other hand, when the external magnetic field is parallel to the base and perpendicular to the arms, the Lorentz force will act on the arms of the U-shaped cantilever making one of the arms to move up and the other down and vice versa while no Lorentz force acts on the base and this is called mode 2 and represents the antisymmetric up and down vibrations of the arms moving in opposite directions in the z -direction. In the third mode (mode 3) the external magnetic field is perpendicular to the current in all parts of the cantilever and the direction of the force on the base and arms will be either inwards or outwards with the arms vibrating in the y -direction while the base vibrates in the x -direction but are all in phase with each other. These three modes of vibrations provide a possibility for the measurement of the magnitude and direction of magnetic fields in all three directions (3-D).



(a) Mode-1



(b) Mode-2



(c) Mode-3

Fig 3-4 The three modes of vibration of a U-shaped cantilever

3.3 Simulation and modeling of the device

The methodology of this research consists of two sections: first simulation of the device and second justification of the results by mathematical modeling.

3.3.1 Device simulation software

CoventorWare simulation software from Coventore Inc [25] is used in this study to perform finite element simulation that offers new possibilities regarding the fabrication, design and analysis of the micromachined U-shaped cantilever. The software is a versatile tool which can be used to quickly build models for microelectromechanical system (MEMS) devices with full control on device parameters.

The major components of CoventorWare are accessed from the Function Manager window as shown in Figure 3.5. From the upper portion of the Function Manager window, you can access the Material Properties Database and the Process Editor. It has navigation tabs for accessing the Architect, Designer, and Analyzer functions. It also contains menu options for file management, help options, and several tools. CoventorWare ANALYZER is composed of numerous numerical approaches to solving the partial differential equations of mathematical physics. Chief among these are the 3-D finite-element method (FEM) of MemMech and the 3-D boundary-element method (BEM) of MemElectro. CoventorWare supports both system-level and physical design approaches.

The system-level approach involves use of behavioral model libraries with a high-speed system simulator. The system-level MEMS design can be used to generate a 2-D layout for physical level verification. The physical approach starts with a 2-D layout and involves building a 3-D model, generating a mesh, and simulating using FEM or BEM solvers. Custom reduced-order macromodels can be extracted for use in system simulations. Finally, the verified 2-D layout can be transferred to a foundry for

fabrication. CoventorWare has numerous options, including design libraries and a variety of 3-D physics solvers. Various entry and exit points allow import and export of files from and to other third-party software.

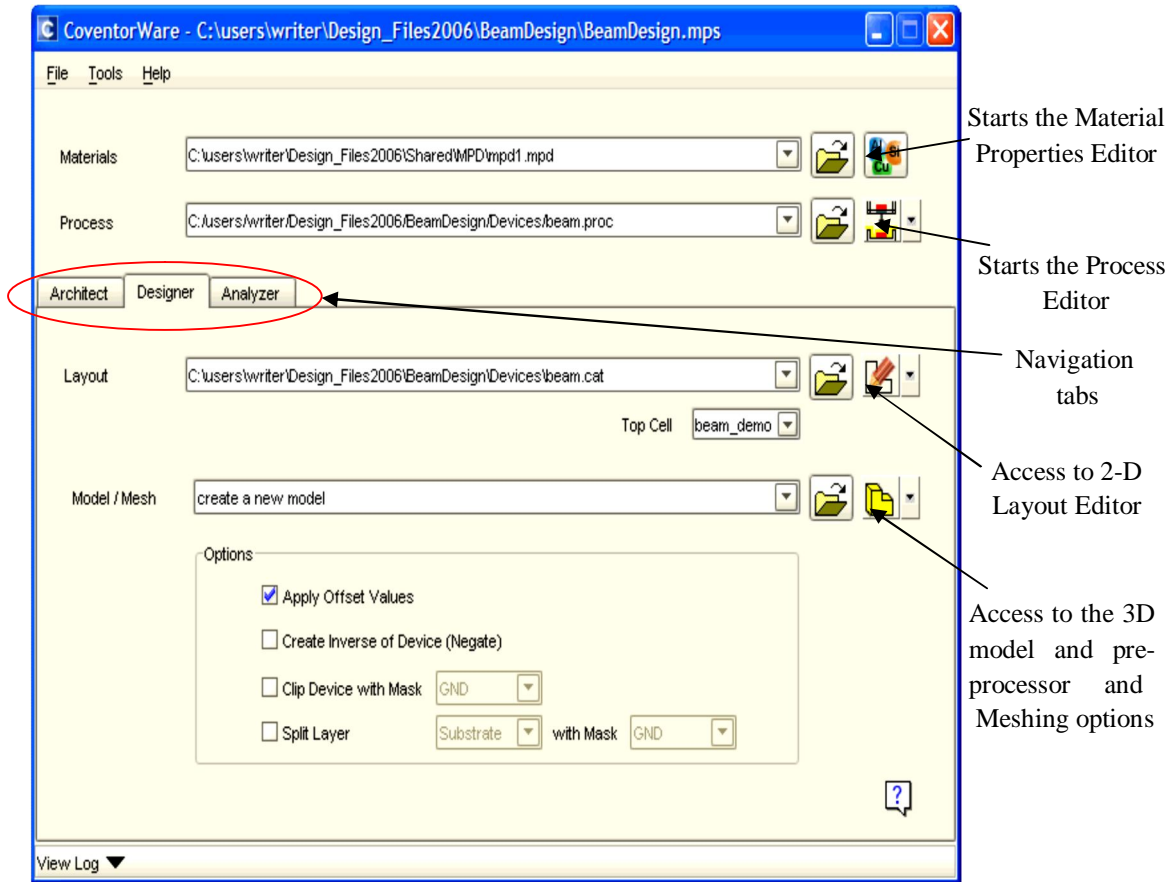


Fig 3-5 The main window of the Coventor soft ware

Figure 3.6 shows the flow chart of the methodology followed in CoventorWare to design and characterize the U-shaped cantilever. The simulation work of the research methodology is presented and summarized in this flowchart as detailed in the following sections.

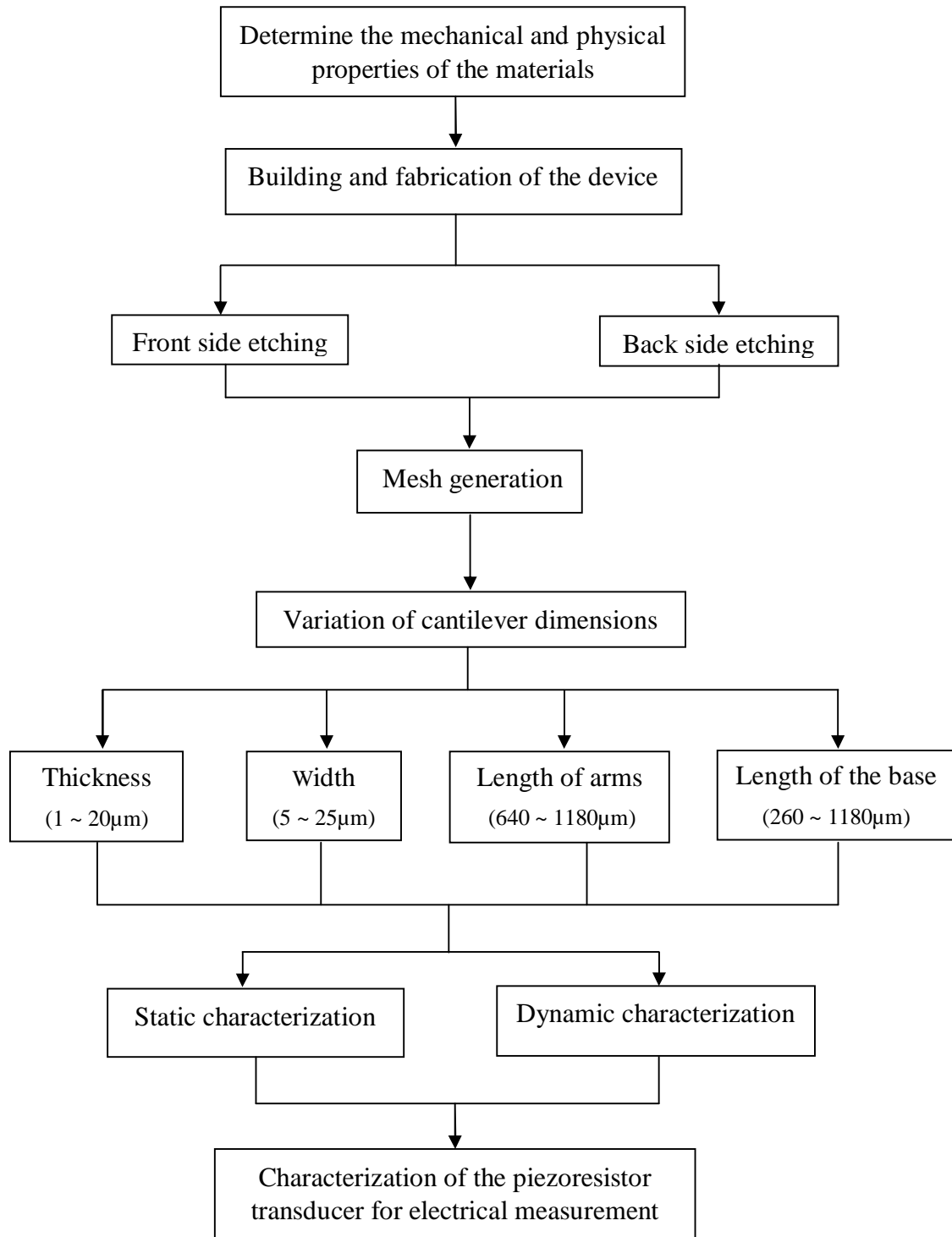


Fig 3-6 Flow chart of the methodology in CoventorWare

3.3.2 Materials selection

In CoventorWare environment, the designer tab is used to fabricate the U-shaped cantilever. Conventional CMOS fabrication steps and bulk micromachining is used. The first steps is material selection and determination of the physical and mechanical properties of interest such as Young's modulus of elasticity, density and electrical conductivity of the materials used in the design as shown in Material Properties Database (MPD) in figure 3.7.

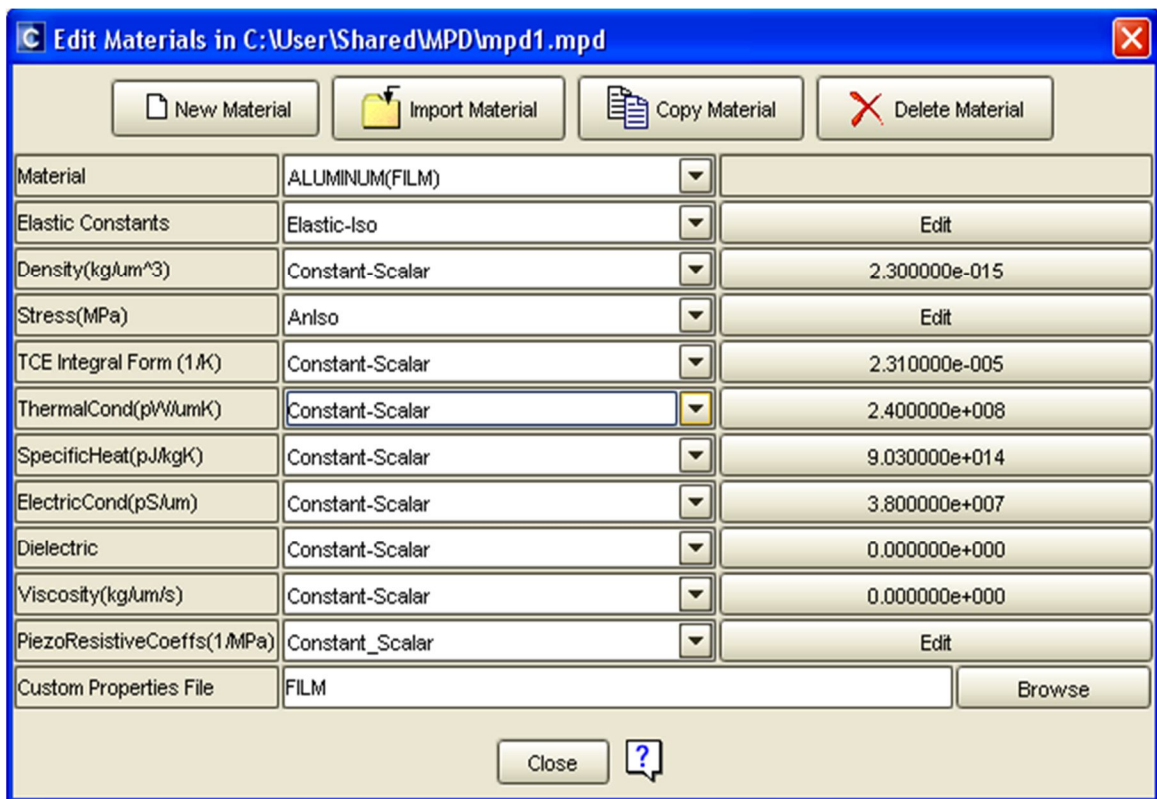


Fig 3-7 Material Properties Database (MPD) window in CoventorWare

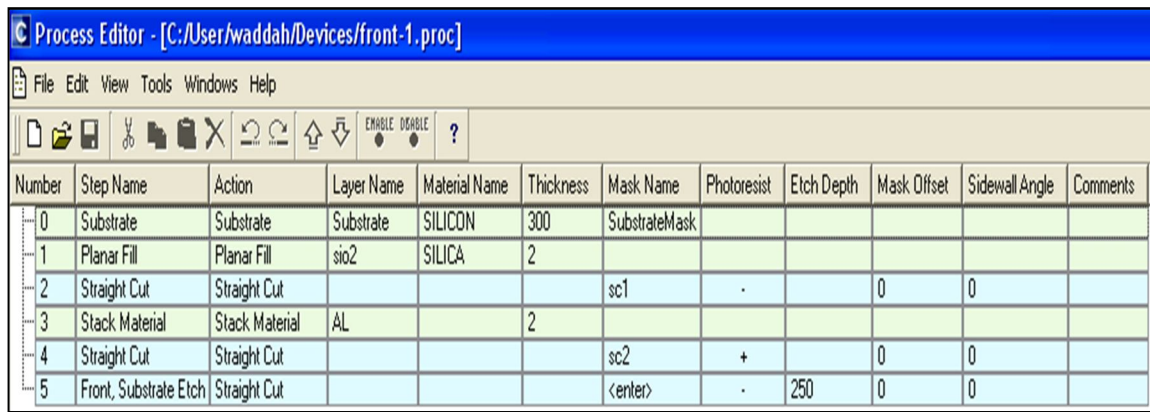
The Materials field specifies a database file that stores all the material properties used by the solvers during the computation phase. This database file has a *.mpd* extension. A generic MPD file is included with the installation and is placed in each user's *Shared\mpd* directory. This step is repeated for all materials used in fabrication which is shown in table 3.1.

Table 3-1 Properties of materials used in the software

Material	Silicon(Si)	Silicon oxide (SiO ₂)	Aluminum (Al)
Thickness (μm)	300	2	5
Function of layer	Substrate	Insulation	Conductor
Young's modulus (Gpa)	140	70	69
Density(g/cm-3)	2.33	2.2	2.3
Poisson's ratio	0.496	0.18	0.33
Electrical Conductivity (S/m)	1.2×10^3	7.0×10^{-10}	3.8×10^7

3.3.3 Device design

To build the device layers, the Process Editor icon from the function manager is clicked to open it. This process field specifies the file that contains the deposit and etches sequence needed to build a device. Using this Process Editor, SiO₂ insulating layer, followed by aluminum layer, is deposited on the silicon substrate. These layers are patterned by using straight cut photoresist photolithography to leave a U-shaped structure anchored at the arms ends to the SiO₂ insulating layer on the silicon substrate. As a post processing step, the front side or back side of the silicon substrate is then anisotropically etched to release the cantilever from the substrate. The thickness of the layers is determined in this step as shown in figure 3.8.



The screenshot shows the Process Editor window with the following table of process steps:

Number	Step Name	Action	Layer Name	Material Name	Thickness	Mask Name	Photoresist	Etch Depth	Mask Offset	Sidewall Angle	Comments
0	Substrate	Substrate	Substrate	SILICON	300	SubstrateMask					
1	Planar Fill	Planar Fill	sio2	SILICA	2						
2	Straight Cut	Straight Cut				sc1	.		0	0	
3	Stack Material	Stack Material	AL		2						
4	Straight Cut	Straight Cut				sc2	+		0	0	
5	Front, Substrate Etch	Straight Cut				<enter>	.	250	0	0	

Fig 3-8 Process Editor for layer deposition and patterning

Under designer navigation tab, the “Layout” function manager provides access to 2-D Layout Editor as shown in figure 3.9. The device is created by drawing its dimensions along the two axes (x, y) for the length and width while the thicknesses has already been determined in the Process Editor shown in figure 3.8.

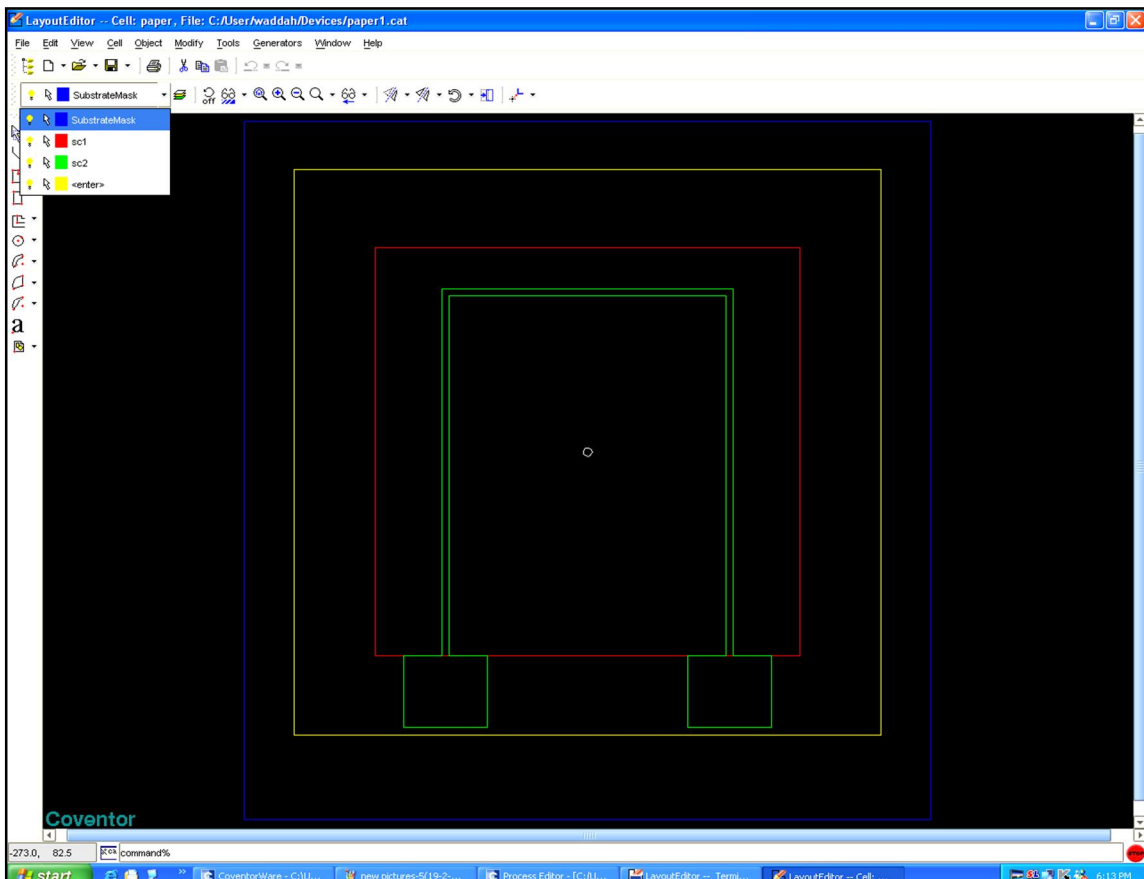
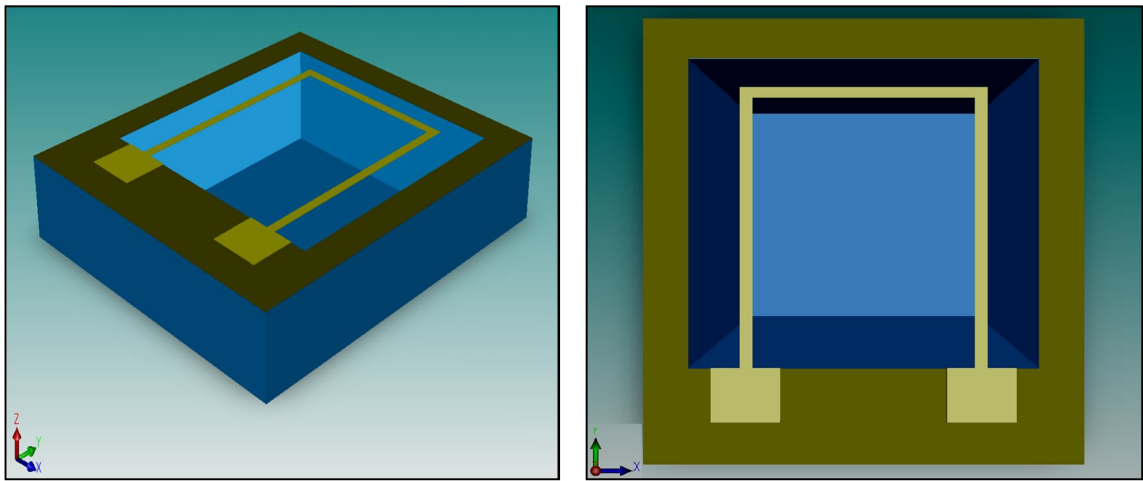


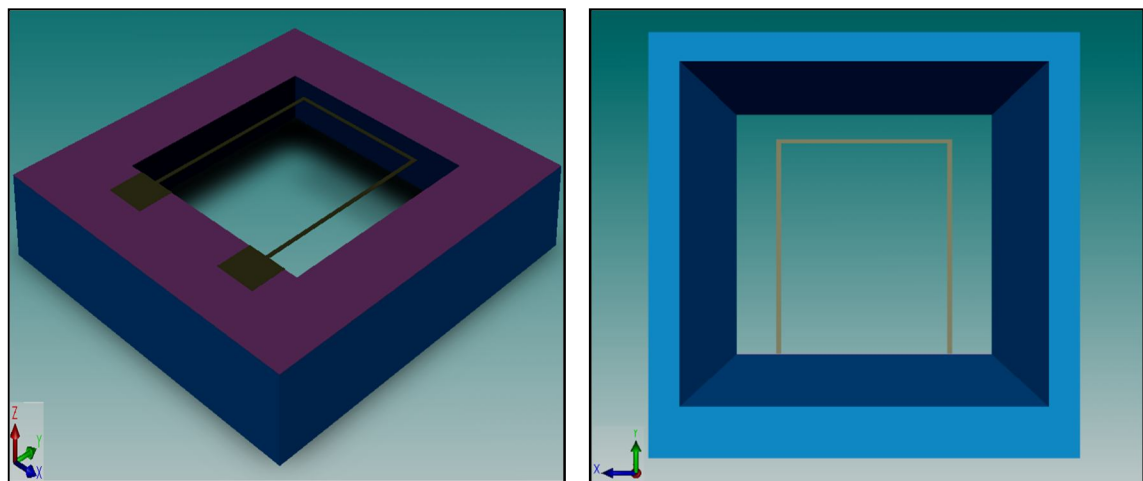
Fig 3-9 2-D Layout Editor showing layout of the U-shaped cantilever

The *Model/Mesh* function manager in figure 3.5 is accessed to create the 3-D structure of the device after drawing the 2-D device layout in the previous step. Two types of bulk micromachining techniques are used to release the vibrating U-shaped cantilever; Front-side bulk micromachining (FSBM) or back-side bulk micromachining (BSBM). As the cost of the post-process is strongly affected by the need for alignment, FSBM is the

preferred method for actual industrial fabrication. Figures 3.10 (a) and (b) show typical results of the 3-D structure of the U-shaped cantilever device generated after BSBM and FSBM etching, respectively.



(a)



(b)

Fig 3-10 3-D solid model of the (a) front side and (b) back side etched U-shaped cantilever

3.3.4 Mesh creation

The model must now be meshed so the geometry of the structure can be reduced to a group of simpler finite element bricks and presented to the solver for finite element analysis. The meshing method is first selected, after which mesh is created for the beam, insulator layer, and the substrate. The mesh, part, and face information are stored in the project database. This database information is used in solver simulation. The software is capable of handling a wide variety of designs. It has some finite capability limits, but the resource limits of the platform on which it is run often dominate a decision on how complex of a mesh to create. Design complexity increases solver computation times. Computation time is influenced by the structure of the design and the number of computational nodes created during the meshing process. A tradeoff between solution accuracy and computation time is considered when deciding on the type of mesh structure and meshing components to use. The target solver can also be configured to accommodate large designs with adjustment of tool control parameters and alternate solution methods. Some adjustments may reduce accuracy, but will allow the software to run complex problems. The Mesh tool partitions and meshes the solid model for finite element method FEM of the simulation to generate a mesh and name parts and surfaces of the device. The resulting mesh can then be used by the Analyzer solvers for a variety of FEM simulations. The meshing functions take place from within the Preprocessor. Different types and accuracy of meshing can be created and saved for solid model. These may be different types of meshes corresponding to different types of simulations or they may be different mesh densities of a single type for a mesh convergence study, or a combination of both. Meshing Guidelines for Solvers for CoventorWare suggests the type of meshing that is recommended for each solver. Tetrahedra mesh is suitable selection for mechanical simulation (MemMech).

Figure 3.11 shows that the accuracy of the results obtained from simulation studies depends on the mesh size selected. It indicates the accuracy level of the different tetrahedral meshing for one simulated result of the natural frequency by calculating the

error ratio between the theoretical value and the simulation value for one sample of the cantilever. This is done to decide on how fine a mesh to use to obtain reasonably accurate results. The smaller the error ratio obtained the higher the accuracy of the simulation. It is observed that the error ratios for the mesh of 10 and 5 have a value of 0.07 and 0.071, respectively. These values are not significantly different and therefore the mesh value of 10 is used for the simulation work to shorten the simulation time and obtain reasonably good accuracy especially for the cantilever part where the characterization focuses. Figure 3.12 shows the mesh of the 3D solid model of the U-shaped cantilever.

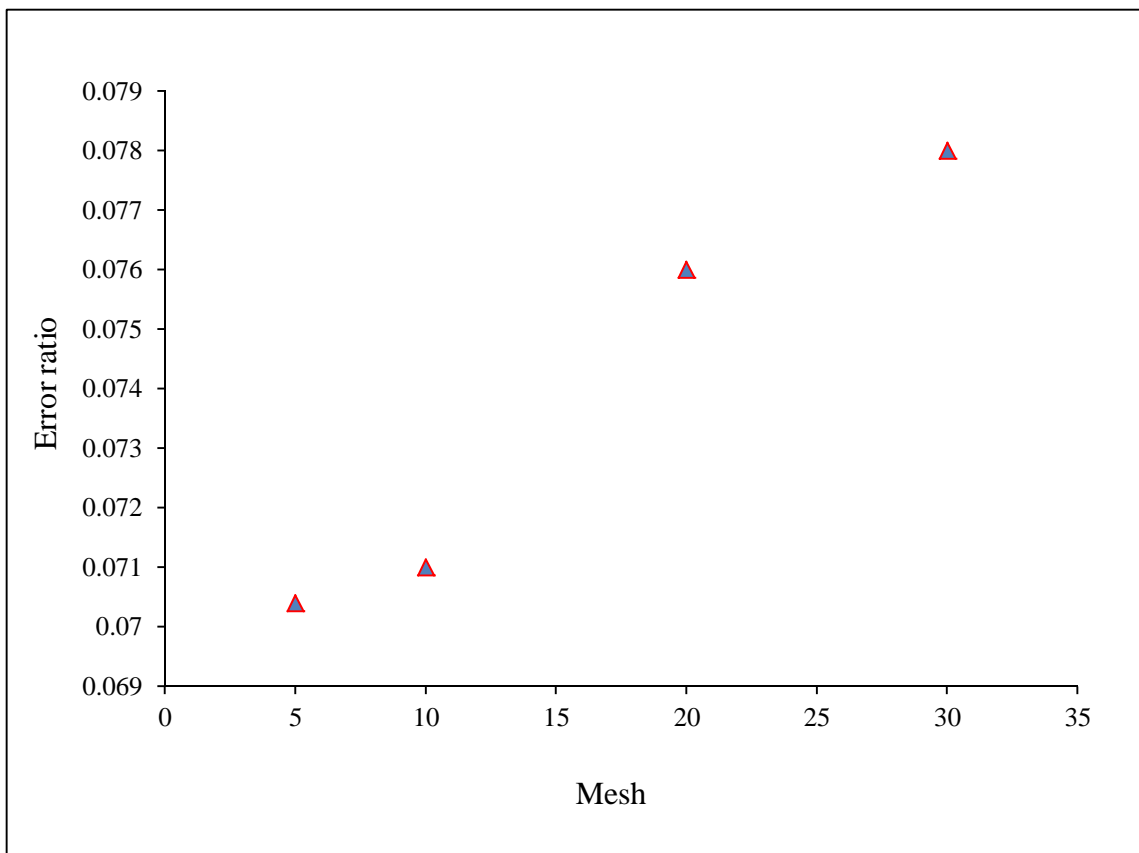


Fig 3-11 Compared accuracy of the different values of mesh

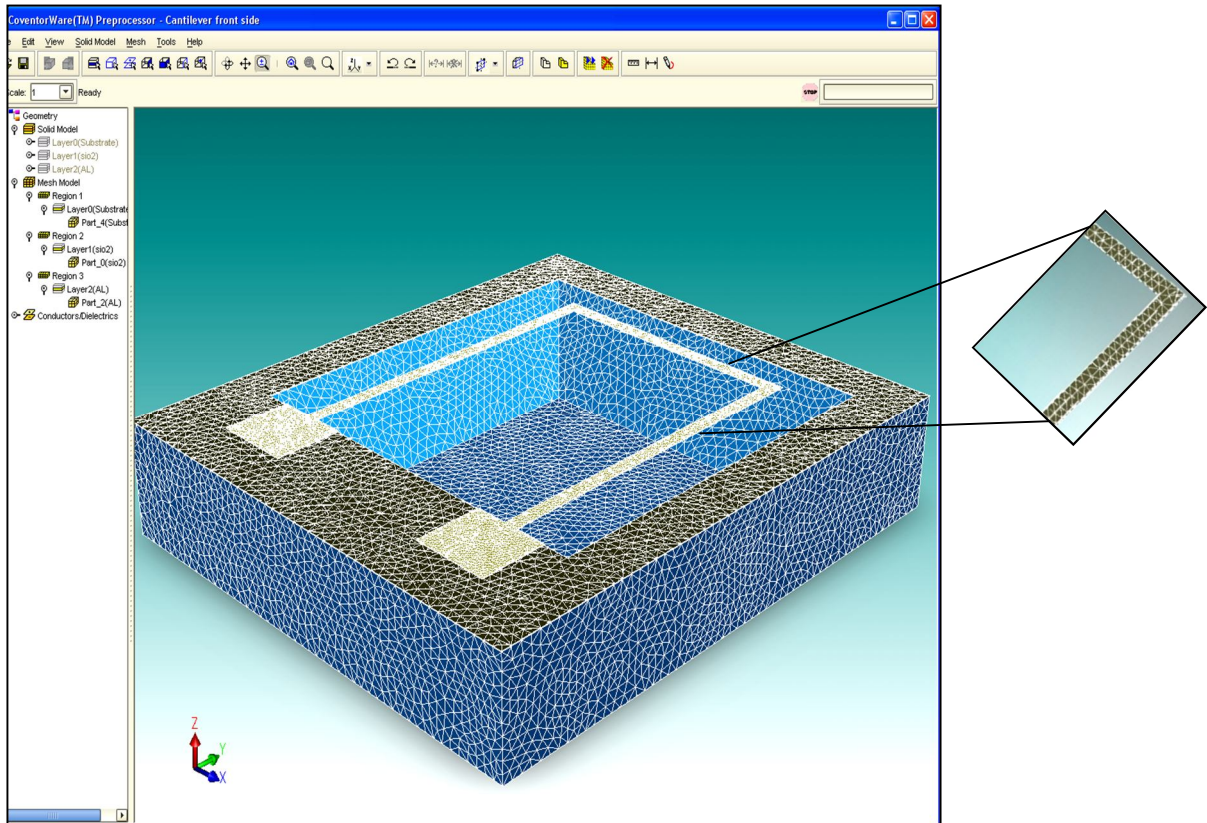


Fig 3-12 The mesh results of the 3D solid model of the device

3.3.5 Simulation and characterization of the U-shaped cantilever

Clicking on the Analyzer tab opens a window that allows access to the solvers. From this tab you can run a MEMS or microfluidics solver, view the results from a previous run, or view the model in the Preprocessor. Selection of the analyser enables the core electrostatic, mechanical, and electromechanical solvers, as well as special domain solvers for modeling piezoresistance, inductance and resistance, optics, and package thermomechanical interaction. Solvers for creating reduced-order models for MEMS mixed-mode system-level simulation are also enabled. MeMech option in the MEMS analyzer tab Performs analysis of mechanical deformation and stresses used for simulating the effect of applied force on the modal vibration of the cantilever. Figure 3.13 shows the MemMech window Settings dialog. A force in μN is applied to the cantilever faces in a certain direction to generate the required displacement. The force is

selected close to the actual Lorentz force expected to act on the cantilever for a given mode based on the direction of the magnetic field under detection to produce minimum and detectable vibration within the elastic limit of the U-shaped cantilever. Two options, Linear or Nonlinear option (see fig 3.13), can be selected for the solution. If the Linear analysis is selected, the software calculates displacement with the assumption that there is a linear relationship between the applied loads and the model deflection while the stiffness of the model is considered constant. Linear analysis is less compute-intensive than nonlinear analysis and is often adequate for design purposes. If Nonlinear analysis is selected, the software calculates displacement with the assumption that the stiffness of the model is dependent on displacement; the initial flexibility can no longer be multiplied by the applied load to calculate the displacement for any load. In a nonlinear analysis the stiffness of the structure has to be assembled and inverted many times during the course of the analysis, making it much more expensive to solve than a linear analysis. Nonlinear analysis may be more appropriate for simulations modeling contact, for models in which the magnitude of the displacements affects the response of the structure, for models in which the material elasticity varies as loads are increased, and for frequency extraction.

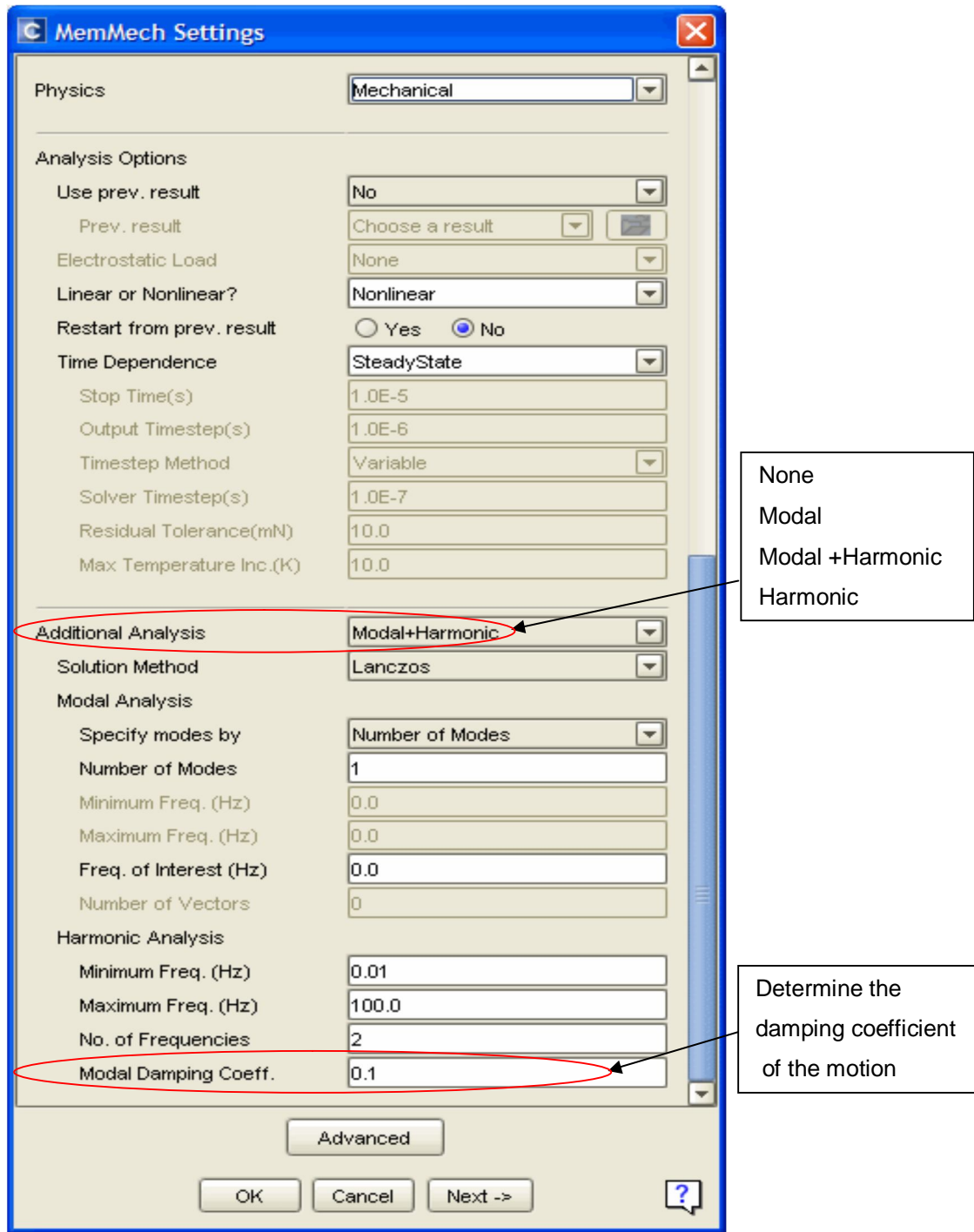


Fig 3-13 MemMech Settings dialog box of the CoventorWare

The appropriate Lorentz force is calculated using equation 2.2 when such cantilever, through which a current is passing, is placed in the magnetic field and it deflects due to the action of the Lorentz force. If the direction of the magnetic induction vector is parallel to the cantilever arms, then the Lorentz force acts on the cantilever base in the direction of z -axis as shown in Figure 3.4 (a).

The magnitude of the Lorentz force (in the case of homogenous magnetic field) is given by the approximate expressions $F_b = iB(b-w)$ where i is the applied electric current, b and w are the length of base and the width of one of the legs, respectively, of the U-shaped cantilever and B is the magnetic induction. The length of the section of the base for which the Lorentz force is calculated is taken to be $b-0.5w-0.5w = b-w$ based on the current behavior through the cantilever [6]. The same procedure is followed for mode 2, but in this case the length is taken to be $l-0.5w$ and thus the force is $F_l = iB(l-0.5w)$ for both arms, one in $+ve$ z -direction while the other in $-ve$ z -direction as show Figure 3.4 (b). However, for mode 3 the force of $F_b = iBb$ acts on the base in y -direction while simultaneously a force of $F_l = iBl$ acts on both arms in the x -direction (refer to Figure 3.4 (c)). Table 3.2 shows the calculated values of the Lorentz forces induced on the base and arms of the U-shaped cantilever by an external magnetic field in the range of from 2 to 12 mT when a current of 100 mA flows through the cantilever.

Table 3-2 Calculated values of forces applied to the base and both arms of the cantilever

Magnetic flux (mT)	Force at the base (μN)	Force at the arm (μN)
2	0.15	0.2
4	0.3	0.4
6	0.45	0.6
8	0.6	0.8
10	0.75	1
12	0.9	1.2

In order to simulate the behavior of the cantilever under the forces considered, as explained in chapter 2, two methods of characterization are used; static and dynamic characterization. Static characterization is realized by applying a constant force to the base or arms of the cantilever corresponding to the macroscopic force on the wire which is created by the Lorentz force for the three modes considered. On the other hand the dynamic characteristics is realized when a periodic force of the same magnitude as the static case, representing the force due to an alternating current in the device placed in an external static magnetic field, is applied to the base and/or the arms. This force is applied in such a way as to excite one of the three modes of vibration based on the direction of the external magnetic field under detection. From MemMech setting in Figure 3.13, the Model+Harmonic analysis is selected. The periodic Lorentz force is applied at different frequencies centered on the resonant frequency for a given mode. This range of frequencies of vibration is selected after estimating the value of the natural frequency in order to obtain the output values of the cantilever deflection as functional of vibration frequency.

The appropriate Lorentz force is applied to the cantilever is calculated using equation 2.2 to estimate the range of the force that is to be applied. The values of the force are selected based on the value of the current and external magnetic field. Different forces are applied, corresponding to the Lorentz force (external magnetic field), for the three modes of vibration of the cantilever to investigate the linearity of the system (relationship between the displacements and the forces applied). The software calculates displacement with the assumption that there is a linear relationship between the applied loads and the model. The stiffness of the model is considered constant and the flexibility of the structure need only be calculated once. The linear response of the structure to other load cases can be found by multiplying the new vector of loads.

Also in the software the Modal_Damping Coefficient is an important parameter used when performing a harmonic analysis. It introduces damping in the MemMech setting (see Figure 3.13) and is a convenient way of including the important absorption of

energy without modeling the effects in details for the simulation. This setting is expressed as a fraction of the critical damping for each eigenmode. For an analysis based on modal superposition, one of the ways of introducing damping is to use a fraction of critical damping for each eigenmode which by default is given the value of 0.1 or 10% of critical damping. This damping is a mathematical concept introduced in association with the eigenmodes of the system. Thus, it cannot be extended to nonlinear applications in which the equations of motion of the system are integrated directly and in which the natural frequencies of the system are constantly changing because of nonlinearities. Different value of the damping_coefficient is used to determine the effect of the damping for the response of the cantilever.

The characterization procedure is repeated for the different modes of the cantilever vibration by varying the dimensions to investigate the effect of the thickness, width, length of the arms and length of base for the vibration response, resonant frequency and sensitivity of the cantilever. The effect of the dimensions can be realized by varying one dimension of cantilever and keeping others constant. The results can be viewed after the simulation processing is finish from mechanical solver drop-down menu of the software results window. Table 3.3 shows the selected values of the various dimensions of the U-shaped cantilever used in the study.

Table 3-3 Dimensions of the Aluminium cantilever determined in the software

Dimension	Values selected (μm)
Thickness	1, 2, 5, 10, 15, and 20
Width	5, 10, 15, 20, and 25
Length of arm	640, 700, 760, 820, 880, 940, 1000, 1060, 1120, and 1180
Length of base	260, 360, 460, 560, 660, 760, 860, 960, 1060, 1120, 1180, 1240

3.3.6 Piezoresistor for output signal measurement

In this last step the procedure of conversion of the mechanical deflection to electrical measurement is explained. This part performs a piezoresistive analysis using a piezoresistor model and a cantilevered beam, and demonstrates how to use Analyzer's MemPZR module and Architect components to simulate the piezoresistive effect. The MemPZR solver uses the finite element method to model piezoresistive behavior. Architect has several components that can be used to model piezoresistive behavior, and it also has components that allow the user to input Analyzer MemPZR solver results. The CoventorWare design environment facilitates the design of multiple piezoresistive sensors of arbitrary shape and size in MEMS devices. To match process parameters, such as diffusion depth, the user may independently control the process-dependent geometry of each resistor. In a two-step solution, the software solves the beam mechanical problem and then applies the beam stress results to solve for the resultant piezoresistive change. Figure 3.14 illustrates the set up of all boundary conditions for the separate beam and piezoresistor. Figure 3.14 (a) shows the cantilevered beam part and (b) shows the piezoresistor with grown in the cantilever while (c) illustrates the combined model showing geometry placement of them.

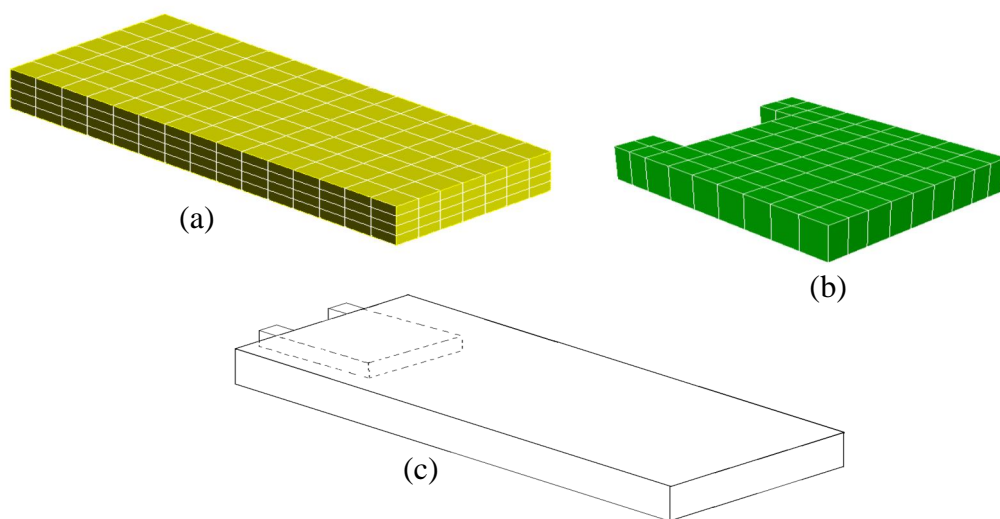


Fig 3-14 Preprocessor view of (a) meshed cantilevered beam, (b) meshed piezoresistor and (c) combined geometry of beam and piezoresistor

In piezoresistive tab (MemPZR) some of the previous results from the mechanical simulation is applied on the piezoresistor transducer of polysilicon which is grown on the silicon beam with three different dimensions based on dimensions of the cantilever as shown in Table 3.4. The length of the cantilever beam used is 1000 μm , the thickness of the SiO_2 insulator layer is 0.5 μm and the same thickness 0.5 μm of the aluminum layer.

Table 3-4 The thickness of the silicon beam and piezoresistor grown inside

Si beam thickness (μm)	Piezoresistor thickness (μm)
2	0.6
5	3
9	6

After the piezoresistor segment is designed, the original value of the resistance in (Ω) is determined by applying a voltage of 5 volt to this resistor as shown in Figure 3.15 and the software will calculate from the value of the current through it.

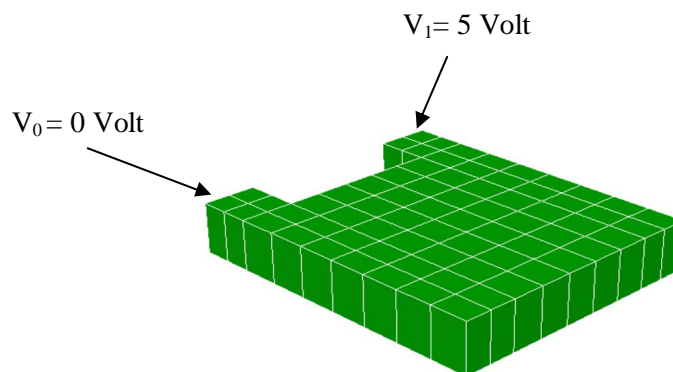


Fig 3-15 Applied voltage to the Piezoresistor Model

A stress of the deflection result of the cantilever beam from a previous MemMech run is specified and applied to the piezoresistor. Figure 3.16 shows the Settings dialog box of the MemPZR.

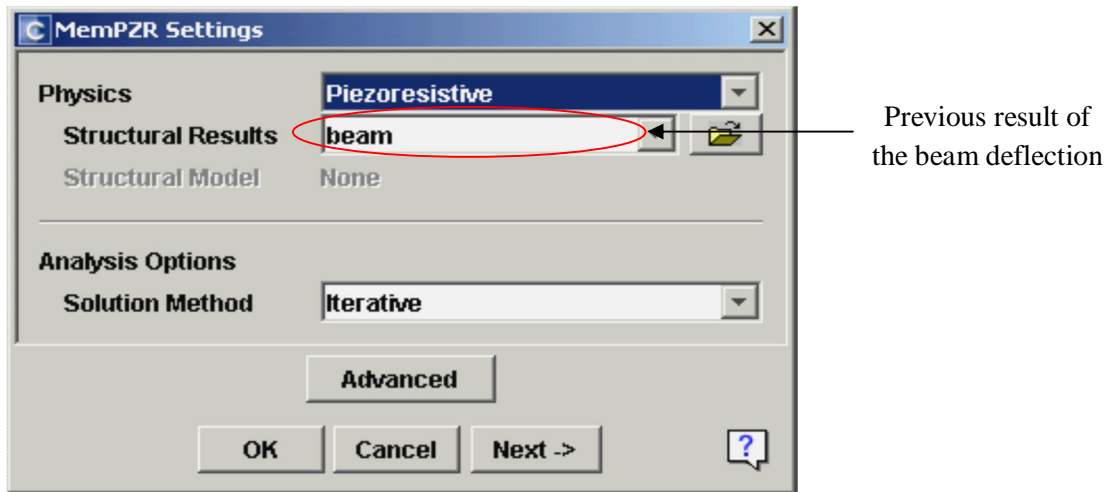


Fig 3-16 Settings Window of MemPZR

This step results in a change of the current (*% Change in Current*) through the piezoresistor after applied the deflection of the cantilever, from which the value of the change in the resistance of the piezoresistor ΔR_p is calculated. MemPZR first calculates an unstressed current through the piezoresistor device and then compares the value with the stress solution number, computing the percentage difference. Figure 3.17 shows the piezoresistive material embedded in a U-shaped beam, while figure 3.18 shows the cross sectional view of the arm width and arm Length of the beam and a polysilicon piezoresistor embedded inside the Si beam of the U-shaped cantilever device.

The value of the piezoresistor at (Ω) is depending on its dimensions to convert this result to electrical signals when from the Wheatstone bridge depend on the value of the change of the resistor of the piezoresistor ΔR_p already explained at the theory (Chapter-2).

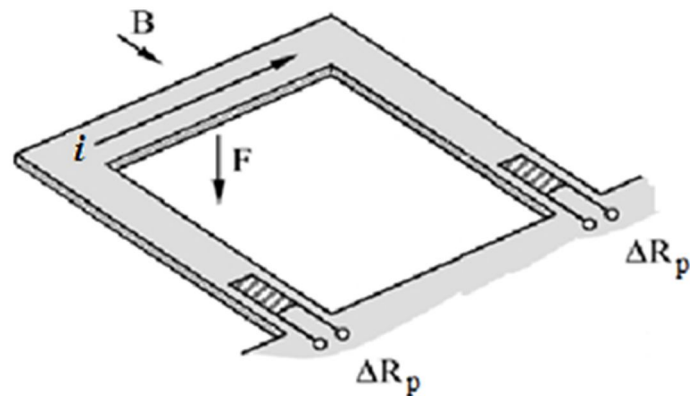


Fig 3-17 U-shaped cantilever with incorporation of piezoresistors

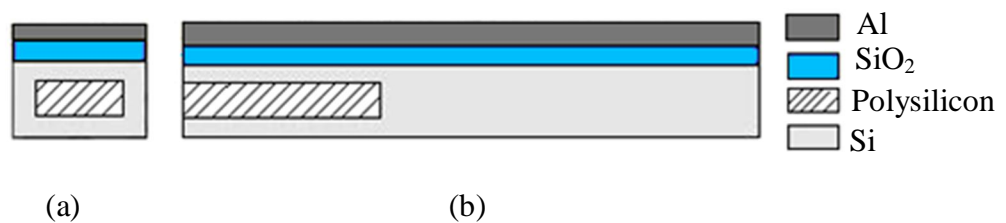


Fig 3-18 Cross sectional view of the (a) arm width (b) arm Length of the U-shaped cantilever device with polysilicon piezoresistor

The resistance of the piezoresistor is dependent on its dimensions. In order to convert the change in resistance to electrical signal, a well-known electrical circuit called Wheatstone bridge configuration is used to measure the output voltage given by: as indicated in figure 3.19. Normally all resistors are chosen equal to each other, resulting in zero output voltage. For the U-shaped cantilever, the mechanical strain generated by the bending translates into a change of gauge resistances placed closely to the anchor of the suspended “U-shape” as shown in figure 3.17. The bridge configuration with voltage supply is the most popular interconnection of piezoresistors. Both gauges (namely R_1 and R_4) are arranged in a Wheatstone Bridge together with two reference resistors (namely R_2 and R_3) deposited over the bulk. Figure 3.19 illustrates this arrangement of gauges and reference resistors [28]. For sensor applications at least one of the resistors has to be dependent on the measured parameter.

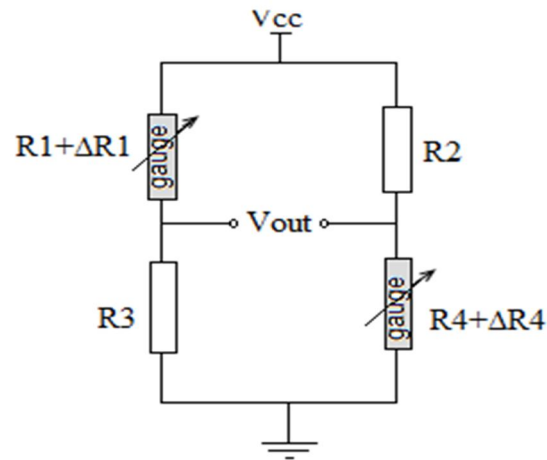


Fig 3-19 Wheatstone's bridge circuit diagram for strain gauges [28]

The change of the resistance is then used to transform the response of the cantilever into electrical signal. The differential output voltage (V_{out}) of the Wheatstone bridge may be written:

$$V_{out} = V_{cc} \frac{R_2 \cdot R_3 - (R_1 + \Delta R_1) \cdot (R_4 + \Delta R_4)}{((R_1 + \Delta R_1) + R_3)(R_2 + (R_4 + \Delta R_4))} \quad (3.2)$$

Thus when the bridge is balanced ($R_2 \cdot R_3 = R_1 \cdot R_4$) there is no change in the piezoresistors R_1 and R_4 ($\Delta R_P = \text{zero}$) and the output voltage is null. Otherwise the output voltage can be measured. As previously mentioned, measurement of low magnetic flux of the order of the earth's magnetic field is achieved by using piezoresistive gauges. Due to low signal level available across the gauges, amplification and very high gain with low noise must be used after the Wheatstone bridge circuit [27, 31, 46].

The electronic workbench program (multisim) is used to design a simple circuit of the Wheatstone bridge to achieve the voltage output of the measurement. The sensitivity of the system can then be calculated as the ratio between the voltage output and the external magnetic field.

3.4 Mathematical modeling

As mentioned in chapter 2 the Lorentz force due to a static external magnetic field acting on direct current (DC) for the static mode or an alternating current (AC) for the dynamic mode through the a cantilever excites it to vibrate in various modes depending on the direction of the current in a conductor wire in the cantilever. Theoretical equations and modeling is conducted to justify the simulation results obtained for the three vibration modes of the U-shaped cantilever. Firstly, for static motion as given in equation 2.3 in chapter 2 the value of stiffness k of the cantilever rectangular beam is given by [28, 30]

$$k = \frac{3EI}{l^3} \quad (3.3)$$

Where E denotes Young's modulus, and I moment of inertia I is given by:

$$I = \frac{1}{12} h^3 w \quad (3.4)$$

where geometrical values selected for the width (w) and thickness (h) depends on the wire flexural vibration mode. The k is now:

$$k = \frac{3EI}{l^3} = \frac{Eh^3 w}{4l^3} \quad (3.5)$$

Secondly, using equation 2.5 of a general simple dynamic problem is applied to the dynamic behavior of the cantilever beam (see Figure 3.20) and classical Euler-Bernoulli beam dynamics equation [14, 45] which given by:

$$EI \frac{\partial^4 \psi}{\partial \zeta^4} = p \quad (3.6)$$

where, the curve ψ describes the deflection of the beam at some position x , y , or z and p is a distributed load, in other words, a force per unit length F/l .

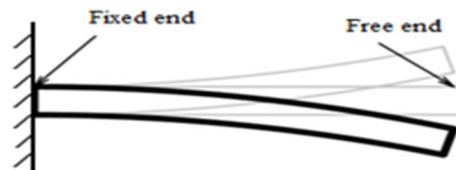


Fig 3-20 Cantilever beam motion

Assuming that the flexural vibrations of the cantilever are small compared to its dimensions (and therefore the effect of shear deformation and rotary inertia are negligible) the oscillations of the cantilever can be described by the classical Euler-Bernoulli beam dynamics theory leading to a set of three (one for each cantilever arm and one for the cantilever base) to give another combine equation [45]:

$$EI \frac{\partial^4 \psi}{\partial \zeta^4} + \frac{m}{l} \frac{\partial^2 \psi}{\partial t^2} + \frac{D}{l} \frac{\partial \psi}{\partial t} = 0 \quad (3.7)$$

Where ζ is the spatial coordinate along the cantilever ζ is (x , y , or z direction), m the effective mass of the beam, t is the time, and $\psi(\zeta, t)$ is the time dependant transverse deflection. This equation can be adopted to analyze the problem of the cantilever beam motion. If $\rho l h w$ is substituted for m , where ρ is the density, h is the thickness and w is the width of the cantilever beam, equation 3.6 becomes:

$$EI \frac{\partial^4 \psi}{\partial \zeta^4} + \rho h w \frac{\partial^2 \psi}{\partial t^2} + \frac{D}{l} \frac{\partial \psi}{\partial t} = 0 \quad (3.8)$$

In order to determine the effect of the dimensions (thickness, width, length of the arm, and length of the base) on the resonant frequency of the three modes of vibration, here is need to justify the mechanical equations in chapter 2 by the U-shaped cantilever based on

some assumption for various modes of vibration. Assuming that the two arms of the cantilever are identical, the U-shaped cantilever in mode 1 is equivalent to two regular cantilevers with half the mass of the base placed at their tips as shown in Figure 3.21 (a). To analyze the U-shaped structure, the stiffness (k) for a single cantilever in equation (3.5) is multiplied by 2 for mode 1 vibration to take care of the two arms with half mass of base to give

$$k = \frac{6EI}{l^3} = \frac{Eh^3w}{2l^3} \quad (3.9)$$

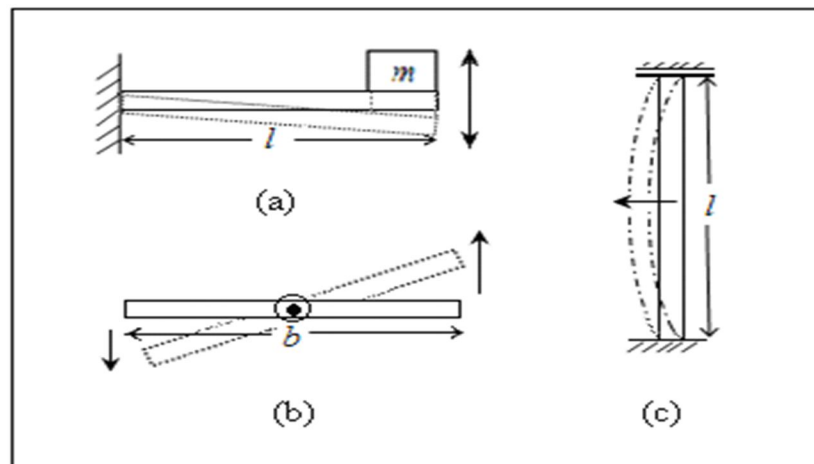


Fig 3-21 Model for mechanical vibration of a U-shaped cantilever in (a) mode 1, (b) mode 2 and (c) mode 3

While the resonant frequency (f_0) is determined from

$$f_0 = \frac{1}{2\pi} \sqrt{\frac{k}{m_{eff}}} = \frac{1}{2\pi} \sqrt{\frac{Eh^2}{2\rho l^3(b/2+l)}} \quad (3.10)$$

Where m_{eff} is the effective mass of the cantilever given by the sum of mass of half base, $m_b/2 = \rho bhw/2$ and mass of arm, $m_{arm} = \rho hwl$ to give $m_{eff} = \rho wh(b/2+l)$.

To analyze the antisymmetrical flexural vibration mode (mode 2) of the U-shaped structure we considered the model in Figure 3.21 (b) where half of the base of the cantilever is replaced by a uniform cantilever anchored at the midpoint of the base and the arms are replaced by a lumped mass $m = \rho lhw$, where l is length of the arm of the cantilever. The total effective mass, m_{eff} , will then be $\rho wh (b/2 + l)$. k is calculated using equation (3.3) but replacing the length l by half of the length of the base $b/2$. The base then moves with a stiffness constant given by $k/2$ since there are two forces acting in opposite directions on the base. The modified equation becomes

$$k = \frac{1}{2} \left(\frac{3EI}{\left(\frac{b}{2}\right)^3} \right) = \frac{Eh^3w}{b^3} \quad (3.11)$$

And the resonant frequency is now

$$f_0 = \frac{1}{2\pi} \sqrt{\frac{k}{m_{eff}}} = \frac{1}{2\pi} \sqrt{\frac{Eh^2}{\rho b^3 (b/2 + l)}} \quad (3.12)$$

Figure 3.21 (c) shows the one-dimensional model for mode 3. Unlike mode 1 and mode 2, the width of the cantilever in mode 3 becomes its thickness and the thickness becomes its width. The base now moves slightly since the mechanical force on the base is assumed to be a bit more than the Lorentz force in the opposite direction.

The theoretical value of k for mode 3 can be determined using equation (3.13) assuming the stiffness for a clamped-clamped beam with a force at midspan [28].

$$k = \frac{192EI}{l^3} \quad (3.13)$$

The motion is assumed moving by four times of the stiffness. That is when the base is considered rigid and no displacement on it and the displacement just on the both arms see Figure 3.21 (c). So the resonant frequency using the effective mass of one arm $m_{eff} = \rho h w l$ to give by:

$$f_0 = \frac{1}{2\pi} \sqrt{\frac{192EI}{\rho h w l^4}} = \frac{1}{2\pi} \sqrt{\frac{192Ew^2}{12\rho l^4}} \quad (3.14)$$

Theoretically, it is expected that the vibration characteristics of the U-shaped cantilever in mode 3 depends on the ratio between the length of the base and arm (b/l) due to two forces acting on the base in opposite directions, one of the forces is the Lorentz force and the other is the mechanical force due to the pressure produced by the motion of both arms as shown in Figure 3.22. Theoretically three submodes for mode 3 are expected to be observed. First is when the motion of the base is the same as that of the arms, that is, inwards or outward as shown in Figure 3.23 (a). Second, is when the base is considered fixed or rigid, because the Lorentz force equal to and in opposite direction to the mechanical force produced by the motion of both arms as shown in Figure 3.23 (b). Third is when the base moves out when the arms move in or vice versa as shown in Figure 3.23 (c), where the mechanical force on the base greater than the Lorentz force.

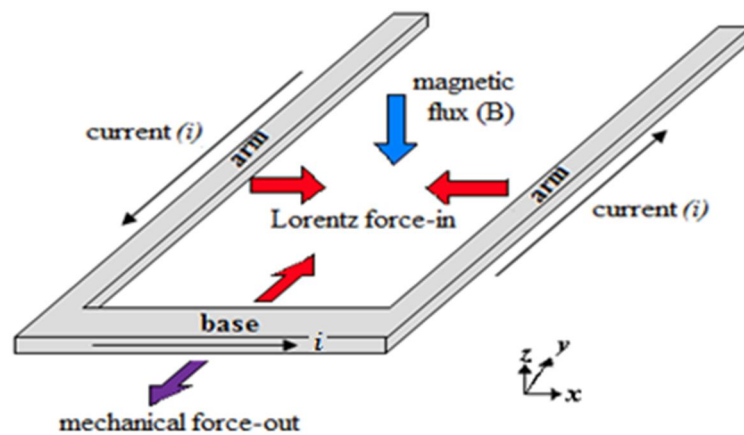


Fig 3-22 Mode 3 of the cantilever-two forces acting on the base

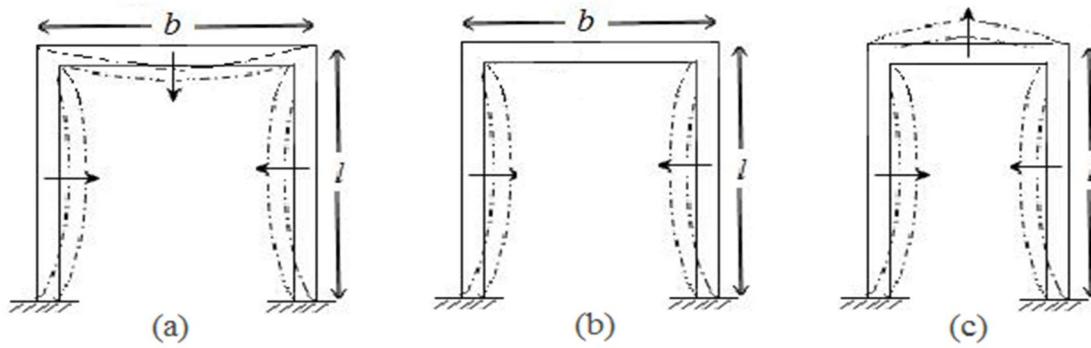


Fig 3-23 Three different submodes for mode 3

The value of the resonant frequency of these submodes of mode 3 is depend on the ratio between the length of the of the base and length arm (b/l). To obtain the value of resonant frequency, we have to multiply equation (3.14) by a new factor. The value of this new factor depends on the b/l value.

Chapter 4

RESULTS AND DISCUSSION

4.1 Static and Dynamic Characterization and Modeling

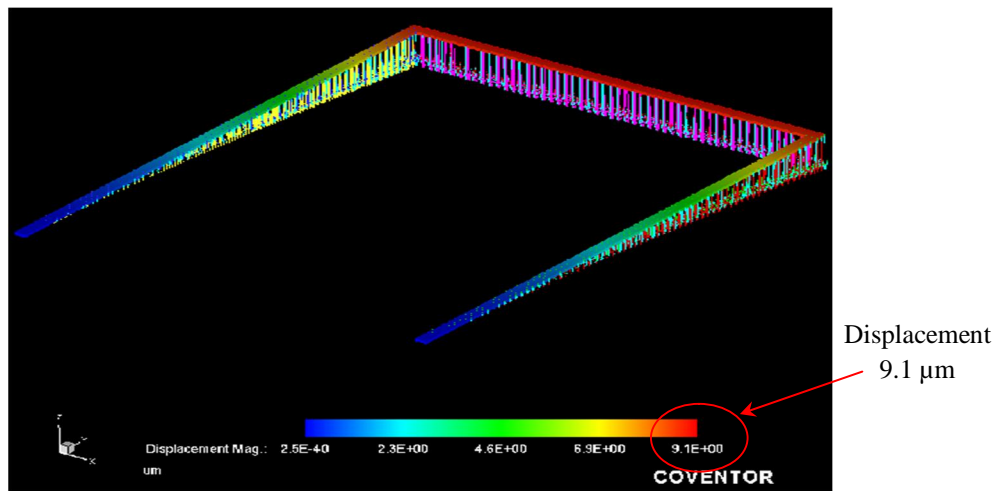
An Al U-shaped cantilever with a thickness of 5 μm , width of 20 μm , arms length of 1000 μm and a base length of 760 μm is initially considered for the characterization. The U-shaped cantilever is subjected to various forces in order to excite the three modes of vibration expected when the Lorentz force acts on the current through the arms and base. The forces were applied in both the static and dynamic modes. Mathematical modeling was also carried out to verify the simulation results.

4.1.1 Static Characterization

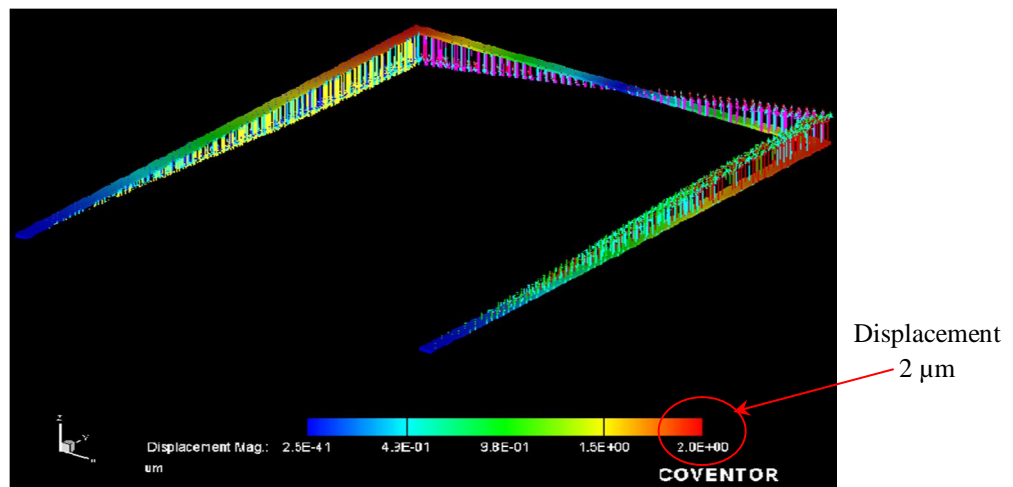
When the dc current carrying U-shaped cantilever is placed in an orthogonal static external magnetic field the Lorentz force acts on it whose magnitude is calculated using equation 2.2. This produces various deflections on the arms and/or base of the current-carrying U-shaped cantilever as described in section 3.3.5. By assuming a current of 100 mA, an external static magnetic field of 12 mT for the cantilever of length of the base (b) and arms (l) of 760 μm and 1000 μm , respectively, a value of 0.9 μN and 1.2 μN is calculated for the forces acting on the base and both arms of the cantilever, respectively. These forces represent the Lorentz forces due to the constant dc current in a static magnetic field that is perpendicular to the arms or base. Figures 4.1 (a), (b) and (c) show the results of the cantilever deflection for mode 1, mode 2 and mode 3 respectively.

Figure 4.1 (a) for mode 1 shows a maximum displacement of $9.1 \mu\text{m}$ on the base when the constant force of $0.9 \mu\text{N}$ is applied on the base in the $-ve z$ -direction. Fig. 4.2 shows a maximum displacement of $2.0 \mu\text{m}$ at the extremity of both arms in the z -direction when the force of $1.2 \mu\text{N}$ is applied in opposite directions on each arm corresponding to the Lorentz force for mode 2. Figure 4.1 (c) shows the maximum displacement of 15 nm when a force of $1.2 \mu\text{N}$ is applied to the arms in opposite direction ($+ve x$ -direction and $-ve x$ -direction) and a force of $0.9 \mu\text{N}$ is applied to the base in the $-ve y$ -direction corresponding to the Lorentz force for mode 3.

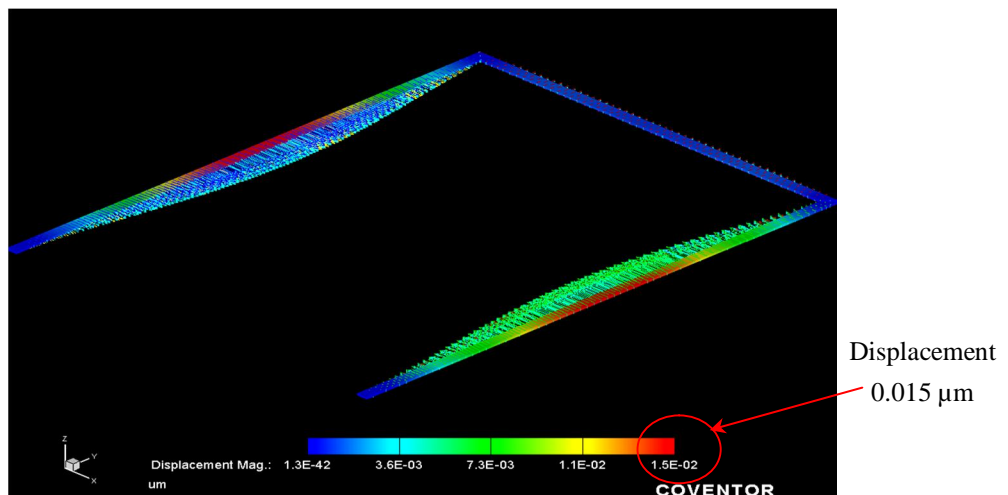
It is observed that in mode 3 there is a small displacement in the x -direction at the base. The base experiences a very small net displacement because the inward Lorentz force is balanced by the outward mechanical force that is induced on the base when an inward force is applied to both the arms simultaneously. From the displacement for the three modes it can be deduced that the sensitivity of the system is highest for mode 1, followed by mode 2 and lowest for mode 3.



(a) Model1



(b) Mode 2



(c) Mode 3

Fig 4-1 3D simulation of constant applied force (a) $0.9 \mu\text{N}$ downward on the base (mode 1), (b) $1.2 \mu\text{N}$ applied to the arms in opposite direction (mode 2) and (c) $1.2 \mu\text{N}$ and $0.9 \mu\text{N}$ inwards on the arms and base respectively (mode 3)

4.1.2 Dynamic Characterization

As explained in chapter 3, section 3.3.5, on the other hand, the dynamic mode is realized when a periodic force, representing the force due to an alternating current in the device placed in an external static magnetic field, is applied to the cantilever. In this situation, if the cantilever is driven by a periodic Lorentz force near its natural frequency, resonance occurs and a considerably large displacement results which increases the sensitivity of the device. Similar situations are observed for the two other modes. So the displacement of the cantilever is significantly large when a periodic force is applied at its natural frequency for the three modes of vibration as compared to a constant force (static case). Figure 4.2 show the graph for the simulation results of the maximum displacement as a function of the frequency for mode 1 when a periodic force with amplitude of $0.9 \mu\text{N}$ is applied at various frequencies around the resonant frequency 1 from 0 Hz to 7000 Hz. Figures 4.3 and 4.4 show the frequency response of mode 2 and mode 3, respectively. The actual data for these results are included in Appendix-A. A maximum amplitude of of the displacement of about 45, 2, $0.06 \mu\text{m}$ at resonant frequency of 3.019, 8.244 and 86.893 kHz is observed for mode 1, mode 2 and mode 3, respectively.

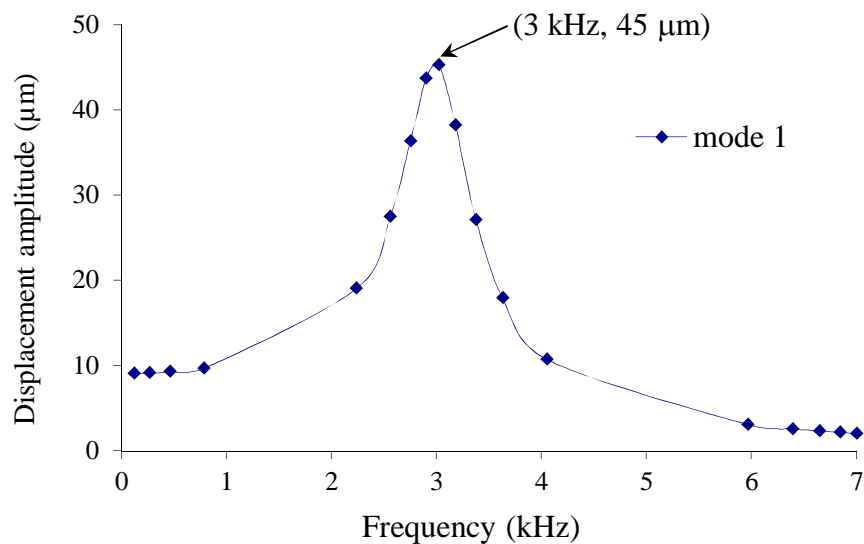


Fig 4-2 Maximum displacement versus frequency for a periodic force of $0.9 \mu\text{N}$ amplitude applied to the base of the cantilever (mode 1)

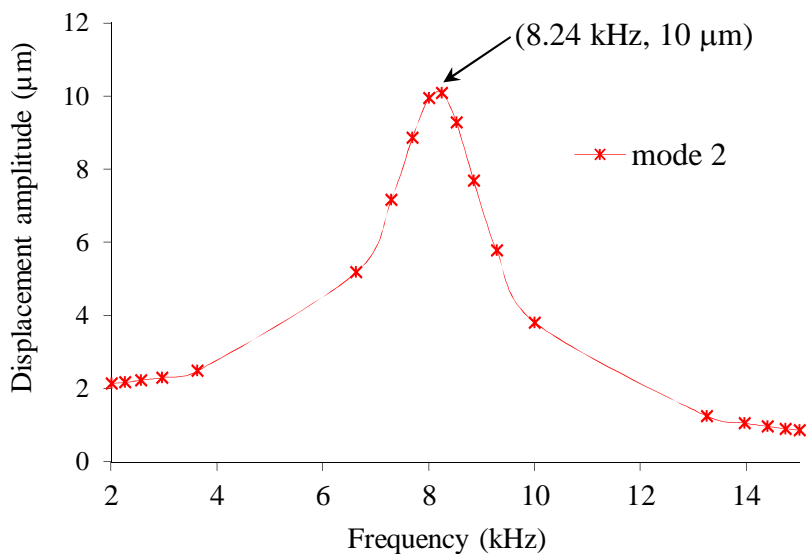


Fig 4-3 Maximum displacement versus frequency for a periodic force of $1.2 \mu\text{N}$ amplitude applied to the arms of the cantilever (mode2)

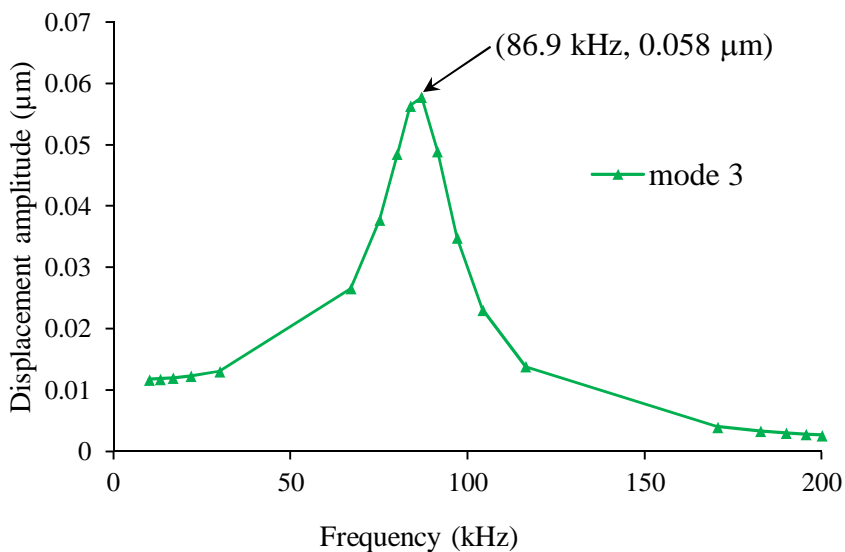


Fig 4-4 Displacement versus frequency for a periodic force of $0.9 \mu\text{N}$ amplitude applied to the base and $1.2 \mu\text{N}$ to both arms of the cantilever (mode3)

4.1.3 Comparison between the static and dynamic modes

Table 4.1 compares the maximum displacement and sensitivity (in μm per μN) of the cantilever for the static and dynamic cases for the same applied Lorentz force on the arms and base produced by assuming the current of 100 mA and external static magnetic field of 12 mT.

Table 4-1 Maximum displacement and sensitivity of the cantilever in the three modes of vibration for static and dynamic cases

Type of the mode	Static displacement (μm)	Resonant displacement amplitude (μm)	Static sensitivity ($\mu\text{m}/\mu\text{N}$)	Resonant sensitivity ($\mu\text{m}/\mu\text{N}$)
Mode 1	9.10	45.20	10.1	50.2
Mode 2	2.00	10.00	1.67	8.33
Mode 3	15×10^{-3}	0.06	12×10^{-3}	50×10^{-3}

It can be deduced from table 4.1 that the displacement of the cantilever is significantly large when a periodic force is applied at its natural frequency (resonant frequency) for all modes of vibration indicating higher sensitivity of about five times as compared to the static modes. Therefore a high sensitivity of the system is achieved when the system is operated at the resonant frequency because the output measurement of the piezoresistor transducer or optical read out technology is dependent on the deflection of the cantilever. It is also observed that the value of the resonant frequency is smallest for mode 1 and largest for mode 3 and depends on some physical and mechanical parameters like the mass (m) and stiffness coefficient (k) as already explained in the mathematical expressions in chapter 2.

4.2 Effect of the cantilever dimensions on its dynamic characteristics

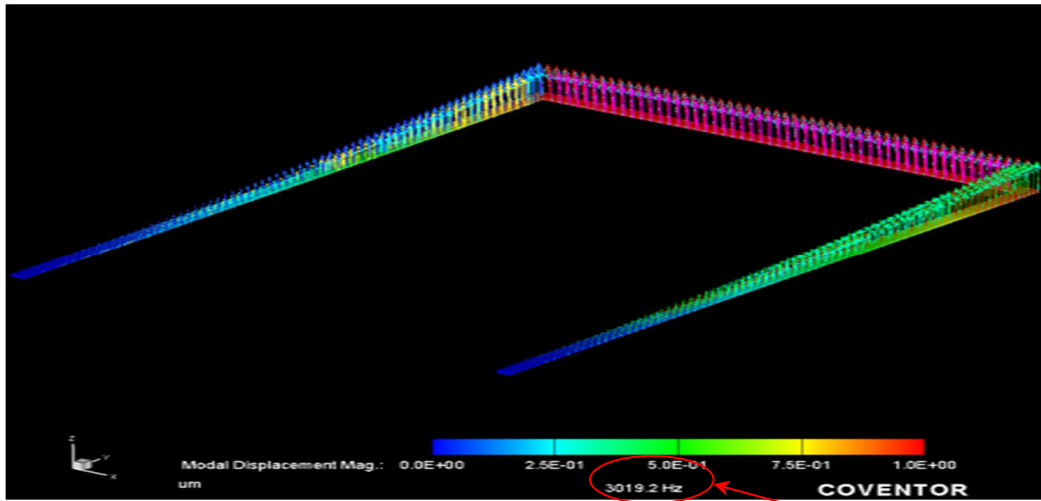
The frequency response of the cantilever is obtained by a frequency sweep in the resonance neighborhoods for various thicknesses, widths, lengths of arms and lengths of the base to obtain the dynamic characteristics of the mechanical system when a periodic force of a given amplitude equivalent to the Lorentz force is applied. Furthermore the simulation results were justified with results of mathematical modeling obtained from mathematical equations 3.10, 3.12 and 3.13 for mode 1, mode 2 and mode 3, respectively. The same parameters of the U-shaped cantilever such as thickness, width, length of base length of the arms were also varied in the mathematical modeling.

4.2.1 Variation of the cantilever thickness

Cantilever thicknesses (h) of 5, 10 and 15 μm are used to investigate its effect on the resonant frequency and response of the cantilever for the three modes of vibration. The other dimensions of the cantilever were kept constant at 20 μm , 1000 μm and 760 μm for the width, length of the arms and length of base, respectively.

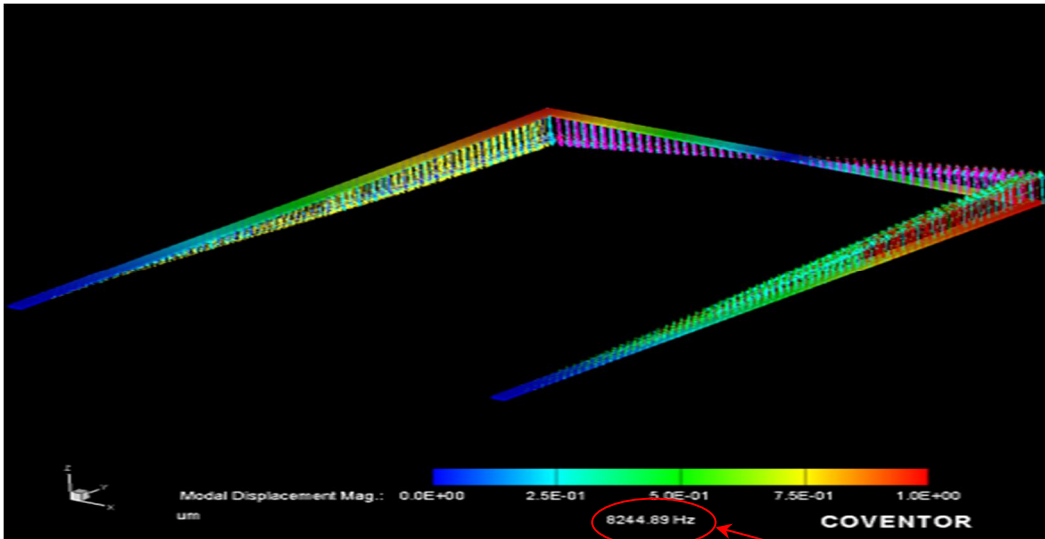
Figure 4.5 (a), (b) and (c) show vector representation of the displacement of a 5 μm thick U-shaped cantilever for the three modes of vibration. The value of the resonant frequency is 3.019 kHz, 8.244 kHz and 86.893 kHz for mode 1, mode 2 and mode 3, respectively.

Similar figures for the vector displacement of a 10 μm thickness U-shaped cantilever for the three modes are included in Appendix (B). The values of the resonant frequencies for the 10 μm thickness cantilever are found to be 6.009 kHz for mode 1, 15.646 kHz for mode 2 and 86.775 kHz for mode 3. And 8.999 kHz for mode 1, 22.064 kHz for mode 2 and 86.717 kHz for mode 3 for 15 μm thick U-shaped cantilever.



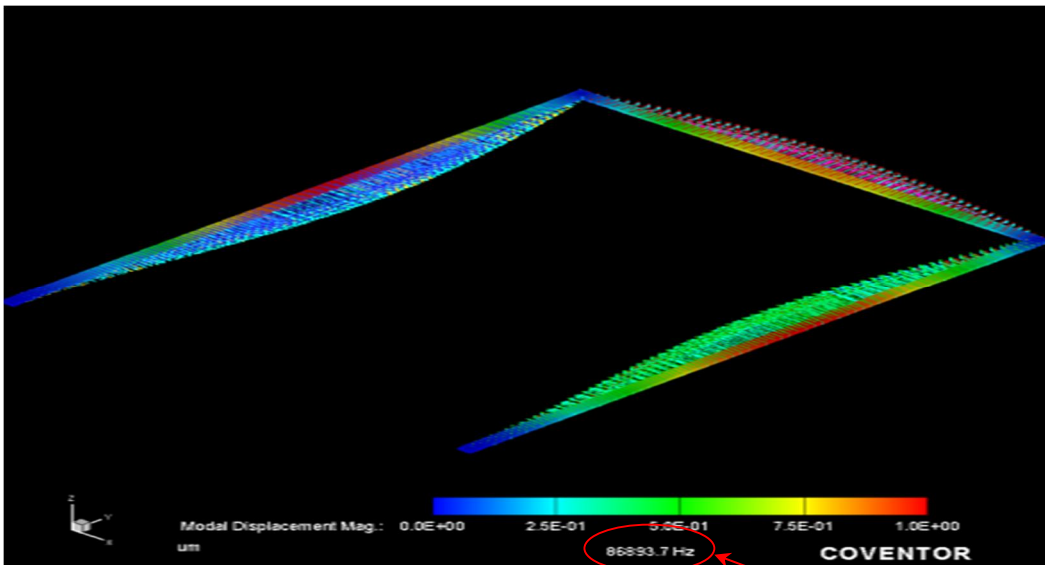
(a) Mode-1

The value of resonant frequency 3019.2 Hz



(b) Mode-2

The value of resonant frequency 8244.09 Hz



(c) Mode-3

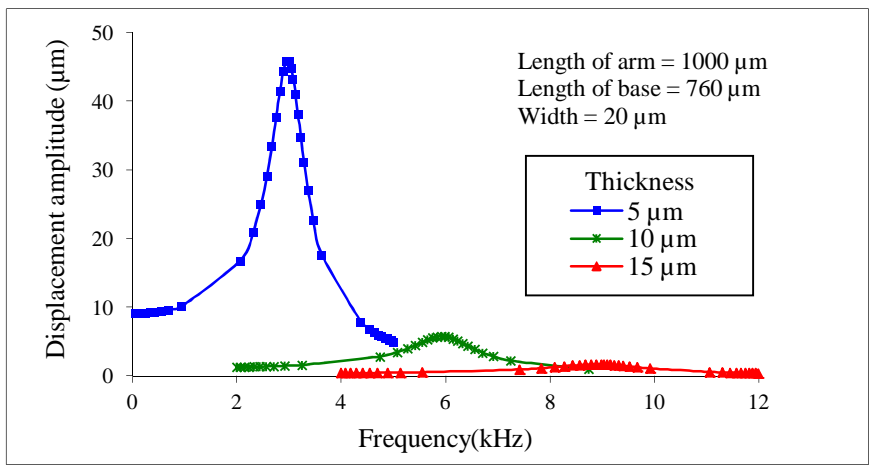
The value of resonant frequency 86893.7 Hz

Fig 4-5 Vector representation for the three modes for a 5 μm thick U-shaped cantilever

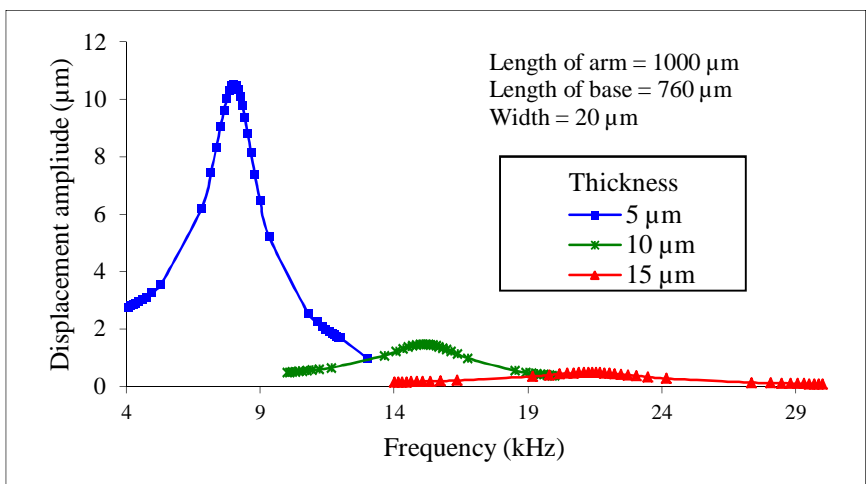
Figure 4.6 (a), (b) and (c) show the effect of cantilever thickness on its maximum displacement profile as a function of frequency for mode 1, 2 and 3, respectively. These figures also show that the sensitivity decreases when the thickness increases for mode 1 and mode 2. The smallest thickness has the highest sensitivity for mode 1 and mode 2 while there is no change in the sensitivity of mode 3.

Theoretical calculations for the resonant frequencies using equations (3.10), (3.12) and (3.14) for mode 1, 2 and 3 for six values of the thickness of the U-shaped cantilever were also obtained in order to confirm that the results obtained by simulation are justifiable for the three modes of vibration. The calculations procedures presented in Appendix (C).

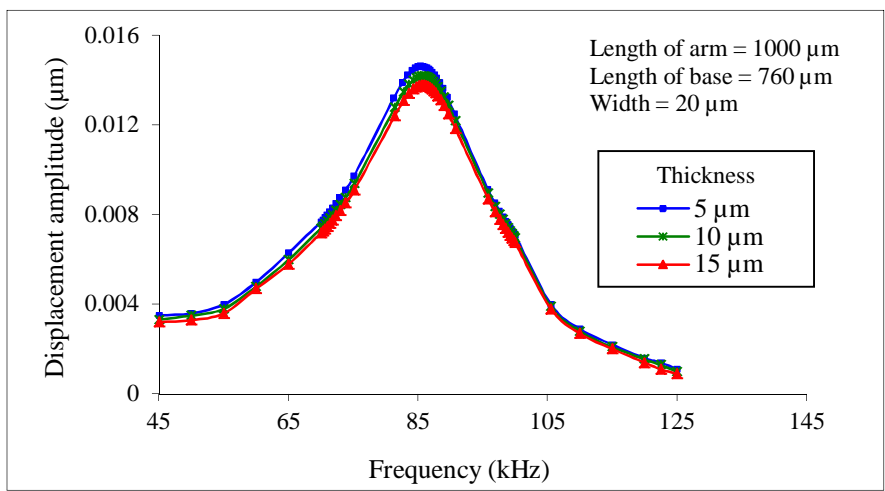
It is observed that the resonant frequencies for modes 1 and 2 are significantly influenced by the thickness of the cantilever with the resonant frequency increasing with increasing thickness. While for mode 3 the resonant frequency is independent of thickness. Table 4.2 and Figure 4.7 show the simulation and theoretical results for the six values of the thickness of the U-shaped cantilever.



(a) Mode 1



(b) Mode 2



(c) Mode 3

Fig 4-6 Maximum displacement of U-shaped cantilever versus frequency at various thicknesses for the three modes of vibration

Table 4-2 Theoretical and simulation results of resonant frequency for various thicknesses of the U-shaped cantilever for the three modes of vibrations

Thickness (μm)	Resonant frequency (kHz)					
	Mode 1		Mode 2		Mode 3	
	Simulation	Theoretical	Simulation	Theoretical	Simulation	Theoretical
1	0.62	0.55	1.74	1.23	86.66	82
2	1.21	1.10	3.35	2.46	86.64	82
5	3.00	2.80	8.08	6.16	86.58	82
10	6.00	5.50	15.00	12.33	86.58	82
15	8.99	8.20	21.52	18.50	86.6	82
20	11.9	11.0	26.91	24.67	86.66	82

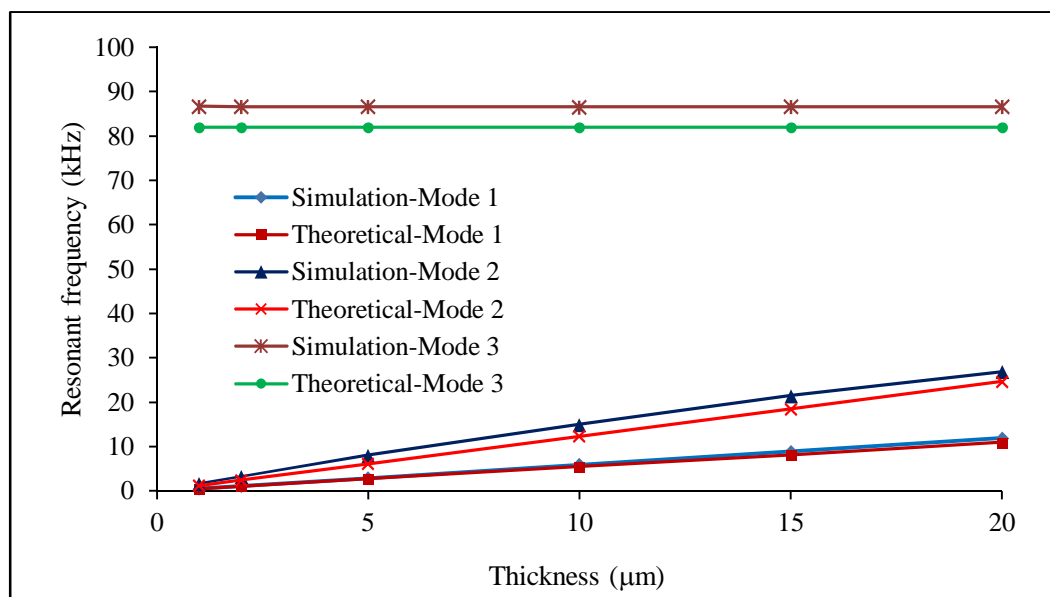
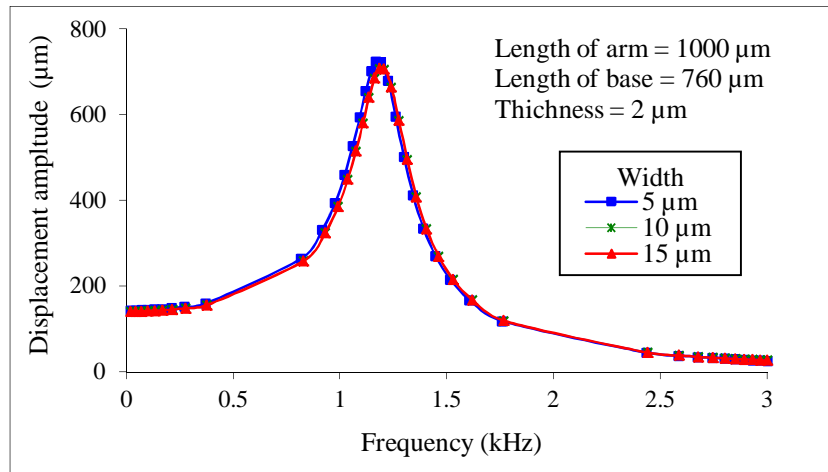


Fig 4-7 Theoretical and simulation results of resonant frequency versus thickness for the three modes of vibration

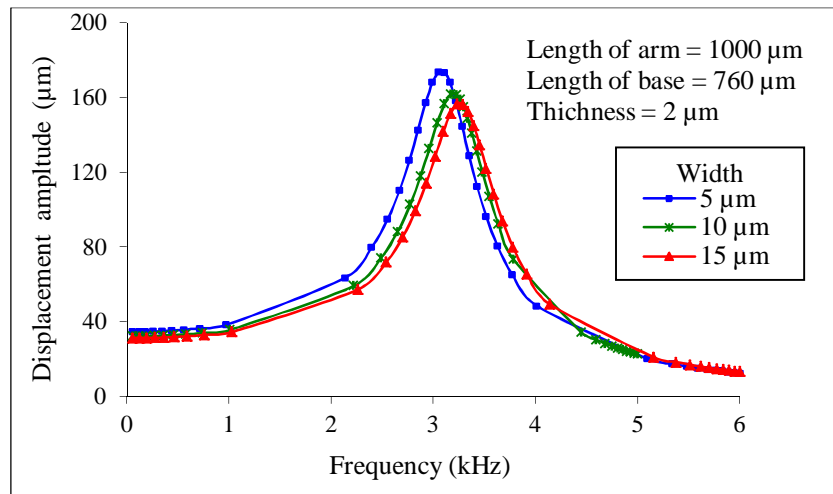
4.2.2 Variation of the cantilever width

A width (w) of 5, 10 and 15 μm is used to investigate its effect on the resonant frequency of the cantilever for the three modes of vibration, while the thickness, length of arms and length of base were kept constant at 2 μm , 1000 μm , and 760 μm , respectively. Figures 4.10 (a) and (b) show that the resonant frequencies for modes 1 and mode 2 are independent of the width of the U-shaped cantilever, while for mode 3, as shown in Figure 4.8 (c), the resonant frequency increases with increase in width.

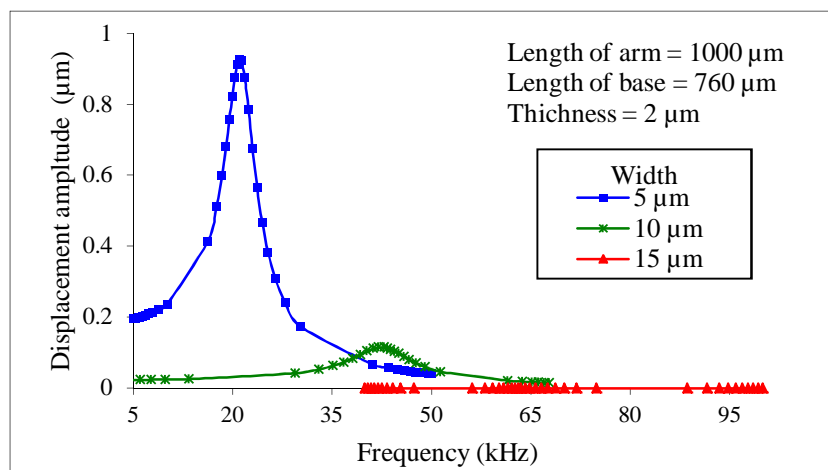
Unlike the thickness effect, the sensitivity decreases when the width is increased for mode 3 while there is no change in the sensitivity of mode 1 and mode 2. Theoretical calculations of the resonant frequencies using equations (3.10), (3.12) and (3.14) for mode 1, 2 and 3 respectively for five values of the width of the U-shaped cantilever were also obtained in order to confirm that the results obtained by simulation are justifiable for the three modes of vibration. Table 4.3 and Figure 4.9 shows the simulation and theoretically derived results for five values of the width of the cantilever. The steps of the theoretical calculations are presented in Appendix (B). For mode 1 and mode 3 the simulation results in table 4.3 are agree by small relative error (error ratio) from with the calculation results. However, relative error of 28% between the calculation and the simulation results of mode 2 obtained due to the calculation only based on the cantilever dimension and ignores the cantilever is fixed to the SiO_2 and Si layers in one end of both of the arms.



(a) Mode 1



(b) Mode 2

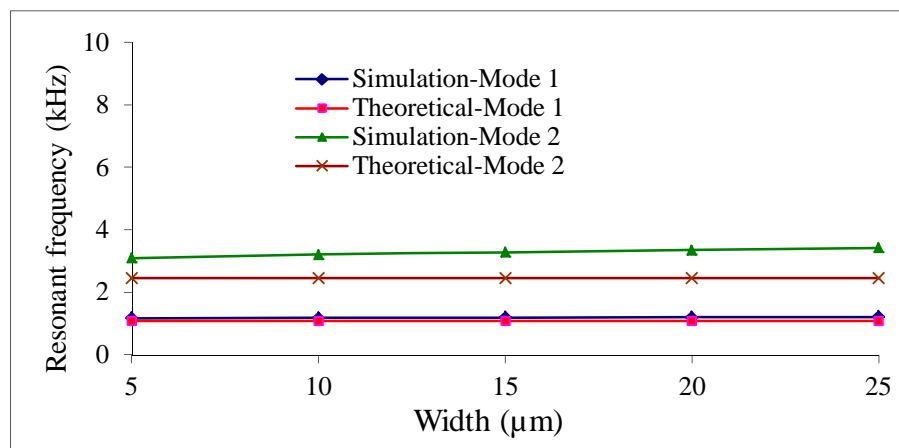


(c) Mode 3

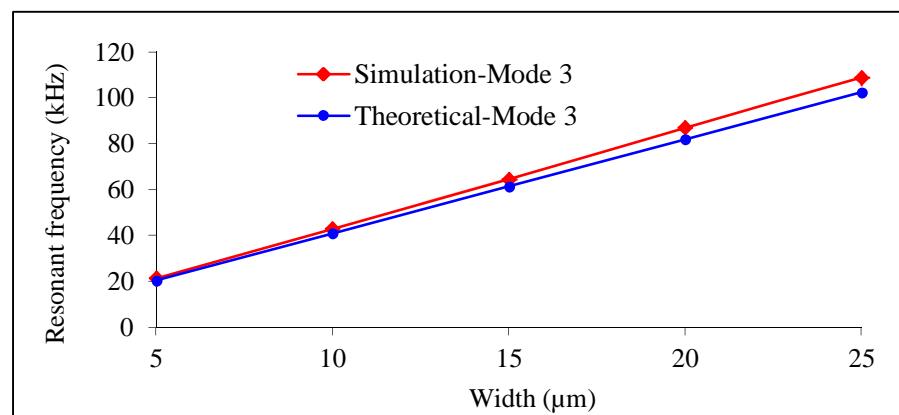
Fig 4-8 Maximum displacement of U-shaped cantilever versus frequency at various widths for the three modes of vibration

Table 4-3 Theoretical and simulation results of Resonant frequency for various widths for the three modes of vibration

Width (μm)	Resonant frequency (kHz)					
	Mode 1		Mode 2		Mode 3	
	Simulation	Theoretical	Simulation	Theoretical	Simulation	Theoretical
5	1.177	1.1	3.110	2.46	21.24	20.5
10	1.190	1.1	3.220	2.46	42.80	41.0
15	1.200	1.1	3.290	2.46	64.58	61.5
20	1.213	1.1	3.359	2.46	86.89	82.0
25	1.223	1.1	3.433	2.46	108.80	102.5



(a)



(b)

Fig 4-9 Theoretical and simulation results of resonant frequency versus cantilever width for (a) mode 1 and mode 2 (b) mode 3

4.2.3 Variation in length of arms

Variation in the length of the arms (l) affects all the three modes of vibrations of the U-shaped cantilever, but its effect is more pronounced for mode 1 and mode 3. Table 4.4 and Figures 4.11 shows the effect of the length of the arms for the resonant frequency at different values of arms length and thus different values of the ratio between the base and arm b/l , while the base length is held constant at $760 \mu\text{m}$ for (a) mode 1 and 2 (b) two behaviors of mode 3 (mode 3a and mode 3c) explained in chapter 3 last section. Mode 3a occurs when the ratio between the length of base and length of arm $b/l < 0.82$, and mode 3c when $b/l > 0.82$. Figure 4.10 shows samples of the simulation results of the three submodes for mode 3.

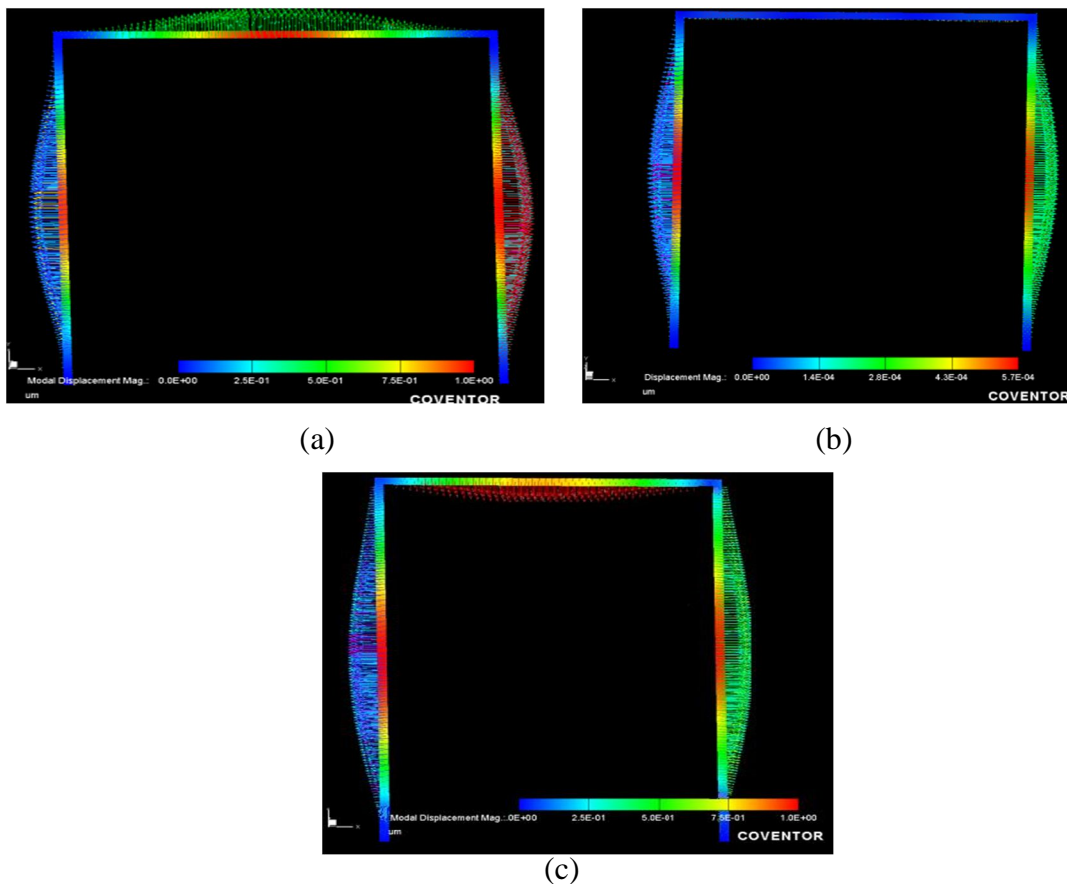
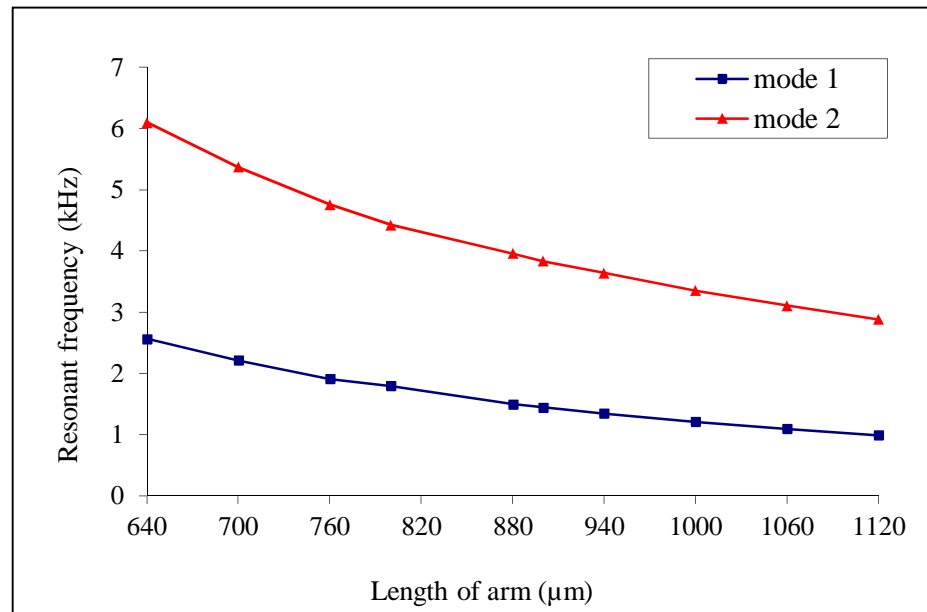


Fig 4-10 Simulation results of the three submodes for mode 3 of the cantilever's mechanical vibration for (a) $l = 1000 \mu\text{m}$, $b = 1000 \mu\text{m}$, $b/l > 0.82$, (b) $l = 1000 \mu\text{m}$, $b = 820 \mu\text{m}$, $b/l = 0.82$ and (c) $l = 1000 \mu\text{m}$, $b = 760 \mu\text{m}$, $b/l < 0.82$

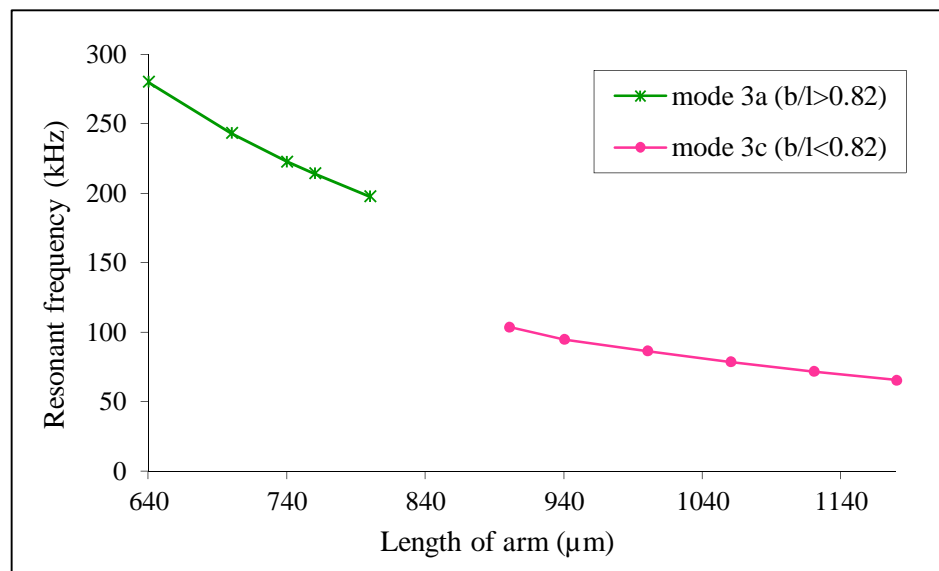
For length of base in the interval between 800 to 880, the ratio of length of base to length of arm b/l is taken to be 0.82 (mode 3b). In this case the base is fixed and the motion is only in the arms of the cantilever and the resonant frequency (f_0) is about 120 kHz.

Table 4-4 Simulation results of the length of the arms effect on the value of the resonant frequency for mode 1, mode 2, mode 3a ($b/l > 0.82$) and mode 3b ($b/l < 0.82$)

Length of the arms (μm)	Resonant frequency (kHz)			
	Mode 1	Mode 2	Mode 3a	Mode 3c
640	2.570	6.100	280.340	
700	2.217	5.377	243.501	
760	1.912	4.766	223.001	
800	1.810	4.431	214.401	
880	1.500	3.966	197.700	
900	1.45	4.841		104.002
940	1.348	3.642		95.011
1000	1.213	3.359		86.649
1060	1.097	3.113		78.901
1120	0.993	2.887		72.009
1180	0.917	2.733		65.803



(a)



(b)

Fig 4-11 Simulation results of the resonant frequency versus length of arms for (a) mode 1 and 2 (c) mode 3a and mode 3c

These graphs of the effect of the length on resonant frequency shows the same trend with that reported by the Jeng-Nan Hung et al [32], who applied the same characterization methodology as that in the current work and K. Brueckner, et al. [49].

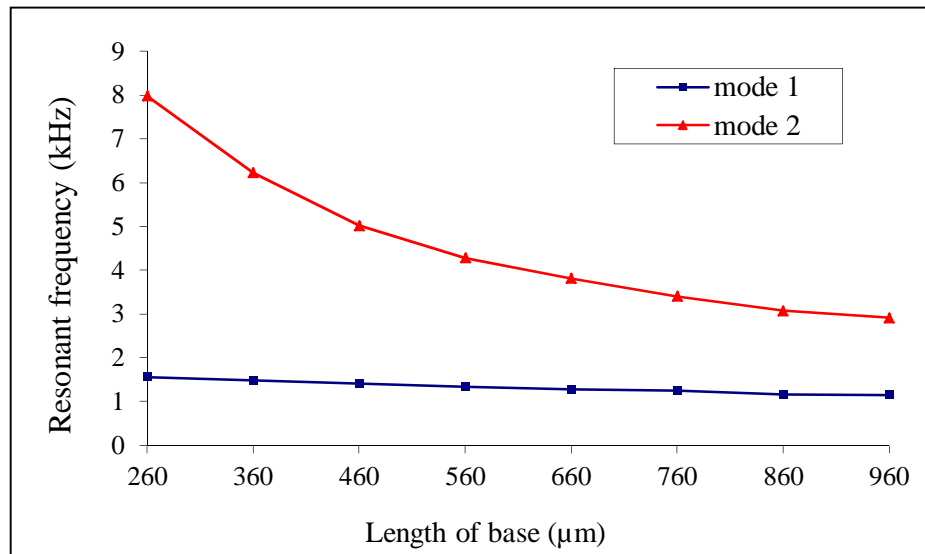
They however used different material of beam structure, polysilicon beam in [32] and two layers of Au deposited over SiC or AlN beam in [49].

4.2.4 Variation in length of the base

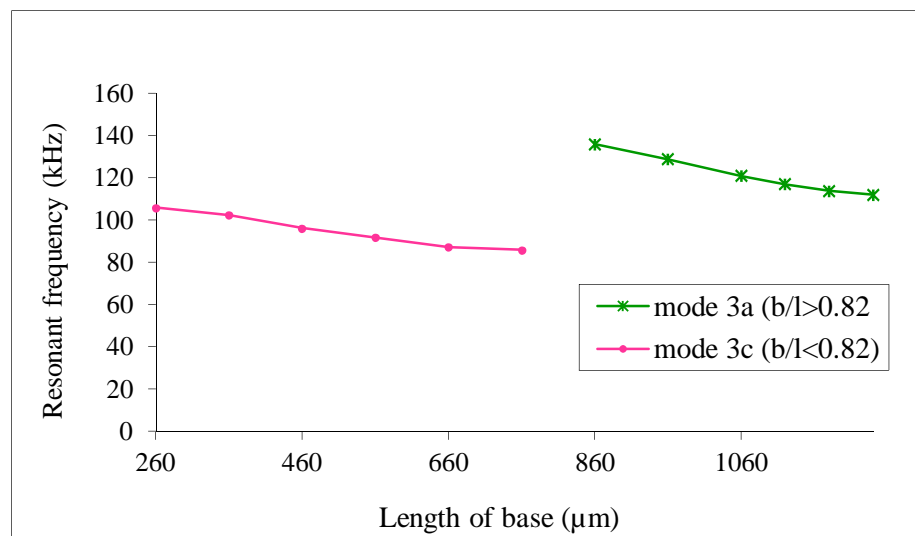
Table 4.5 and Figures 4.12 (a and b) show the resonant frequency for (a) mode 1 and 2 and (b) mode 3a and mode 3c of U-shaped cantilever as a function of the length of base while the length of arms are held constant at 1000 μm thus giving different values for the ratio between the base and arm b/l . It is observed that increasing the length of the base (b) results in a decrease in the resonance frequency for mode 2 and 3, while the resonant frequency for mode 1 is independent of the length of base.

Table 4-5 Simulation results of the effect of length of base on the resonant frequency for mode 1, mode 2, mode 3a ($b/l > 0.82$) and mode 3b ($b/l < 0.82$)

Length of base (μm)	Resonant frequency (kHz)			
	Mode 1	Mode 2	Mode 3c	Mode 3a
260	1.564	7.985	106.001	
360	1.493	6.227	102.520	
460	1.417	5.024	96.345	
560	1.35	4.288	91.877	
660	1.292	3.819	87.334	
760	1.256	3.411	86.800	
860	1.175	3.083		136.001
960	1.156	2.921		128.800
1060	1.093	2.685		121.00
1120	1.069	2.568		117.001
1180	1.077	2.545		113.901
1240	1.087	2.539		112.0



(a)



(b)

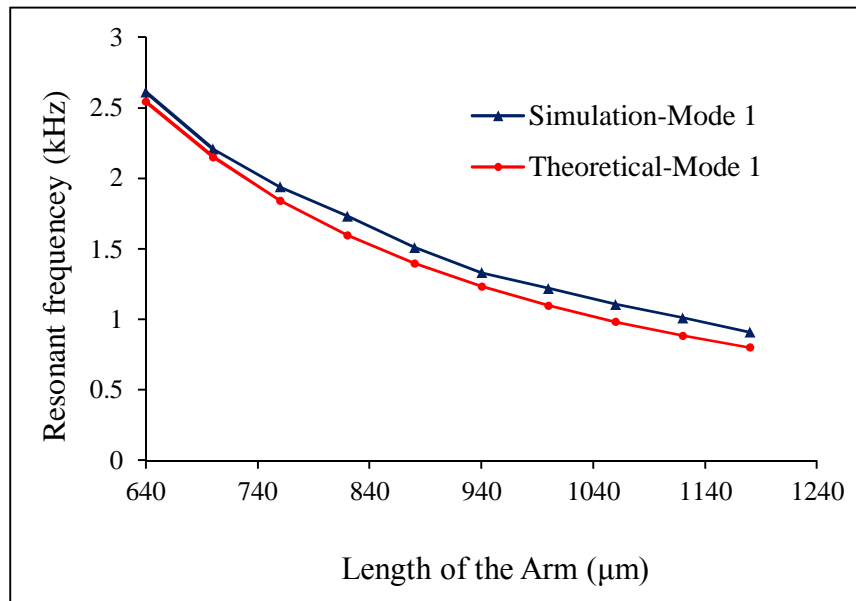
Fig 4-12 Simulation results of the resonant frequency versus length of the base for (a) mode 1 and 2 (b) mode 3a and mode 3c

Table 4.6 and Figure 4.13 (a) and (b) compare the theoretical calculations and the simulation results of the resonant frequencies at various lengths of arms for mode 1 and mode 2. The thickness, width and length of base are held constant at 2, 20, and 760 μm respectively. As mentioned earlier in section 3.4 and 4.2.3, the value of the resonant

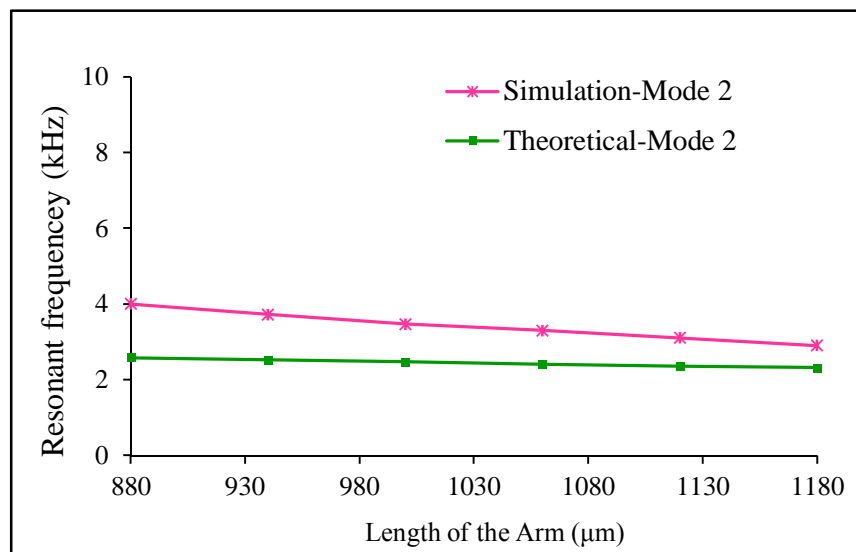
frequency for mode 3 depends on the ratio between length of base and length of arm (b/l). The results indicated three situations arising for mode 3 as a result of application of the Lorentz force in this mode. These situations are termed mode 3a for the ratio $b/l > 0.82$, mode 3b for $b/l = 0.82$ and mode 3c for $b/l < 0.82$ (see Figure 4.10). When the base is stationary due to the balance between Lorentz force and the mechanical force on the base as described in section 3.4 for mode 3, in this situation the motion due to the Lorentz force is just on both arms. Therefore, in order to theoretical obtain the values of the stiffness and resonant frequency for mode 3b, we assume the motion of the cantilever as equivalent to that given for a clamped-clamped beam [34] and so we use equations 3.13 and 3.14 to obtain 104 kHz as the value for the resonant frequency. However, for mode 3a and mode 3c, the motion of the U-shaped cantilever is much more complicated and involves all parts of the cantilever. The resonant frequency calculated for mode 3b is considered as the standard value and it is multiplied by a given factor in order to obtain the theoretical values of the resonant frequency for the other two modes (mode 3a and mode 3c). This factor is found to be a function of (b/l). For instance for mode 3a the factor is found to be equal to $2.121 \times b/l$ while it is equal to $1.0574 \times b/l$ for mode 3c.

Table 4-6 Simulation and theoretical resonant frequency for various length of arms for mode 1 and 2

Length of arm (μm)	Resonant frequency (kHz)			
	Mode 1		Mode 2	
	Simulation	Theoretical	Simulation	Theoretical
880	1.51	1.40	4.00	2.58
940	1.33	1.23	3.72	2.52
1000	1.22	1.10	3.47	2.46
1060	1.10	0.98	3.30	2.41
1120	1.01	0.88	3.10	2.36
1180	0.91	0.80	2.90	2.32



(a)



(b)

Fig 4-13 Simulation and theoretical resonant frequency versus length of arm for (a) mode 1 and (b) mode 2

Table 4.7 and Figure 4.14 show the theoretical calculation and the simulation results of the resonant frequency as a function of the length of arms for mode 3a and mode 3c. The thickness, width and base are held constant at 2, 20, and 760 μm , respectively.

Table 4-7 Simulation and theoretical resonant frequency various length of the arms for mode 3a and 3c

Length of the arms (μm)	Resonant frequency (kHz)			
	Mode 3a		Mode 3c	
	Simulation	Theoretical	Simulation	Theoretical
640	280.34	261.90		
700	243.50	239.50		
760	223.01	220.60		
800	214.40	204.01		
880	197.70	190.50		
940			95.01	88.90
1000			86.64	83.57
1060			78.90	78.85
1120			72.01	74.60
1180			65.80	70.80

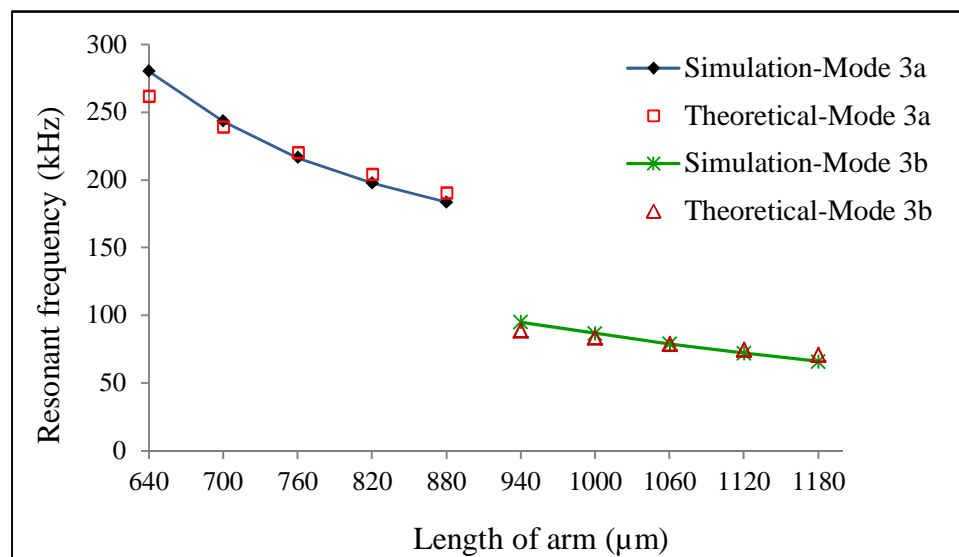


Fig 4-14 Simulation and theoretical resonant frequency versus length of arm for mode 3a and 3b

4.3 Relationship between applied force and displacement

The relationship between the applied force and the response of the cantilever (displacement) is investigated in this section for the static and dynamic mode situations.

4.3.1 Static mode

Figure 4.15 shows the simulation and theoretical values of the cantilever displacement as a function of a constant applied force for the three modes. A perfectly linear graph is obtained with different slopes for the three modes indicating highest sensitivity for mode 1 followed by mode 2 and lowest for mode 3. Using equations 3.9, 3.11 and 3.13, the stiffness of the cantilever is calculated and found to be 0.093, 0.469 and 47.6 for mode 1, mode 2 and mode 3, respectively. The displacement is calculated using equation 2.3. The calculation procedures and the actual data may be found in the Appendix (C).

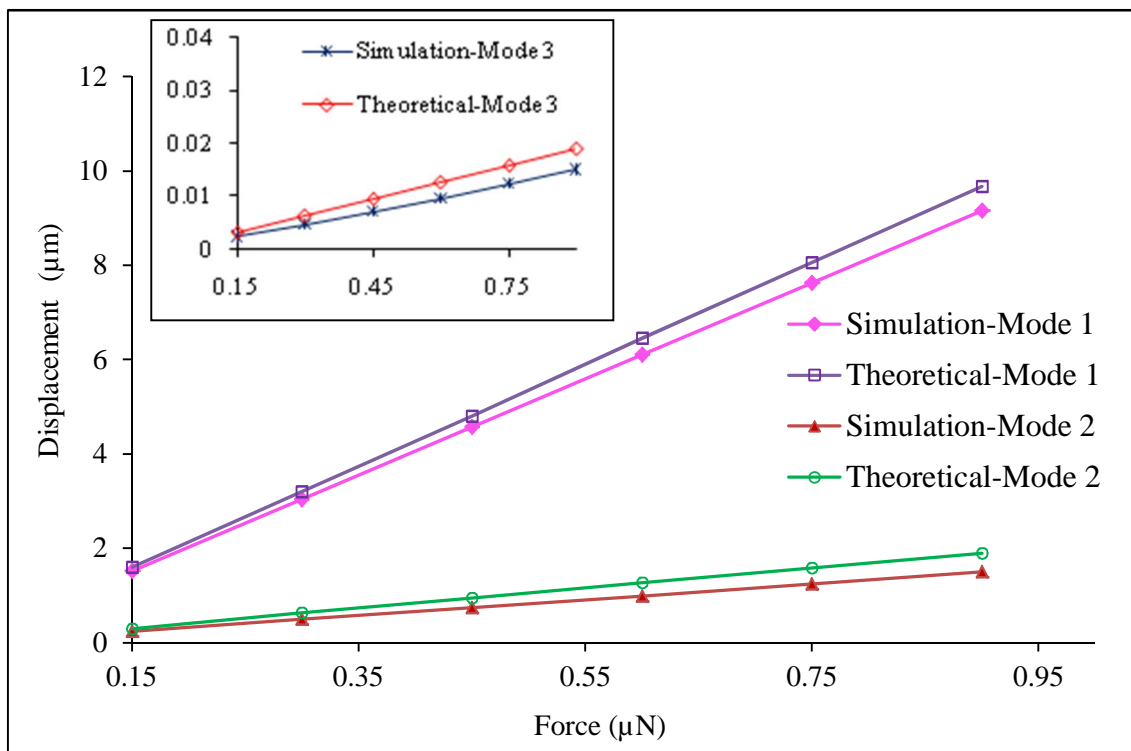
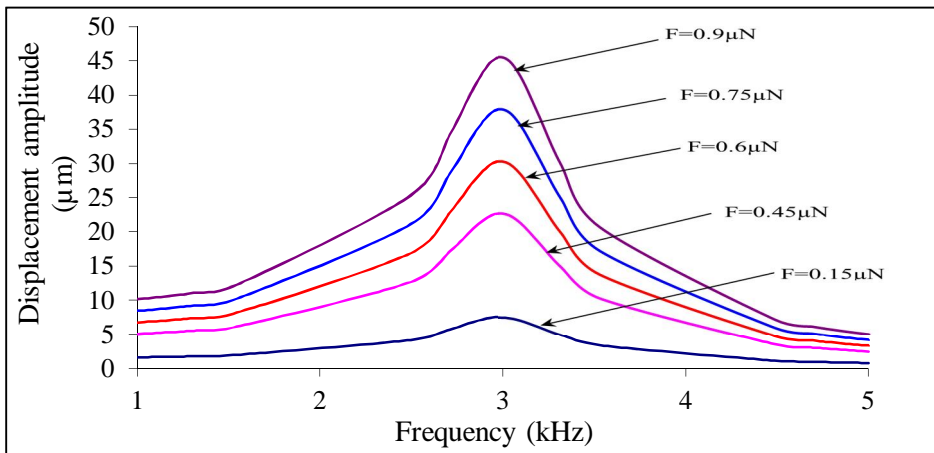


Fig 4-15 Simulation and theoretical values of the displacement as function of a constant applied force for the three modes

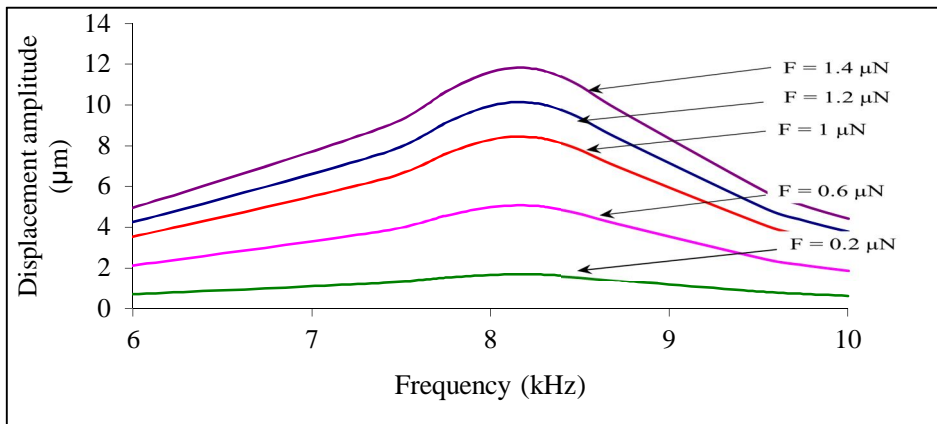
4.3.2 Dynamic mode

Figure 4.16 (a), (b) and (c) show the frequency response as function of the periodic applied force for mode 1, 2 and 3, respectively. The displacement amplitude is found to be a linear function of the applied force. Figure 4.17 shows that the simulation and theoretical values of the displacement amplitude is a linear function of the periodic applied force at the resonant frequency for the three modes.

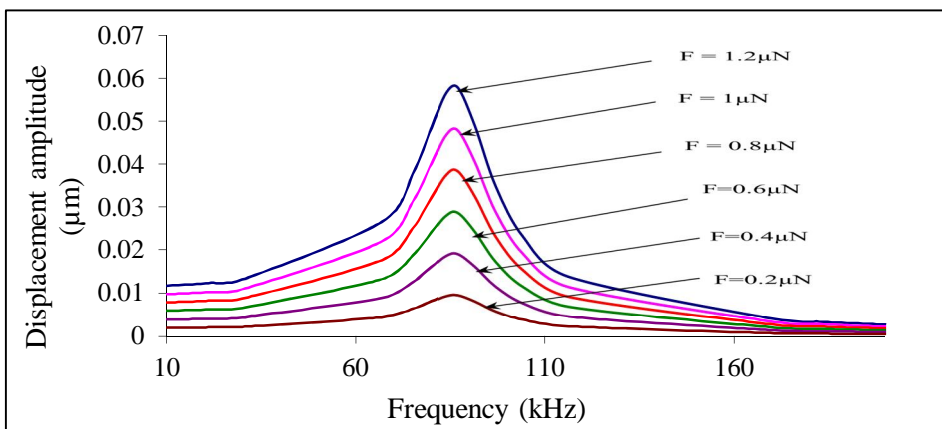
Equation 2.4 and its solution which is given in equation 2.5 were used to calculate the maximum displacement at the resonant frequency for the three modes of vibration. Furthermore, Figure 4.17 shows that the slopes of the graphs for the three modes are different being highest for mode 1 followed by mode 2 and lowest for mode 3 which indicates correspondingly highest sensitivity for mode 1 and lowest for mode 3. The calculation procedures and the actual data included in Appendix (C).



(a) Mode 1



(b) Mode 2



(c) Mode 3

Fig 4-16 Displacement amplitude versus frequency at various applied periodic force for the three modes of vibration

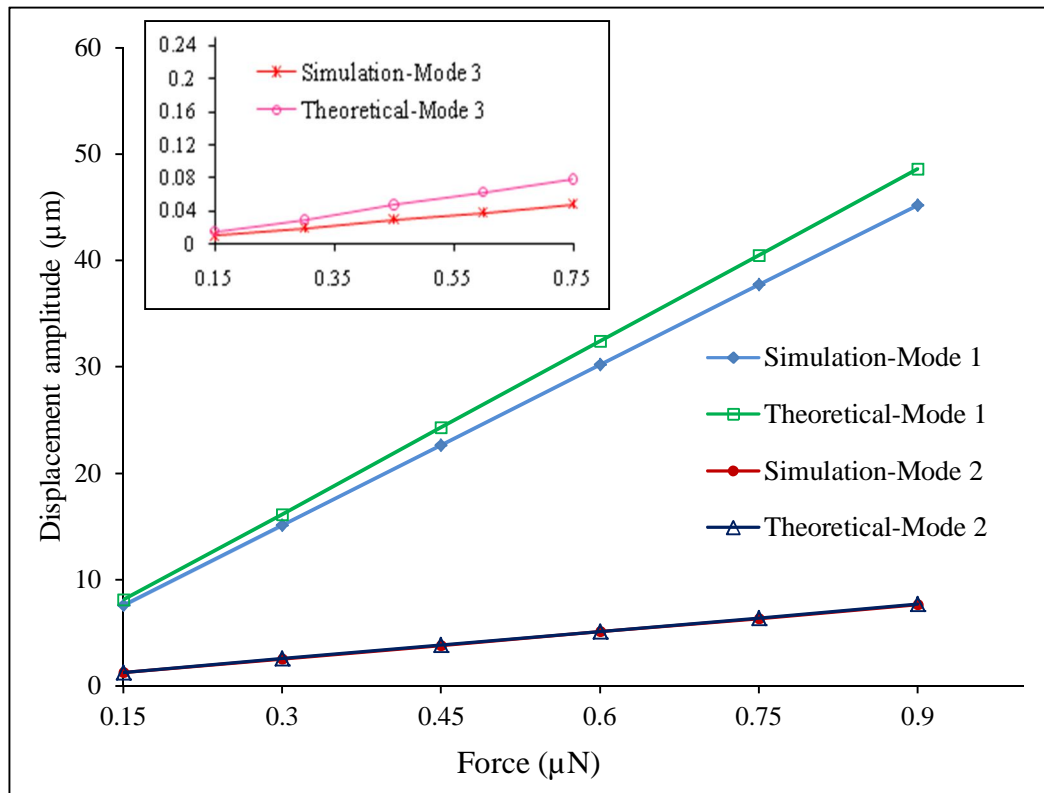


Fig 4-17 Simulation and theoretical values of the displacement amplitude at resonance frequency as function of a periodic applied force for the three modes

4.4 Mechanical quality factor

The mechanical quality factor (Q -factor) is an important parameter in this study. Its value depends on a number of parameters such as mass, stiffness and damping coefficient of a vibrating system. Figure 4.18 shows a typical frequency response of vibrating U-shaped cantilever. Using equation 2.7, the value of Δf_{-3dB} may be calculated. For example, for mode 1 the maximum displacement is about $45 \mu\text{m}$ and the $-3dB$ of this value is about $32 \mu\text{m}$ while the values for f_{res} , f_1 , and f_2 taken at $32 \mu\text{m}$ is found to be 3019.495 Hz , 2654.467 Hz and 3297.35 Hz , respectively. Therefore, Δf is found to be 632.883 Hz and the Q -factor is determined to be 4.8 . Table 4.8 shows the Q -factor determined for the three modes of vibration at same damping factor (d) of 0.1 . It is observed that the Q -factor is the same for all three modes of vibration at a given damping coefficient. The low Q -factor of 4.8 implies high energy loss in the vibration and low sensitivity due to

the big damping factor of 0.1 is considered. This value of the damping is selected just to characterize the mechanical behaviors of the system in a stable range of the displacement. The next section damping coefficient effect presents that the Q -factor depends on the damping coefficient.

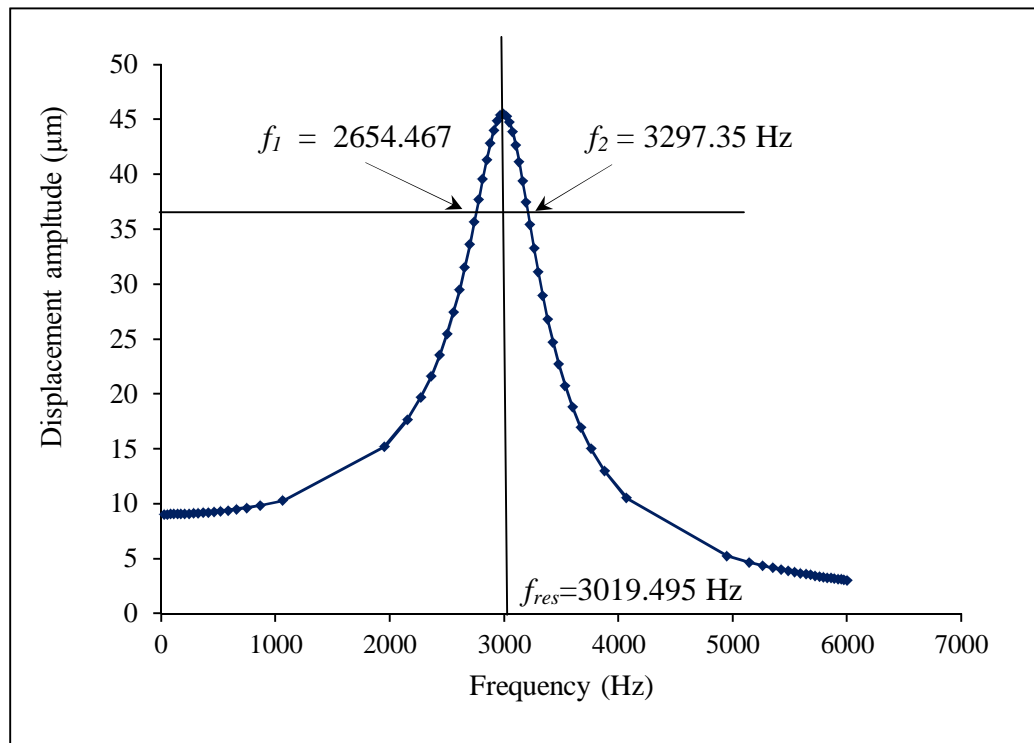


Fig 4-18 Frequency response of the cantilever and bandwidth at -3dB of the amplitude for mode 1

Table 4-8 Calculated Q -factor for mode 1, mode 2 and mode 3

Mode	f_{res} (Hz)	Δf (Hz)	Q -factor
Mode 1	3019.5	632.88	4.8
Mode 2	8244	1686.5	4.9
Mode 3	86893.7	17711	4.9

4.5 Effect of damping-coefficient

As mentioned in section 2.1.5 the damping coefficient is an important parameter for the system response at all modes of vibration. Figure 4.19 shows the displacement amplitude as a function of frequency for mode 1 at the same applied periodic force of amplitude $0.15 \mu\text{N}$ and values of the damping coefficient of 0.01, 0.05 and 0.1. As mentioned in the methodology chapter these values of the damping coefficient are selected and applied observe the effect of the damping and the motion environment on the cantilever response (maximum displacement) of vibration. The displacement amplitude at the resonant frequency is about 75.4 , 15.1 and $7.54 \mu\text{m}$ for the damping coefficients of 0.01, 0.05 and 0.1, respectively. Table 4.9 shows the values of the maximum displacement for various values of the damping coefficients for the three modes of vibration while Figure 4.20 shows the displacement amplitude as a function of the damping coefficient. It is observed that the maximum displacement decreases exponentially as the damping coefficient increases.

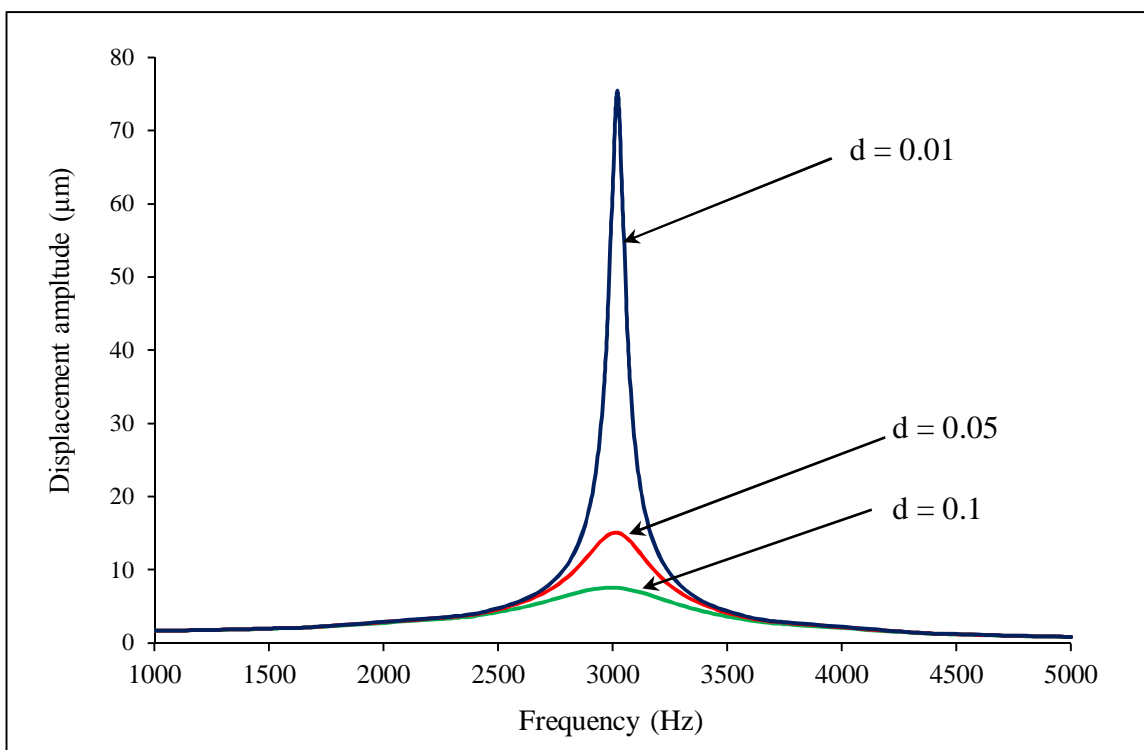


Fig 4-19 Frequency response for mode 1 at different values of the damping coefficient

Table 4-9 Maximum displacement at the resonant frequency for various values of the damping coefficient for the three modes of vibration

Damping coefficient	Maximum displacement (μm)		
	Mode 1	Mode 2	Mode 3
0.1	7.54	1.68	2.37E-03
0.08	9.44	2.10	2.97E-03
0.06	12.58	2.80	3.95E-03
0.05	15.10	3.36	4.74E-03
0.04	18.87	4.21	5.93E-03
0.02	37.75	8.41	1.18E-02
0.01	75.40	16.80	2.37E-02
0.008	94.40	21.01	2.97E-02
0.006	125.80	28.01	3.95E-02
0.005	151.01	33.02	4.74E-02
0.004	188.70	42.05	5.93E-02
0.002	377.50	84.10	1.18E-01
0.001	754.60	168.00	2.37E-01

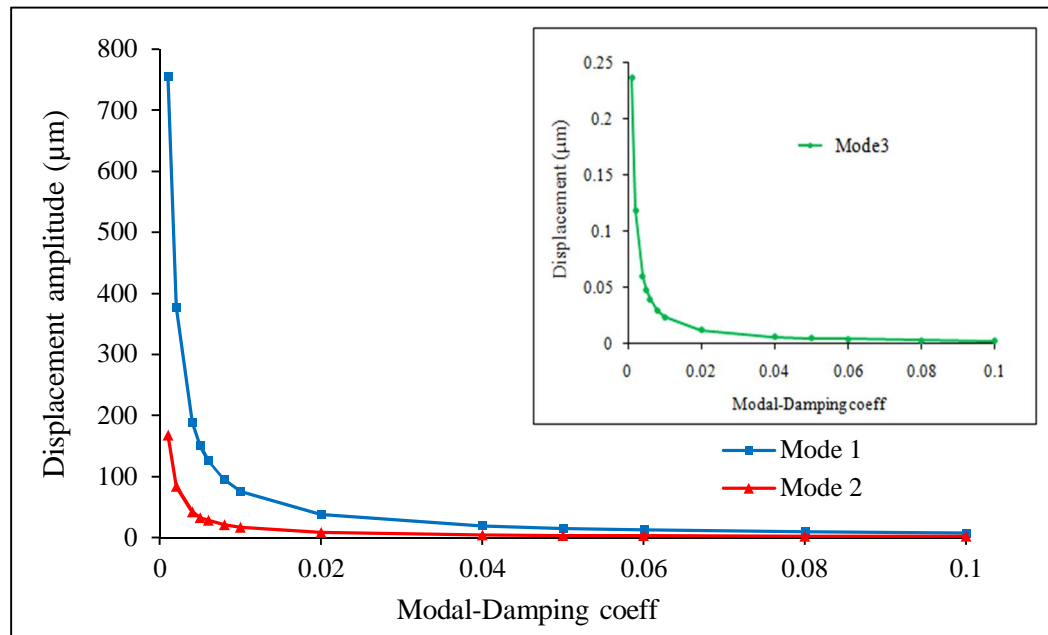


Fig 4-20 Maximum displacement at the resonant frequency versus damping coefficient for the three modes of vibration

Figure 4.19 also shows that the Q -factor of the system is dependent on the damping coefficient. The Q -factor decreases as the damping coefficient increases since the value of the bandwidth (Δf) is inversely proportional to the damping coefficient. Table 4.10 shows the value of Δf and Q -factor for the three modes of vibration at three different values of damping coefficient. Q -factor of 60 is achieved for 0.01 damping coefficient and it can be improved to ten times of this value by decreasing the damping of the vibration system.

Table 4-10 Calculated Δf and Q -factor for the three modes for various damping coefficients

Damping_coeff.	Mode 1		Mode 2		Mode 3	
	Δf	Q -factor	Δf	Q -factor	Δf	Q -factor
0.01	50	60.3	137.8	59.8	1445.82	60.1
0.05	326	9.3	858.7	9.6	9260	9.4
0.10	633	4.8	1686.5	4.9	17711	4.9

4.6 Piezoresistor transduction

A simple technique to measurement the external magnetic field is by the transduction of the deflection produced by the Lorentz force into electrical signal by using piezoresistor technology. This section simulates these transduction procedures. Figure 4.21 shows cross sectional view of a sample 100 μm length of the polysilicon piezoresistor grown in the silicon layer of the arm of the cantilever device to realize the electrical measurement.

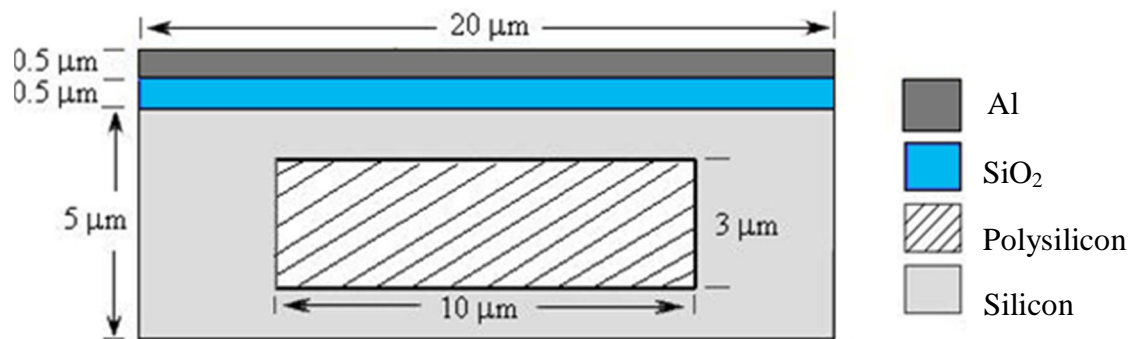


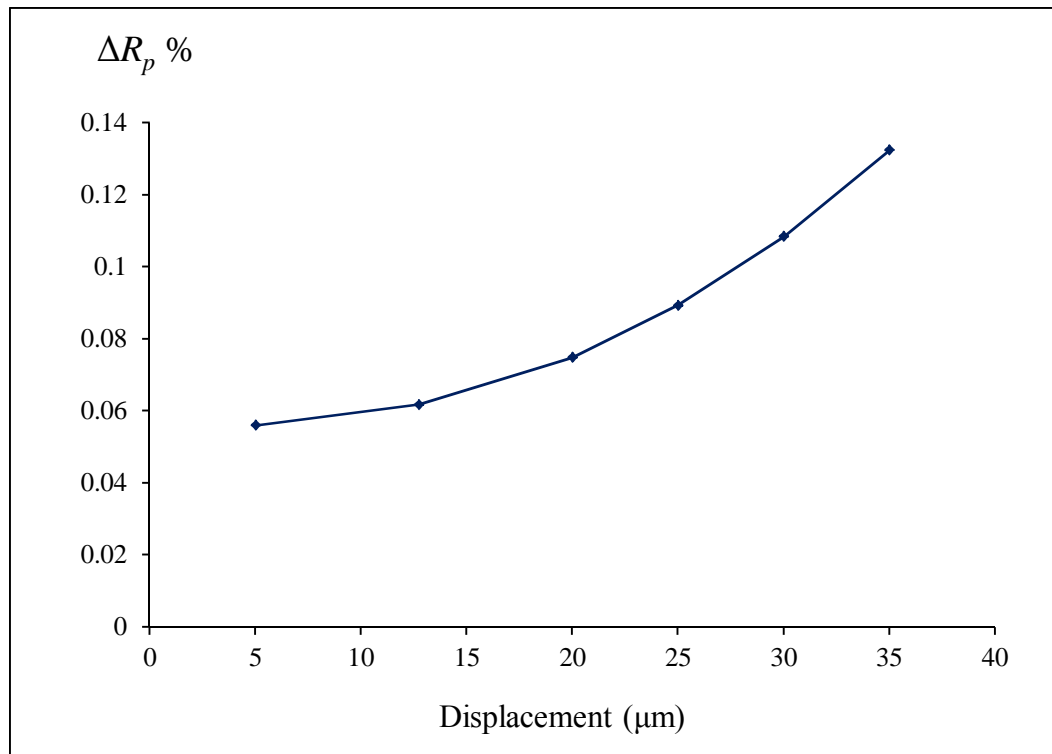
Fig 4-21 Cross sectional view of the arm of the U-shaped cantilever device with embedded polysilicon piezoresistor

4.6.1 Effect of arms deflection on Resistivity

To investigate the change in the resistance of the piezoresistor, the constant force applied to the cantilever is varied in mode 1 and the different deflections resulting recorded. The percent change in resistance (ΔR_p %) from the original value of piezoresistor resistance R_p (unstressed position of the piezoresistor) is then obtained. R_p from the simulation result for the indicated dimensions in Figure 4.23 is equal to 1709.83 Ω . Table 4.11 and Figure 4.22 show the results of ΔR_p % for different values of the cantilever deflections. It is observed that the change in resistance of the piezoresistor increases nonlinearly with increase in the displacement of the cantilever. The results agree quite well with experimental result presented by Vincent B, et al [4] and Tyler Lane [38].

Table 4-11 Simulation results of ΔR_p % for different values of the cantilever deflections

Displacement (μm)	ΔR_p %
5	5.60E-02
12.74	6.18E-02
20	7.48E-02
25	8.93E-02
30	1.08E-01
35	1.32E-01

**Fig 4-22** ΔR_p % various cantilever deflections for mode 1

The values of ΔR_p % obtain by simulation as shown in table 4.11 are used to deduce the values for ΔR_p in Ω mathematically and then to apply this change in the resistance on the

Wheatstone bridge circuit discussed in Figure 3.19 in section 3.3.6 to achieve the voltage output measurements. As mentioned in the methodology of the research, Multisim Electronic Workbench is used for the design and simulation of this electrical circuit. The simulation software will realize the output as percent values of the original (unstressed) value of the piezoresistor as given in equation 2.17. The value obtained is then used to calculate the change in the resistance in Ω by using equation 2.18. As an example, at 5 μm deflection of the cantilever in $-z$ direction in mode 1, the value of $\Delta R_p\%$ is 0.056 as shown in Table 4.11. The unstressed resistance value is calculated to be equal to 1709.83 Ω and thus ΔR_p is calculated to be 0.96 Ω . Therefore the actual resistor values for the circuit diagram of Wheatstone bridge shown in Figure 3.19 become as shown in Figure 4.23.

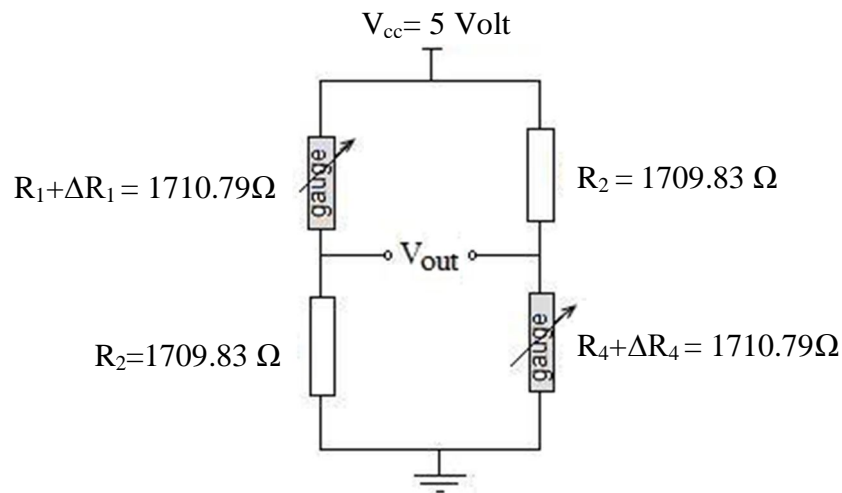


Fig 4-23 Conditioning circuit for strain gauges at 5 μm deflection of the cantilever in $-z$ direction

After simulating the circuit in the electronic workbench software, the output voltage V_{out} is found to be 1.405 mV and equation 3.2 is used to determine the calculated value to validate and compare and the values are found to be 1.4033. Table 4.13 and the Figure 4.24 show the calculated values of ΔR_p and the estimated output voltage (mV) of the measurement circuit for different values of the cantilever deflection shown in Table 4.12.

Table 4-12 Calculated values of ΔR_p (Ω) and simulation results of the voltage output for different values of the cantilever deflections

Displacement (μm)	ΔR_p (Ω)	Output voltage (mV)
5	0.96	1.403
12.74	1.057	1.545
20	1.279	1.855
25	1.535	2.243
30	1.857	2.714
35	2.257	3.298

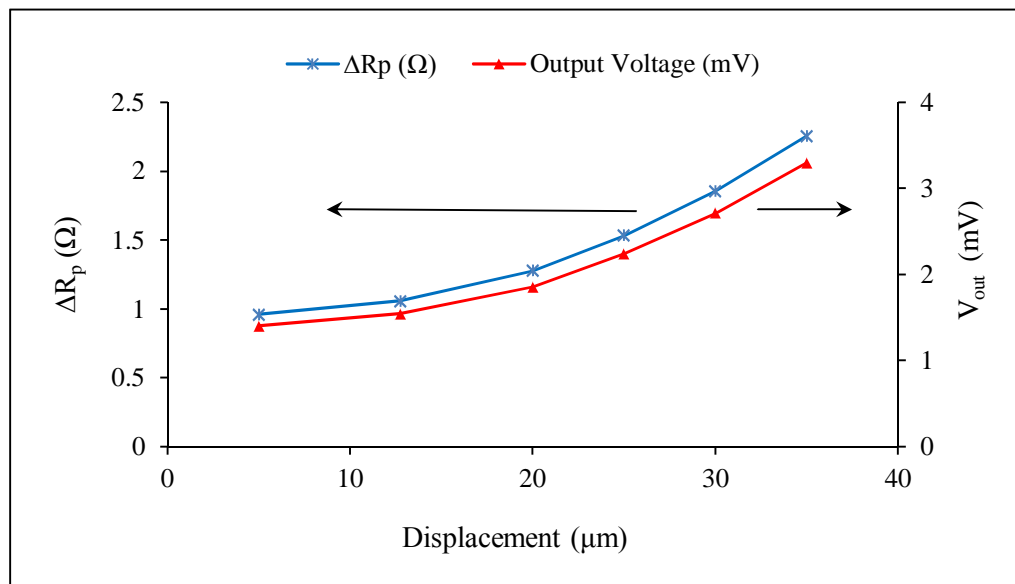


Fig 4-24 Calculated values of ΔR_p and estimated output voltage (mV) versus cantilever deflection

For a length of the base (b) of $760 \mu\text{m}$, when the cantilever is excited by 100 mA alternating current to detect an external static magnetic field of 10 mT , the force induced on the base of the cantilever in mode 1 will have amplitude of $0.74 \mu\text{N}$. This periodic force will produce a periodic deflection with a maximum displacement along the arms of the cantilever of about $12.74 \mu\text{m}$. This displacement amplitude produces a change in

resistance ΔR_p of 1.057Ω in the piezoresistive polysilicon. This value is calculated by taking ΔR_p % to be 6.18×10^{-2} % of the original value of the resistance and results in an alternating voltage with a maximum amplitude of about 1.545 mV at the resonant frequency (f_o) of 4.55 kHz for the cantilever with the given dimensions. On the other hand, for mode 2 at the same Lorentz force of 1 μ N acting on both arms of the cantilever, the displacement is about 3 μ m and the percent change (ΔR_p %) of 0.0551 % to produce 0.94 Ω and 1.3 mV output voltage. While the smallest output voltage for mode 3 is estimated to be about 0.05 μ V.

4.6.2 Sensitivity estimation

The electrical signal output of about 1.545 mV induced by the Lorentz force due to an external static magnetic field of 10 mT in mode 1 results in a sensitivity that is estimated from equation 2.19 to be 0.155 V/T. Table 4.13 compares the sensitivity of the system for the three modes. The output voltage (V_{out}) calculated in this study is obtained directly from the Wheatstone bridge. However, due to the low signal level available across the gauges, on-chip amplification with very high gain of up to 1000 times and low noise is required [10, 31]. The different values of the ΔR_p % and sensitivity are compared in Figure 4.25 for three different values of the piezoresistor thickness based on the thickness of the cantilever beam. Vincent B, et al [46] reported that they observed 14 mV/T static sensitivity and 530 $mV_{r.m.s}/T$ dynamic sensitivity for mode 1 but for the different dimensions of the cantilever and piezoresistor transducers.

Table 4-13 Sensitivity for mode 1, mode 2 and mode 3

Type of the mode	Sensitivity (V/T)
Mode 1	0.155
Mode 2	0.13
Mode 3	0.05×10^{-3}

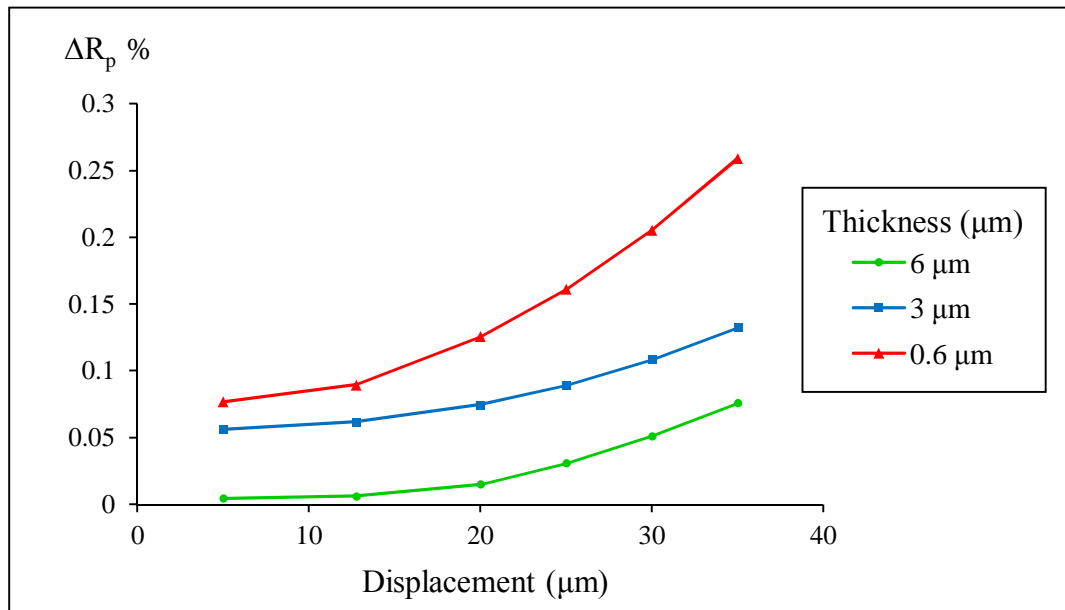


Fig 4-25 Simulated values of ΔR_p % various cantilever deflections for various beam thickness

It is noted that the graph is not linear and it is largest, indicating highest sensitivity, for small thicknesses. Table 4.14 presents the comparison of piezoresistor resistance and resonant displacement and the percentage change of the resistance for three different thicknesses of the U-shaped cantilever and the embedded piezoresistor when the same force is applied to the cantilever (mode 1) corresponding to Lorentz force at the 10 mT of the external magnetic flux. Table 4.15 shows the theoretically determined sensitivities.

Table 4-14 Simulation results showing changes in various parameters for different thicknesses of the piezoresistor

Thickness of Si beam (μm)	Thickness of piezoresistor (μm)	resistance (Ω)	Resonant Frequency (kHz)	Maximum displacement (μm)	ΔR_p %
2	0.6	5557	2.117	117.6	2.50
5	3	1709.83	4.55	12.74	6.1759E-2
9	6	570	8	2.5	1.9002E-2

Table 4-15 Calculated values of the voltage output and the sensitivity for difference thickness of piezoresistor

Thickness of piezoresistor (μm)	voltage output (mV)	sensitivity (V/T)
0.6	63.5	6.4
3	1.55	0.16
6	0.49×10^{-3}	0.05×10^{-3}

As mentioned in section 4.6.2 due to the low signal level available across the gauges, amplification circuit with a high gain can be used after the Wheatstone bridge circuit.

As a summary, the highest value of the percent change in resistance (ΔR_p) % is obtained at the highest displacement of the cantilever when the cantilever is driven at the resonant frequency. Experimental work by Laurent Latorre, et al in [50] agree with these results just for mode 1.

Chapter 5

CONCLUSION AND RECOMMENDATIONS

5.1 CONCLUSION

This chapter presents the main purpose of the study and major conclusions from the progress achieved. This is followed by the limitation of the study and finally some recommendations are given for future research.

The purpose of this study is to design and characterize a MEMS-based U-shaped cantilever device capable of detecting magnetic fields from static to low frequency. Analytical models describing 3-D vibration modes for U-shaped cantilever devices that are actuated by the Lorentz force and their verification by simulation is discussed. It is shown that when the cantilever is driven at or near its natural frequency by a periodic force, a large displacement is realized as compared to a static force for both modes. The results obtained indicated static sensitivities of 10.1, 1.67 and $12 \times 10^{-3} \mu\text{m}/\mu\text{N}$ while the resonant sensitivities are about five times the static sensitivity with values of 50.2, 8.33 and $48.3 \times 10^{-3} \mu\text{m}/\mu\text{N}$ for mode 1, mode 2 and mode 3, respectively. This high response of the device in the dynamic mode is useful for increasing sensitivity in the measurement of an external magnetic field.

Results show that the resonant frequency is directly proportional and the sensitivity inversely proportional to the thickness of the cantilevers for mode 1 and 2 while they are independent of the thickness for mode 3. However unlike mode 1 and 2, the resonant frequency in mode 3 increases with increasing width of the U-shaped cantilever. The theoretically calculated values for the resonant frequencies in all modes agree quite well with the simulation results. Three quality factors are determined according to the type of the mode and the damping coefficient. When the selected three values of the damping coefficient of 0.1, 0.05, and 0.01 of the critical damping is applied, Q -factors of 4.9, 9.3 and 60 for modes 1, 2 and 3, respectively, are realized.

The graph of displacement as a function of the applied force is shown to be perfectly linear in both the static and dynamic situations. The percentage change in resistance, $\Delta R_p\%$, of a polysilicon peizo-resistor is found to be proportion to the cantilever deflections. The estimated sensitivity from the output voltage of a Wheatstone bridge circuit setup for thicknesses of the cantilever of 6, 3, and 0.6 μm is found to be about 0.06, 0.16, and 64 V/T respectively.

5.2 Recommendations and Limitations of Research

Some important issues are not covered in this research such as the elastic limit of the cantilever for the three modes of vibration. Thus, the maximum range of the measurement of the magnetic flux under detection is not determined.

This research investigated three modes of vibration for an external magnetic field that is perpendicular to the current through the cantilever. And the angel (θ) in equation 2.1 is equal to 90 thus $\sin \theta$ is equal to 1. However if the magnetic field is diagonal to the currents in any or all of the three modes of vibration, the situation will be a combination between two or the three modes described and characterized in this research.

In the last part of this research piezoresistor transducers are demonstrated as a simple method for the measurement without going into details of how it will be applied to the U-shaped cantilever. There is need to do an in-depth study of the amplification and conditioning circuits and investigate the effect of some parameters such as the ambient temperature on the sensitivity of the system. Also there are some materials which are more sensitive and have higher gauge-factor compared to polysilicon such as lead-Zirconate Tetanate, it can be use for the small magnetic field under detection.

The motion of the base has also not been exhaustively treated for the observed submodes of mode 3 that depends on whether the based is static or in motion. The optical readout method of measurement may be useful to determine the type of mode and thus the direction of the external magnetic field especially for the combined modes. It is also possible to design smart circuit consisting of piezoresistor transducers in various configurations to determine the magnitude and direction of a magnetic field by matching the frequency of the excitation current with the resonant frequency value and then tracking which mode of vibration is excited.

REFERENCES

- [1] T. Thundat, E. A. Wachter, S. L. Sharp and R. J. Warmack, "Detection of mercury vapour using resonating microcantilevers," *Appl. Phys. Lett.* vol. 66, pp1695-1697, 1995.
- [2] N. Nugaeva, K. Y. Gfeller, N. Backmann, H. P. Lang, M. Duggelin and M. Hegner "Micromechanical cantilever array sensors for selective fungal immobilization and fast growth detection," *Journal of Biosensors and Bioelectronics-ELSEVIER*, vol. 21, pp. 849–856, 2005.
- [3] J. Bausells "Micro- and nano-electromechanical systems for [bio] molecular analysis," Institut d'Estudis Catalans, Barcelona *Contributions to Science*, 3 (1), pp. 67–78, 2005.
- [4] B. Vincent, B. Yves, L. Laurent and N. Pascal, "Monolithic piezoresistive CMOS magnetic field sensors," *Sensors and Actuators A*, vol.103, pp. 32-23, 2003.
- [5] L. Latorre, V. Beroulle and P. Nouet, "Design of CMOS MEMS Based on Mechanical Resonators Using a RF Simulation Approach," *IEEE transactions on computer-aided design of integrated circuits and systems*, vol. 23, pp. 962-967, 2004.
- [6] Z. Djuric, I. Jokic, M. Frantlovic, D. Randjelovic, D.V. Radovic, M. Smiljanic and Z. Lazic, "Fabrication and Characterization of AFM Golden Microcantilevers and Measurement of Small Electromagnetic Forces," *26th International Conference on MICROELECTRONICS (MIEL 2008)*, 2008.
- [7] A. Agoston, F. Keplinger and B. Jakoby, "Evaluation of a vibrating micromachined cantilever sensor for measuring the viscosity of complex organic liquids," *Sensors and Actuators A* 123–124 pp. 82–86, 2005.
- [8] P.I. Oden, G. Y. Chen, R. A. Steele, R. J. Warmack and T. Thundat, "Viscous Drag Measurement Utilizing Microfabrication Cantilevers," *Appl. Phys. Lett.*, vol. 68, pp. 3814-3816, 1996.

- [9] R. Berger, C. Gerber, H. P. Lang and J. K. Gimzewski, "Micromechanics: a toolbox for femtoscale science: towards a laboratory on a tip," *Microelectron. Eng.*, vol. 35, pp. 375-379, 1997.
- [10] N. Dumas, L. Latorre and P. Nouet "Low noise CMOS amplifier for a piezoresistive magnetic field sensor," *18th Conference on Design of Circuits and Integrated Systems (DCIS'03)*, Ciudad Real, Spain, pp. 639-644, 2003.
- [11] J. Fritz, M. K. Baller, H. P. Lang, H. Rothuizen, P. Vettiger, E. Meyer, H. J. Güntherodt, Ch. Gerber and J. K. Gimzewski, "Translating Biomolecular Recognition into Nanomechanics," *Science* 288, pp. 316-318, 2000.
- [12] O. Enders, F. Korte and H. A. Kolb, "Lorentz-force-induced Excitation of Cantilevers for Oscillation-mode Scanning Probe Microscopy," *Surf.InterfaceAnal.*, vol. 36, pp. 119-123, 2004.
- [13] L. Voiculescu, M. E. Zaghoul, R. A. McGill, E. J. Houser and G. K. Fedder, "Electrostatically Actuated Resonant Microcantilever Beam in CMOS Technology for the Detection of Chemical Weapons," *IEEE, Journal of SENSOR*, vol. 5, pp. 641-647, 2005.
- [14] F. Keplinger, R. Beigelbeck and F. Kohl, "Simultaneous Measurement of Two Magnetic Field Components Using a U-Shaped Cantilever Device," *3rd IEEE Conference on Sensors*, pp. 1450-1453, 2004.
- [15] R. Holzer, I. Shimoyama, and H. Miura, "Lorentz Force Actuation of Flexible Thin-Film Aluminum Microstructures", *Proc.IEEE-RSJ Intelligent Robots and Systems*, vol. 2, pp. 156-161, August, 1995.
- [16] F. Keplinger, S. Kvasnica, A. Jachimowicz, F. Kohl, J. Steurer and H. Hauser "Lorentz force based magnetic field sensor with optical readout," *Journal of Sensors and Actuators- ELSEVIER*, A 110, pp. 112-118, 2004.
- [17] D. Lange, O. Brand and H. Baltes, *CMOS Cantilever Sensor Systems- Atomic Force Microscopy and Gas Sensing Application*. springer, Verlag Berlin Heidelberg New York, 2002.

- [18] Å. Forslund, "Designing a Miniaturized Fluxgate Magnetometer," MSc. Thesis in Physical Electro technology Stockholm, April 2006.
- [19] R. L. Reese, *University Physics*. London, England: A Division of International Thomson Publishing Inc: 2000.
- [20] A. Hieriemann, *Integrated Chemical Microsensor Systems in CMOS Technology*. springer, Verlag Berlin Heidelberg New York, 2005.
- [21] L. Latorre, P. Nouet, Y. Bertrand, Ph. Hazard and F. Pressecq, "Characterization and modeling of a CMOS-compatible MEMS technology," *Sensors and Actuators* vol. 74 pp 143–147, 1999.
- [22] V. Berouille, Y. Bertrand, L. Latorre and P. Nouet, "Test and Testability of a Monolithic MEMS for Magnetic Field Sensing," *Journal OF ELECTRONIC TESTIN*, Theory and Applications 17, 439–450, 2001.
- [23] A. Gupta, R. Bashir, G. W. Neudeck, and M. McElfresh, "Design of Piezoresistive Silicon Cantilevers with Stress Concentration Region (SCR) for Scanning Probe Microscopy (SPM) Applications," *International Conference on Modeling and Simulation of Micro systems (MSM)*, pp 617-620, 2000.
- [24] Franz Keplinger, Samuel Kvasnica, Hans Hauser "Micro Machined Sensor for Measuring High Magnetic Fields," *16th European Conference on Solid-State Transducers, Magnetic sensor* pp 1225-1228, 2002.
- [25] www.coventorware.com, valid at 12/7/2008.
- [26] Shyam Aravamudhan, Shekhar Bhansali "Reinforced piezoresistive pressure sensor for ocean depth measurements," *Journal of Sensors and Actuators- ELSVEIR*, A 142, pp111–117, 2008.
- [27] M. Elwensspoek, R. wiegerink, *Mechanical microsensors*. springer, Verlag Berlin Heidelberg New York, 2001.
- [28] L. Meirovitch, *Fundamentals of Vibrations*, McGraw Hill, USA, 2001.

- [29] J. S. Walker, *Physics*. Prentice Hall, Upper Saddle River, New Jersey, pp. 380-414, 2002.
- [30] P. Hagedorn, A. D. Gupta, *Vibration and Waves in Continuous Mechanical Systems*. Wiley, England, 2007.
- [31] E. Boujamaa, Y. Soulie, F. Maily, L. Latorre and P. Nouet, "Rejection of Power Supply Noise in Wheatstone Bridges Application to Piezoresistive MEMS," *Proc. of DTIP of MEMS & MOEMS*, Rome, Italy, 2008.
- [32] J. Hung and H. Hocheng, "Resonance Frequency of Polysilicon Microcantilever Beam of Various Dimensions and Root Geometry," *International Workshop on Nanomechanical Cantilever Sensors*, Max-Planck Institute for Polymer Research, Mainz, Germany, 2008.
- [33] R. S. Fearing "Powering 3-Dimensional Microrobots: Power Density Limitations," *Tutorial on Micro Mechatronics and Micro Robotics, University of California*, September 27, 1998.
- [34] Raphael H, Isao S, Hirofumi M, "Hybrid Electro static-Magnetic Microactuators," *IEEE, ICRA*, pp2941-2946, 1995.
- [35] P. Attian and P. Herto "Dependence of the resonant frequency of mocomachined gold microbeams on polarisation voltage," *Journal of microelectronics - ELSEVIER*, vol. 29, pp 543-546, 1998.
- [36] N. Dumas, L. Latorre and P. Nouet, "Low noise CMOS amplifier for a piezoresistive magnetic field sensor", *18th Conference on Design of Circuits and Integrated Systems(DCIS'03)*, Ciudad Real, Spain, pp 639-644, 2003.
- [37] C. H. Edwards and D. E. Penney, *Differential Equations Computing and Modeling*. Second edition, publisher-Prentice Hall, USA, 2000.
- [38] T. L. Waterfall "Design of Piezoresistive MEMS Force," Thesis-Master of Science, University of Brigham Young, 2006.

- [39] G. Villanueva, J.A. Plaza, J. Montserrat, F. Perez-Murano and J. Bausells “Crystalline Silicon Cantilevers for Piezoresistive Detection of Biomolecular Forces” *Microelectronic Engineering*, vol. 85, pp1120-1123, 2008.
- [40] G. Villanueva, J. Montserrat, F. P_erez-Murano, G. Rius and J. Bausells “Submicron piezoresistive cantilevers in a CMOS-compatible technology for intermolecular force detection” *Microelectronic Engineering*, vol. 73-74, pp 480-486, 2004.
- [41] X. Yu, J. Thaysen, O. Hansen, and A. Boisen “Optimization of sensitivity and noise in piezoresistive cantilevers” *Journal of applied physics*. vol. 92, pp. 6296-6301 Num. 10, 2002.
- [42] M. Gad-el-Hak, *MEMS-Application*. Second edition, crcpress Taylor & Francis, New York, 2006.
- [43] H. Baltes, O. Brand, G. K. Fedder, C. Hierold, J. G. Korvink and O. Tabata, *MEMS-CMOS, advanced micro & nanosystem*. WILEY-VCH, Weinheim, Germany. vol 2, 2005, pp 1-68.
- [44] S. Franssila, *Introduction to micro fabrication*. WILY, England, 2004.
- [45] F. Keplinger, R. Beigelbeck, F. Kohl, S. Kvasnica , A. Jachimowicz , and B. Jakoby, “Frequency and Transient Analysis of Micromachined U-shaped Cantilever Devices for Magnetic Field Measurement,” *13th International Conference on Solid State Sensors, Actuators and Microsystems*, pp 630-635, 2005.
- [46] V. Beroulle, Y. Bertrand, L. Latorre and P. Nouet “Micromachined CMOS magnetic field sensors with low-noise signal conditioning,” *IEEE international conference on micro electro mechanical system*, pp. 256-259, 2002.
- [47] Information is available on the World Wide Web at the following address: <http://cmp.imag.fr>, valid at 1/7/2009.
- [48] J. M. Karam, B. Courtois, and J. M. Paret, “Microelectronics Compatible Manufacturing Techniques of Microsystems,” *Mechatronics’ 96*, Besancon, France, 1996.

- [49] K. Brueckner, Ch. Förster, K. Tonisch, V. Cimalla, O. Ambacher, R. Stephan, K. Blau, and M. A. Hein “Electromechanical Resonances of SiC and AlN Beams under Ambient Conditions,” *13th GAAS[®] Symposium – paris*, pp585-588, 2005.
- [50] L. Latorre and P. Nouet “A complete Methodology for Electro-Mechanical Characterization of a CMOS Compatible MEMS Technology,” *IEICE TRANS. ELECTRON NO.4*, vol. E82-C, pp 582-588, 2009.

APPENDIX-A

Actual data of some graphs in the results chapter

Table 1 actual data of the simulation results of the frequency response for the cantilever deflection (mode 1) presented in figure (4.4.a)

Frequency (Hz)	Displacement (μm)
121.3170	9.0742
268.6191	9.1307
462.9312	9.2734
783.9097	9.6997
2235.4819	19.0538
2556.4604	27.4620
2750.7724	36.3548
2898.0747	43.6648
3019.3916	45.2995
3179.3298	38.2251
3373.5251	27.1200
3629.6960	17.9086
4052.8574	10.7159
5966.5341	3.0904
6389.6958	2.5855
6645.8666	2.3411
6840.0620	2.17958
7000	2.05942

Maximum displacement
at resonant frequency

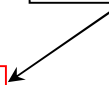


Table 2 the simulation results table of the frequency response for the cantilever deflection (mode 2) presented in Figure (4.5.a)

Frequency (Hz)	Displacement (μm)
2000	2.1419
2250.9150	2.1773
2555.5739	2.2279
2957.4616	2.3088
3621.3286	2.4864
6623.5556	5.1849
7287.4223	7.1769
7689.3100	8.8735
7993.9692	9.9455
8244.8837	10.0930
8516.2998	9.2957
8845.8505	7.6918
9280.5742	5.7798
9998.6816	3.8123
13246.2021	1.2510
13964.3095	1.0629
14399.0332	0.9707
14728.5839	0.9092
15000	0.8632

Maximum displacement
at resonant frequency

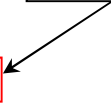


Table 3 the simulation results table of the frequency response for the cantilever deflection (mode 3) presented in Figure (4.6.a)

Frequency (Hz)	Displacement (μm)
10000	0.0117
13089.5361	0.0118
21789.2949	0.0123
29963.5351	0.0130
66930.1796	0.0265
75104.4140	0.0377
80052.8906	0.0485
83804.1796	0.0563
86893.7109	0.0578
91438.2421	0.0489
96956.1718	0.0348
104235.0937	0.0231
116258.9375	0.0138
170634.7656	0.0040
182658.6093	0.0033
189937.5312	0.0030
195455.4687	0.0028
200000	0.0026

Maximum displacement
at resonant frequency




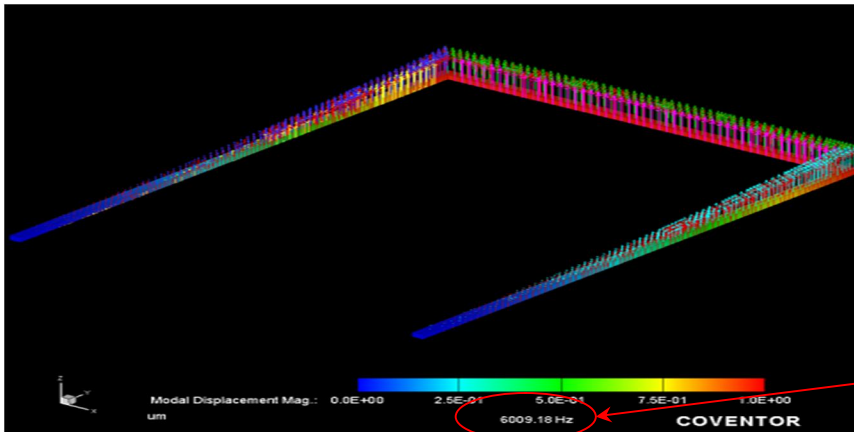
Table 4 the simulation results table of the frequency response for the cantilever deflection (mode 1) for calculation of the band width and Q-factor presented in Figure (4.22)

Displacement (μm)	Frequency (Hz)
9.0599	26.2618
9.0620	53.4879
9.0658	81.7719
9.0713	111.2232
9.0789	141.9700
9.0889	174.1650
9.1016	207.9919
9.1174	243.6745
9.1370	281.4906
9.1612	321.7906
9.1908	365.0279
9.2274	411.8043
9.2728	462.9470
9.3299	519.6445
9.4033	583.7063
9.5011	658.1216
9.6389	748.4761
9.8553	867.6663
10.3118	1064.553
15.2236	1954.941
17.6814	2151.828
19.71	2271.019
21.6357	2361.373
23.5477	2435.788
25.4837	2499.850
27.4601	2556.548
29.4803	2607.690
31.5369	2654.467
33.6116	2697.704
35.6743	2738.004
37.6833	2775.820
39.5856	2811.503
41.3196	2845.330
42.8208	2877.525

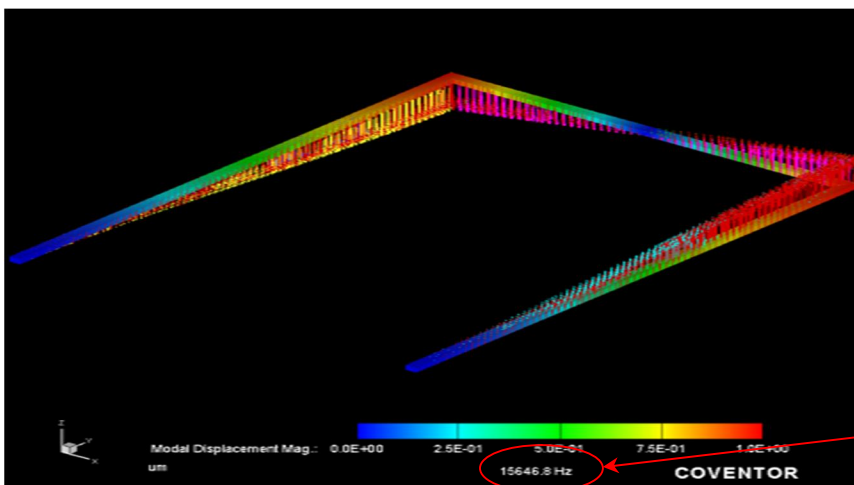
f_1

44.0287	2908.271	
44.8955	2937.723	
45.3939	2966.007	
45.2964	3019.495	← Resonant frequency f_{res}
44.7476	3045.417	
43.8638	3072.292	
42.6574	3100.211	
41.1600	3129.282	
39.4182	3159.631	
37.4876	3191.411	
35.4258	3224.801	
33.2867	3260.023	
31.1170	3287.350	← f_2
28.9534	3337.130	
26.8226	3379.809	
24.7413	3425.981	
22.7173	3476.464	
20.7499	3532.429	
18.8293	3595.664	
16.9344	3669.118	
15.0234	3758.306	
13.0019	3875.957	
10.5285	4070.302	
5.2727	4949.193	
4.6890	5143.538	
4.3858	5261.188	
4.1768	5350.376	
4.0167	5423.831	
3.8868	5487.065	
3.7774	5543.031	
3.6830	5593.513	
3.6000	5639.686	
3.5260	5682.364	
3.4592	5722.144	
3.3984	5759.472	
3.3426	5794.694	
3.2910	5828.084	
3.2431	5859.863	
3.1985	5890.213	
3.1566	5919.28	
3.1172	5947.203	
3.0449	6000.001	

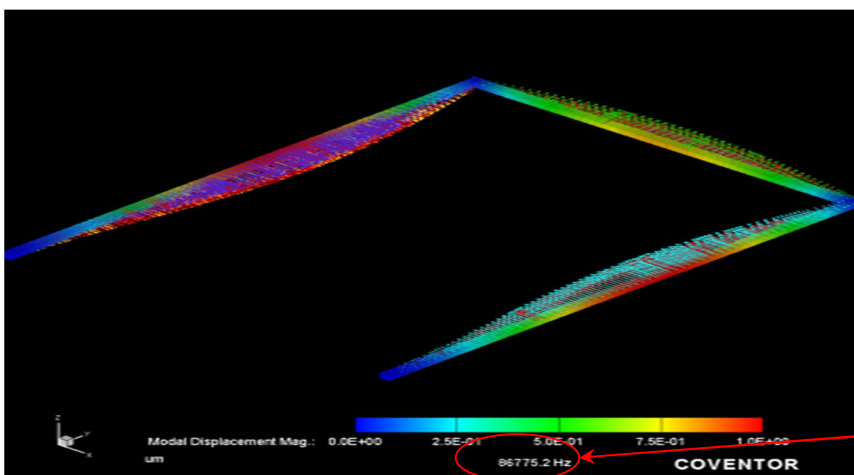
Pictures of some results presented on chapter-4



(a) Mode 1

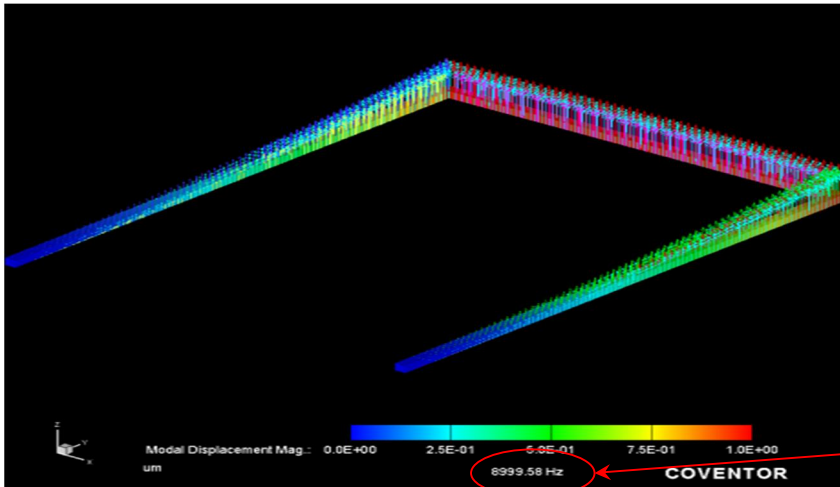


(b) Mode 2



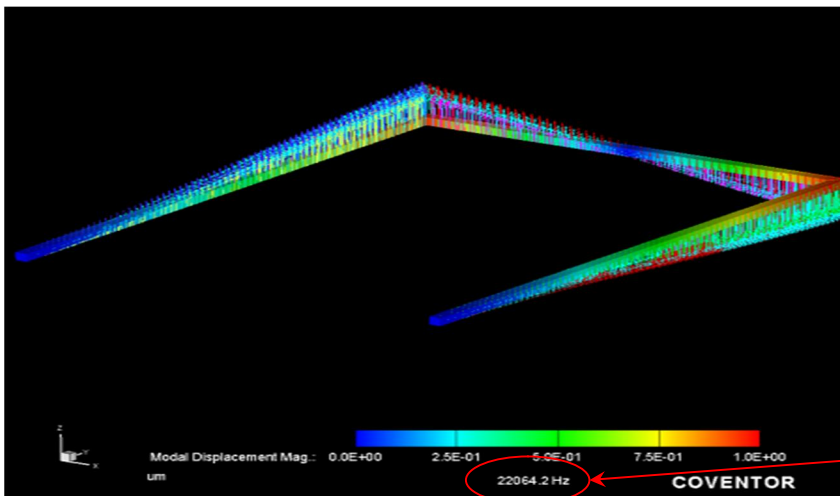
(c) Mode 3

Vector representation of the displacement of a 10 μm thickness U-shaped cantilever for (a) mode 1, (b) mode 2 and (c) mode 3, presented in section 4.1.2



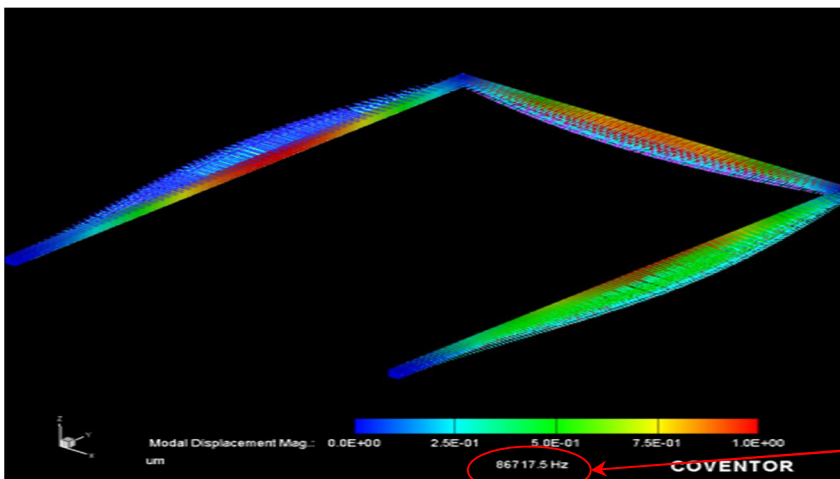
(a) Mode 1

The value of resonant frequency 8999.58 Hz



(b) Mode 2

The value of resonant frequency 22064.2 Hz



(c) Mode 3

The value of resonant frequency 86717.5 Hz

Vector representation of the displacement of a 15 μm thickness U-shaped cantilever for (a) mode 1, (b) mode 2 and (c) mode 3, presented in section 4.1.2

Calculation procedures for validation of the simulation results

Samples of the calculation procedure of the modeling results validation to the simulation results presented in this thesis:

Modeling of the resonant frequency

The effect of the cantilever dimensions on the resonant frequency of the three modes of the cantilever vibration presented in section 4.2.1, 4.2.2 and 4.2.3 for the effect of the thickness h , width w , length of the arm l and base b respectively.

To obtain the results in table 4.2 following actual values are used:

$$E = 70 \times 10^9 \text{ pa}, \rho = 2.3 \times 10^{-15} \text{ kg}/\mu\text{m}^3,$$

$$h = 5 \mu\text{m}, w = 20 \mu\text{m}, b = 760 \mu\text{m} \text{ and } l = 980 \mu\text{m}$$

are substituted in equation (3.10) to calculate the resonant frequency for mode 1 as follows:

$$\begin{aligned} f_0 &= \frac{1}{2\pi} \sqrt{\frac{(70 \times 10^9 \text{ pa}) \times (5 \times 10^{-6} \text{ m})^2}{2(2.3 \times 10^{-15} \times 10^6 \text{ kg/m}) \times (980 \times 10^{-6} \text{ m})^3 (760 \times 10^{-6} \text{ m}/2 + 980 \times 10^{-6} \text{ m})}} \\ &= 2.8 \text{ kHz} \end{aligned}$$

And equation (3.12) is used to obtain the resonant frequency for mode 2

$$\begin{aligned} f_0 &= \frac{1}{2\pi} \sqrt{\frac{(70 \times 10^9 \text{ pa}) \times (5 \times 10^{-6} \text{ m})^2}{(2.3 \times 10^{-15} \times 10^6 \text{ kg/m}) \times (720 \times 10^{-6} \text{ m})^3 (760 \times 10^{-6} \text{ m}/2 + 980 \times 10^{-6} \text{ m})}} \\ &= 6.163 \text{ kHz} \end{aligned}$$

While equation (3.14) is used to calculate the resonant frequency of mode 3a then multiplied the value by the factor of $(1.0574 \times b/l)$ as discussed in section 4.2.4

$$f_0 = \frac{1}{2\pi} \sqrt{\frac{192Ew^2}{12\rho l^4}} = \sqrt{\frac{192(70 \times 10^9 \text{ pa}) \times (20 \times 10^{-6} \text{ m})^2}{12(2.3 \times 10^{-15} \times 10^6 \text{ kg/m}) \times (980 \times 10^{-6} \text{ m})^4}}$$

$$= 104 \text{ kHz}$$

And for these dimensions the correction factor is $1.0574 \times (760/1000) = 0.8$.

And the resonant frequency $104 \times 0.8 = 83.2 \text{ kHz}$

Modeling of the linearity

Section discusses the linear relationship between the applied force and the cantilever deflection for the three modes at the static motion and dynamic vibration presented in Figures (3.15), (3.16) and (3.17)

Static linearity

Using equations 3.9 the stiffness of the cantilever is calculated for mode 1

$$E = 70 \times 10^9 \text{ pa}, \quad \rho = 2.3 \times 10^{-15} \text{ kg}/\mu\text{m}^3,$$

$$h = 5 \mu\text{m}, \quad w = 20 \mu\text{m}, \quad b = 720 \mu\text{m} \quad \text{and} \quad l = 980 \mu\text{m}$$

$$k = \frac{70 \times 10^9 \text{ pa} \times (5 \times 10^{-6} \text{ m})^3 \times (20 \times 10^{-6} \text{ m})}{2(980 \times 10^{-6} \text{ m})^3}$$

$$= 0.093$$

Equation 3.11 used to calculate stiffness of mode 2

$$k = \frac{70 \times 10^9 \text{ pa} \times (5 \times 10^{-6} \text{ m})^3 \times (20 \times 10^{-6} \text{ m})}{(720 \times 10^{-6} \text{ m})^3}$$

$$= 0.47$$

Equation 3.13 used to calculate stiffness of mode 3

$$k = \frac{192 \times 70 \times 10^9 \text{ pa} \times (5 \times 10^{-6} \text{ m}) \times (20 \times 10^{-6} \text{ m})^3}{12(980 \times 10^{-6} \text{ m})^3}$$

$$= 47.6$$

The displacement calculated using equation (2.3) $u = \frac{F}{k}$

The table below presents the comparison of the calculation and simulation result of the displacement vs static applied force for the three modes witch presented in Figure (3.15).

Applied force (μN)	Displacement (μm)					
	Mode 1		Mode 2		Mode 3	
	Simulation	Theoretical	Simulation	Theoretical	Simulation	Theatrical
0.15	1.52	1.6	0.25	0.3	0.0024	0.0031
0.3	3.04	3.2	0.5	0.63	0.0048	0.0063
0.45	4.57	4.8	0.743	0.95	0.0072	0.0094
0.6	6.1	6.45	0.99	1.27	0.0097	0.0126
0.75	7.62	8.06	1.25	1.59	0.0125	0.0157
0.9	9.15	9.67	1.5	1.9	0.015	0.0189

Dynamic linearity at the resonant frequency

Equation 2.4 and its solution which is given in equation 2.5 were used to calculate the maximum amplitude of the displacement at the resonant frequency for the three modes of vibration.

$$\psi_{\max} = \frac{F_0}{c \left(\frac{k}{m} - \left(\frac{c}{2m} \right)^2 \right)^{\frac{1}{2}}}$$

The damping of the system is calculated using equation (2.13)

$$c = d \times c_{crit} = 0.1 \times 2\sqrt{mk}$$

and the values of k already calculated for the three modes and found to be 0.093, 0.663 and 47.6 for mode 1, mode 2 and mode 3, respectively.

For mode 1, $m = \frac{1}{2} \rho wh(l+b) = 312.8 \times 10^{-12}$ kg and $k = 0.093$ So $c = 1.079 \times 10^{-6}$ kg/s

$$\psi_{\max} = \frac{F_0}{0.0185}$$

For mode 2, $m = \frac{1}{2} \rho wh(l+b) = 312.8 \times 10^{-12}$ kg and $k = 0.47$ So $c = 2.425 \times 10^{-6}$ kg/s

$$\psi_{\max} = \frac{F_0}{0.1176}$$

For mode 3, $m = \frac{1}{2} \rho wh(l+b) = 230 \times 10^{-12}$ kg and $k = 47.6$ So $c = 10.5 \times 10^{-6}$ kg/s

$$\psi_{\max} = \frac{F_0}{9.5}$$

The table below presents the comparison of the calculation and simulation result of the amplitude of the displacement vs periodic applied force at the resonant frequency for the three modes witch presented in Figure (3.17).


The large different for the validation of mode 3 obtained because the mass and thus the damping is considered for the arm in this calculation will the base is not completely rigid as explained in section 4.2.3.

Applied force (μN)	Maximum amplitude of the displacement ψ_{max} (μm)					
	Mode 1		Mode 2		Mode 3	
	Simulation	Theoretical	Simulation	Theoretical	Simulation	Theoretical
0.15	7.55	8.1	1.27	1.28	0.01	0.016
0.3	15.1	16.1	2.54	2.552	0.019	0.032
0.45	22.64	24.3	3.81	3.82	0.029	0.047
0.6	30.2	32.4	5.08	5.103	0.038	0.63
0.75	37.74	40.5	6.34	6.378	0.048	0.078
0.9	45.2	48.6	7.61	7.655	0.06	0.09

LIST OF PUBLICATIONS

CONFERENCE PAPERS

Waddah Abdelbagi Talha, John Ojur Dennis, Abdelaziz Yousif Ahmed “Design of a Lorentz Force Actuated Micromachined U-Shaped Cantilever Device for Magnetic Field Detection" Student Conference on Research and Development (**SCOREd 2008**) IEEE. 26-27 November 2008. UNIVERSITI TEKNOLOGI MALAYSIA, Johor Bahru, Malaysia.

John Ojur Dennis, Waddah Abdelbagi Talha, Nor Hisham B Hamid “Characterization and Modeling of 3-D Vibration Modes of a Micromachined U-Shaped Cantilever” The International Conference on Design, Test, Integration and Packaging of MEMS/MOEMS (DTIP 2009)  1-3 April 2009 ISBN: 978-2-35500-009-6, Rome, Italy

Waddah Abdelbagi Talha, John Ojur Dennis, Abdelaziz Yousif Ahmed “Simulation Studies on Vibration Modes of a Micromachined U-shaped Cantilever for Application in Magnetic Field Detection” The International Conference on Control, Instrumentation and Mechatronics Engineering (**CIM 2009**). 2-3 June 2009. Malacca, Malaysia.

JOURNAL PAPERS

Waddah Abdelbagi Talha, John Ojur Dennis, Abdelaziz Yousif Ahmed “Simulation Studies on Vibration Modes of a Micromachined U-shaped Cantilever for Application in Magnetic Field Detection” **IEEE Sensors and Transducers** journal (under review).